NUMERICAL SIMULATION OF THE TRANSITION REGION IN HYPERSONIC FLOW

By
Scott Andrew McKeel

a dissertation submitted to the faculty of
virginia polytechnic institute and state university
in partial fulfillment of the requirements for the degree of
doctor of philosophy
in
Aerospace Engineering

Robert W. Walters, Chairman

Bernard Grossman

Joseph A. Schetz

William H. Mason

Roger Simpson

February 1996
Blacksburg, Virginia

Abstract

NUMERICAL SIMULATION OF THE TRANSITION
REGION IN HYPERSONIC FLOW

by

Scott Andrew McKeel

Committee Chairman: Robert W. Walters
Aerospace Engineering

(Abstract)

The current state of transition region modeling is investigated through a literature search. The six most promising transition region models from the literature search were implemented in the Navier-Stokes code GASP. Baldwin-Lomax is an algebraic turbulence model in which the authors discuss how it can be used to simulate the transition region. Wilcox developed a procedure to use the low-Reynolds number $k-\omega$ model as a transition region model where a roughness strip is used to fix the transition point. Schmidt and Patankar developed production term modifications for low-Reynolds number $k-\epsilon$ models to correct for the problems these models have in simulating the transition region. Warren, Harris and Hassan developed a one equation turbulence model that accounts for the first and second mode disturbances in the transition region. The algebraic transition region model of ONERA/CERT controls the amount of eddy viscosity added to the molecular viscosity. The linear combination model of Dey and Narasimha combines a fully laminar and fully turbulent flow field

through the intermittency to form the transitional flow field.

GASP is a compressible Navier-Stokes code which has a practical lower working limit of $M = .1$. The majority of experimental data for transitional flow exists below this limit. The test cases found above this limit and used here were all in the hypersonic regime. The results from the six transition region models were compared against the experimental test cases found for a variety of cones and ramps. Two models produced inadequate results on these test cases. The Wilcox model did not function as it was intended. The algebraic transition region model overpredicted the heat transfer in the turbulent region for several cases and did not transition in regions of large adverse pressure gradients. Several models performed adequately. The Baldwin and Lomax model provide fast estimates of the transition region. The Warren, Harris and Hassan model, the Schmidt and Patankar model, and the linear combination model produced adequate results on the test cases for this work and are worthy of attention on other test cases.

Modifications were made to the Schmidt and Patankar model and the algebraic transition region model to improve their predictions on the current test cases. A turbulent spot was introduced into the boundary layer for the Schmidt and Patankar model which facilitated in the use of the model. Also, the maximum production allowed was recalibrated and allowed to grow exponentially to improve transition region simulating for the test cases presented here. The empirical transition function from the algebraic transition region model was recalibrated for the hypersonic test cases used in this work.

Acknowledgements

Many thanks need to go out, it was a monumental accomplishment for me to graduate. I thank God for everything.

I thank my parents for believing in me and always being there. I thank all my friends who have always been like family to me.

I am very thankful to Dr. Robert Walters for the patience he showed towards me.

A special thanks must go out to Dr. Andy Godfrey, Dr. Bill McGrory and Dr. Mike Applebaum each of which spent countless hours trying to help me understand CFD.

I thank everyone who has ever been part of the "Sun Room". It has been a lot of fun. It is hard to believe, but I will actually miss this place.

And I thank Chris for everything.

Nomenclature

A^+	Van Driest constant = 26
A	Schmidt and Patankar PTM parameter
B	Schmidt and Patankar PTM parameter
c_p	Specific heat at constant pressure
C_{cp}	Baldwin-Lomax constant = 1.6
C_f	Skin friction coefficient
C_h	Heat Transfer coefficient, $\frac{q_w}{\rho_\infty U_\infty (h_{o\infty} - h_w)}$
C_{Kleb}	Baldwin-Lomax constant = 0.3
C_{mutm}	Baldwin-Lomax constant = 14
C_{wk}	Baldwin-Lomax constant = 0.25
h	Enthalpy
k	Turbulent Kinetic Energy (TKE), $\frac{1}{2}\overline{u_i' u_i'}$ (incompressible), $\frac{1}{2}\frac{\overline{\rho u_i'' u_i''}}{\overline{\rho}}$ (compressible)
K	Clauser constant = 0.0168
k_R	Surface roughness height
k_R^+	Non-dimensional surface roughness height, $\frac{u_\tau k_R}{\nu}$
l_{TKE}	Free Stream TKE reference length, $\frac{k_\infty^{1.5}}{\epsilon_\infty}$
L_{t2}	pressure gradient parameter
M	Mach number
N_0	Narasimha's non-dimensional turbulent-spot formation rate for zero pressure gradients
N_2	Narasimha's non-dimensional turbulent-spot formation rate
P_k	Production term in TKE equation
q	Free stream turbulence level, $\frac{k_\infty}{U_e^2}$

q_w	Wall heat transfer rate
R_k	Wilcox $k-\omega$ constant $= 6$
R_β	Wilcox $k-\omega$ constant $= 8$
R_ω	Wilcox $k-\omega$ constant $= 27/10$
Re_{s_t}	Reynolds number based on transition location
Re_θ	Reynolds number based on momentum thickness
Re_x	Reynolds number based on x
St	Stanton Number, $\frac{q_w}{\rho_e U_e c_p (T_w - T_{aw})}$ (Stainback) $\frac{q_w}{\rho_\infty U_\infty (h_o - h_w)}$ (Kimmel)
T_w	Temperature at the wall
T_{aw}	Adiabatic temperature at the wall
Tu_e	Turbulence intensity, $\frac{\sqrt{{u'_i}^2/3}}{U_e}$
u_j	Velocity in j direction, tensor notation
U	Reynolds averaged steady state velocity
u_τ	Friction velocity, $\sqrt{\frac{\tau_w}{\rho_w}}$
$\vec{V}$	Velocity vector
x_j	Coordinate in j direction, tensor notation
x_{t0}	Stream wise distance to start of transition
x_{t2}	Stream wise location of subtransition
X	Axial distance
y	Normal distance to wall
y^+	Non-dimensional distance to wall, $\frac{\rho\ u_\tau\ y}{\mu}$
t	Time
α_0	Wilcox $k-\omega$ constant $= 1/10$
α_0^*	Wilcox $k-\omega$ constant $= 1/40$
δ_t	Boundary layer thickness
Δs	Length of Wilcox roughness strip
ϵ_t	Algebraic Transition model transition function
γ	Intermittency
κ	Kármán constant $= .41$

μ	Molecular viscosity
μ_{eff}	Effective viscosity
μ_{mol}	Molecular viscosity
μ_t	Turbulent eddy viscosity
ρ	Density
σ	Wilcox $k-\omega$ constant $= 1/2$
σ^*	Wilcox $k-\omega$ constant $= 1/2$
τ_{ij}^T	Reynolds stress tensor
θ	Momentum thickness
θ_{lam}	Momentum thickness of laminar flow field
θ_{t0}	Momentum thickness at x_{t0}
ν	Kinematic viscosity, $\frac{\mu}{\rho}$
χ_1	Momentum thickness parameter for Algebraic Transition model
ω	Vorticity or specific dissipation rate (ϵ/k)

Subscripts

e	Condition at edge of boundary layer
o	Stagnation condition
w	Condition at wall
∞	Free stream condition upstream of shock

Acronyms

CFD	Computational Fluid Dynamics
DNS	Direct Numerical Simulation
GASP	General Aerodynamics Simulation Program
PTM	Production Term Modifications
RANS	Reynolds-averaged Navier-Stokes
TKE	Turbulent Kinetic Energy

Contents

List of Tables

List of Figures

Chapter 1

Introduction

1.1 Overview

In most types of flows, laminar flow will yield to turbulent flow through a transition region that is too often ignored in CFD calculations. The length of the transition region can become a large part of the domain [1], even as long as the length of the laminar region [2]. Skin friction and heat transfer significantly increase in the transition region [1, 3], at times, increasing to the point that a local maxima is reached [4, 5]. It is thus imperative that the transition region be modeled appropriately.

The importance of the transition region has been recognized in many design problems. Many papers [6, 7, 8, 9] have stressed the importance of modeling the transition region in the design of turbine blades. Gas turbine engines are limited by the turbine inlet temperature which is limited by the temperature that the turbine blades can withstand. Turbine blade temperatures are thus pushed to critical material temperatures to achieve a high turbine inlet temperature. Computing accurate heat transfer is very important in designing turbine blades and, since the local maximum in heat transfer usually occurs in the transition region, modeling the transition region becomes almost mandatory. If the region is not modeled, large errors in the prediction of heat transfer are possible.

Hypersonic reentry vehicles such as the National Aerospace Plane and the Space Shuttle show the importance of the transition region [10, 11]. Heat transfer in the

turbulent region can be almost an order of magnitude higher than laminar heating. The transition region must be accounted for to accurately model the heat transfer around these vehicles.

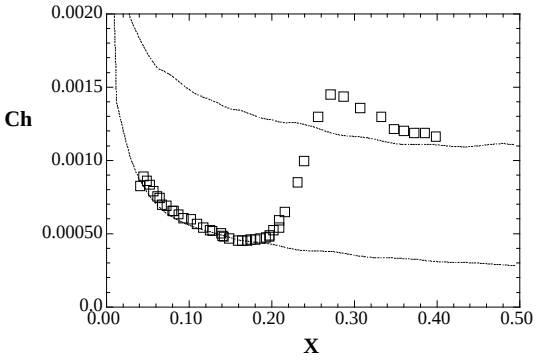

Figure 1.1: Typical Transition Profile

Figure 1.1 shows a typical transition region heat transfer profile on the surface of an axisymmetric cone at hypersonic speeds to illustrate the above points. The lower dotted line is the fully laminar solution and the upper dotted line is the fully turbulent solution. The heat transfer for turbulent flow is much higher than for laminar flow. The experimental data shown starts out laminar in the beginning of the domain, then it slowly rises and reaches a peak higher than the turbulent value at the end of transition. Clearly, the local minimum and maximum in the heat transfer occur in the transition region. The length of the transition region is commonly (and will be in this work) measured as the distance between the minimum and maximum in heat transfer, though Narasimha [12] shows that the transition region extends slightly in front and beyond these boundaries. For the example case presented, the length of the transition region is seen to be a significant part of the domain. In some hypersonic flows, the length of the transition region is longer than the laminar region preceding it [2, 13].

Thus realizing the importance of the transition region and realizing the need to model it in computational fluid dynamics (CFD), the goal of this work is to evaluate the current state of transition region modeling and improve on it. This begins by searching the available literature for methods of modeling the transition region using a

Navier-Stokes code. The most promising transition region models from the literature are then implemented in the General Aerodynamics Simulation Program (GASP) version 2 [14] and tested against a variety of test cases incorporating important flow features such as pressure gradients. Modifications then can be attempted to improve on the accuracy.

1.2 The Physics of Transition

A look into the physics of transition is necessary. While the current work is not a study of the process or physics of transition, knowledge of the physics of what is trying to be modeled or simulated will be helpful.

Transition is very complicated, and a thorough general description of the process for all types of flows would be difficult at best. A good starting point is a discussion of the idealized transition process for flat plate incompressible flow. The information presented here is largely from White [15]. The initial part of the domain is stable laminar flow. Transition does not start at the beginning of the domain. The laminar boundary layer is susceptible to disturbances from both the free stream and the surface itself which is defined to be the receptivity of the boundary layer. The free stream or outer disturbances include acoustic waves, particles in the flow, and pressure fluctuations [16]. Surface disturbances include the roughness of the body as well as any vibrations the body may have [16]. The transition process formally starts where a disturbance in the boundary layer is no longer damped, it becomes unstable. The results is the formation of the two-dimensional Tollmien-Schlichting waves which are the first mode instability of the flow.

While traveling downstream, three dimensional spanwise variations begin to develop in the Tollmien-Schlichting waves. Small amplitude fluctuations develop in velocity and pressure. The flow at this point is still technically laminar. Three dimensional breakdown of the longitudinal vortices begins. The vortices cascade down into smaller scales. Turbulent spots, known as Emmons [17] spots, begin to occur. The spots have the rough shape of an arrowhead [15, 18, 12]. As the spots move downstream, they grow by entraining more and more laminar flow. Eventually, the

growing spots coalesce into a fully turbulent flow. The transition from laminar to turbulent flow is complete. Schlichting [19] and Bertin and Smith [20] show figure 5-28a from White [15] which is a sketch of the transition process.

The above description of the transition region holds only for flows with small disturbances that are primarily random [15]. Flows with strong disturbances in the laminar region bypass the initial steps of the instabilities such as Tollmien-Schlichting waves and this process is known as bypass transition by Morkovin [16]. Of concern to bypass transition is the inner, three-dimensional, nonlinear instability known as bursting.

For compressible flows, most notably flows with a Mach number of 4 or greater, Mack [21, 22] shows that the viscous first mode instability is no longer the dominant mode. The inviscid second mode becomes the most unstable mode. As the Mach number increases, the generalized inflection point moves away from the wall and the viscous instability decreases to the point of being a stabilizing influence and the inviscid instability mechanisms increase [21].

The transition process has a dramatic effect on many integral quantities of importance to engineering. The boundary layer thickness and the momentum thickness roughly double. Skin friction and heat transfer also experience a large increases. These changes occur in the region where the turbulent spots form and coalesce downstream into fully turbulent flow, not in the region where the Tollmien-Schlichting waves start.

1.3 Literature Search

This section presents a survey of the available literature that pertains to modeling the transition region. This includes papers on turbulence models, transition region models and experimental transition data.

The papers are divided into three broad categories: turbulence/transition region models, experimental results, and theoretical studies. Some of the papers present information in multiple categories and in that case they will be put into the section for which they contributed the most value. All sections feature one paragraph summaries

of the papers in chronological order.

1.3.1 Overview of Turbulence/Transition Region Models

Papers that deal with turbulence models or transition region models are listed in this section. Papers that introduce models are listed in chronological order starting with the oldest first. Papers which review models are located at the end of this section once again in chronological order.

An important distinction needs to be made between predicting transition and simulating the transition region. Some models will attempt to predict the location of the start of transition given the free stream conditions. Other models will attempt to simulate the transition region given the location of transition. Others will attempt to do both.

McDonald and Fish [23] present a turbulence/transition region model that uses a turbulence kinetic energy equation in conjunction with algebraic length scale relationships. The model can predict the location of transition as well as simulate the transition region. The model can also account for relaminarization in strong favorable pressure gradients. Comparisons with many experiments are presented with good results. A limitation of the paper is that the turbulent kinetic energy equation is presented in a form for nonhypersonic boundary layers codes which makes it difficult for implementation in full Navier-Stokes codes used for hypersonic flows, like this dissertation. This model is one of the few true turbulence/transition region models available.

Forest [8] developed a procedure for predicting transition and simulating the transition region. The eddy viscosity is modeled with a simple algebraic mixing length. Another term is added to the viscosity to model free stream turbulence effects. To simulate the transition region, the eddy viscosity is multiplied by a factor called the intermittency before being added to the viscosity. The intermittency is defined to have contributions due to Tollmien-Schlichting and due to Taylor-Goertler mechanisms, each of which is defined by formulas presented in the paper. Results are presented for a flat plate, a relaminarizing flow, and a turbine blade in a cascade.

Baldwin and Lomax [24] present an algebraic turbulence model which is very

popular and is implemented in many CFD codes. What is often overlooked in the paper is a procedure for using the model to predict and simulate the transition region. The eddy viscosity is set equal to zero if the maximum eddy viscosity in the profile is less than a constant, in this case 14, times the free stream viscosity. Results are shown in good agreement with experiment.

Arad, Berger, Israeli and Wolfshtein [25] develop a procedure for predicting transitional boundary layer flow in compressible, axisymmetric and flat plate boundary layers. The numerical method used is an extension of the very popular boundary layer method of Patankar and Spalding [26]. This paper aims to quantify the disturbances in the boundary layer that cause transition in terms of an energy and a length scale. For this reason the two equation turbulence model of Ng [27] is used for the turbulent and transitional region. Results are presented against experiments for computed transitional Reynolds number versus free stream turbulence energy levels, the scale of the disturbances and Mach number and a correlation is presented between these quantities. Results for transitional heat transfer or skin friction are not presented.

The process of transition from laminar to turbulent flow is very complicated. Emmons [17, 28] observed that transition starts as turbulent spots which form in the laminar region and propagate downstream, eventually coalescing to form the turbulent region. Narasimha in several published papers [12, 29, 30] develops formulas using this spot theory to compute the intermittency of the transition region, where the intermittency is defined to be the percentage of time that a flow is turbulent at a given location. Dey and Narasimha [31] go on to develop a linear combination transition region model which is used to simulate the transition region. The mean transitional flow is defined to be the combination, using the intermittency, of the mean laminar flow and a mean turbulent flow that starts where the spots are first formed, i.e. where transition starts. Computations presented using this model produced promising results.

Arnal [10] presents an overview of some of the theoretical and experimental issues involved with transition. Much of the paper is devoted to stability theory of boundary layers. There is also much information on different experimental studies that highlight the effect of different parameters on transition. With over 100 references, this paper

is an excellent starting point for general transition knowledge. Transition region modeling is just briefly touched upon but it is very important. An algebraic transition region model is presented which is described in more detail in Singer's papers[4, 5]. The model simulates the transition region by proportioning the amount of eddy viscosity that is added to the molecular velocity through a transition function. No eddy viscosity is added for the laminar part. When the specified transition point is hit, the amount of eddy viscosity added in is slowly increased to a value greater than one to produce the peak at the end of transition of heat transfer or skin friction before it finally hits a value of one for the fully turbulent region. Results given for this model for two experimental cases are excellent.

Standard two equation turbulence models experience problems near the wall. Some modelers use wall functions that prescribe values near the surface. Other modelers have developed low-Reynolds number corrections to the two equations models that enable them to be integrated to the wall, but this also has some problems. An interesting approach comes from the work of Rodi [32] and Fujisawa, Rodi, and Schönung [33] where the two equation model is used in the outer region and a one equation model is used near the wall. Results are presented for a variety of flows including transitional. The transition region is simulated by manipulating a damping constant for the length scale for the eddy viscosity. In the laminar region, the damping constant is adjusted so the eddy viscosity is small, forcing laminar flow. In the transition region, the value of the damping constant is ramped to its fully turbulent value, simulating the transition to turbulent flow.

Schmidt and Patankar [34] develop a modification for low-Reynolds number $k-\epsilon$ models to help them model the transition region. They modify the production term in the turbulent kinetic energy equation so that it is zero at the beginning of the domain and then they slowly let it ramp up as to prolong the length of the transition region. The model is calibrated with the work of Abu-Ghannam and Shaw [1] which correlates the starting point of transition and length with the free stream turbulent kinetic energy for incompressible flow. The model was originally developed for the Lam-Bremhorst [35] low-Reynolds number $k-\epsilon$ model but can feasibly be used for any low-Reynolds number $k-\epsilon$ model. Results are presented against several experimental

data sets including flat plates with no pressure gradient and a favorable pressure gradient as well as turbine blades. The comparisons are very good.

An interesting approach to simulating the transition region is undertaken by Lund [36] who uses the renormalization group theory (RNG) algebraic turbulence model of Yakhot and Orszaga [37] to mimic transition. The basic theory behind the RNG algebraic turbulence/transition region model is an eddy viscosity is computed by using a standard mixing length model and is then rescaled according to its magnitude. A ramp function is used in the rescaling which produces the transitional effects. A sample calculation is done for an incompressible flat plate boundary layer but is not compared to any experimental values.

Wilcox's *Turbulence Modeling for CFD* [38] is a review of many of the aspects of turbulence modeling. Wilcox discusses zero, one, and two equation turbulence models as well as compressibility effects and numerical considerations. He presents in this book and discusses in more detail in a later paper[39], how his two equation $k-\omega$ turbulence model [40, 41, 42, 43, 44] can be used to simulate the transition region. Wilcox developed low-Reynolds number corrections for the model that enable it to predict transition for a Blasius boundary layer. For other flows, the corrections do not produce the correct transition location. Wilcox goes on to use the roughness boundary condition on ω to create a roughness strip which destabilizes the boundary layer and allows the user to set the transition point almost anywhere in the flow. Equations are given for how long the roughness strip should be and what value of roughness should be used. Related papers are by Menter [45, 46, 47] who attempts to improve on the $k-\omega$ turbulence model. Menter[45] deals with the effects of the free stream value of ω on the flow. He effectively states that there is a minimum value that ω must be in the free stream, if it is any lower, the results are affected. Menter [46] develops two new turbulence models based on the $k-\omega$ model. Menter[47] compares the $k-\omega$ model against 3 very popular turbulence models, Baldwin-Lomax [24], Johnson-King [48], Baldwin-Barth [49] for adverse pressure gradient flows. A modification for the eddy viscosity is developed out of this work for the $k-\omega$ model.

Spalart and Allmaras [50] develop a one-equation turbulence model based on a

transport equation for the eddy viscosity which has the advantage over other one-equation models that there is no need to specify algebraic relations for the length scale. Modifications are made to the production and destruction terms and a source term is added to trip transition at a given point. The model is used to simulate the transition region, not predict the location of transition. Unfortunately, no transitional results are presented against experimental data. Strong points of this turbulence model are that it is local which means that it is not dependent on properties that are computed from a select group of grid cells, such as momentum thickness. Also it does not have the convergence and grid problems that plague two equation models.

Warren, Harris, and Hassan [3] expand on the previous work of Young, Warren, Harris and Hassan [51] and Micheltree, Salas and Hassan [52] to develop a one-equation compressible turbulence model with provisions to simulate the transition region. The one-equation used is a form of the turbulent kinetic energy equation with the modeled form of the turbulent transport diffusion different than what is usually seen in the literature. The provisions for the transition region are in the form of the Dey and Narasimha [31] relations for the intermittency used to proportion the length scale for the eddy viscosity. What makes this paper unusual is that the Reynolds stress in the transition region includes non-turbulent and large eddy effects. While the large eddy effects are mentioned and then ignored, formulas are presented to incorporate the effect of the first and second mode disturbances through the eddy viscosity length scale. The issue of a non-constant turbulent Prandtl number is also included. Results are presented for several supersonic cone cases and are very promising.

Two equation turbulence models are able to qualitatively simulate the transition region. The beginning of the region is given a low turbulent kinetic energy which causes the dissipation of k to be greater than the production of k which makes the flow laminar. As the flow progress down the domain, TKE from the free stream diffuses into the boundary layer and eventually the production of TKE exceeds the dissipation and the flow goes through transition. The increasing k also increases the dissipation of k and eventually a balance is reached. This method is not physically correct and it also predicts transition too early in the domain and the length of the region tends to be too short. However, because of the popularity of two equation

turbulence models, many people [11, 53, 54, 55, 56] have tried to overcome these shortfalls by varying the initial conditions in the domain with some limited success.

The popularity of two equation turbulence models has spawned an explosion of new two equation models. Many of these are simply new low-Reynolds number versions of the $k-\epsilon$ model. Others replace k or ϵ with new variables that are supposed to have better behaved governing equations. Several papers exist that review and test the different two equation models available. As mentioned earlier in this chapter, Wilcox's book [38] is a complete review of turbulence models, including two equation models. An excellent two equation model review paper is Patel, Rodi and Scheuerer [57], which compares 8 different two equation turbulence models. Results are presented for velocity profiles, turbulent kinetic energy profiles and skin friction. The paper has a thorough break down of what the different damping terms are trying to accomplish and what their near wall behavior should be. Coakley and Huang [58] compare 5 two equations models. Results are presented for simple flat plate flows and for complex flows with a variety of modeling corrections. Speziale, Abid, and Anderson [59] compares three existing two-equation models with a new one presented in the paper. The asymptotic consistency of the models is discussed and results are shown for a flat plate.

Stephens and Crawford [9] present a dissertation to NASA that examines an early form of the Schmidt and Patankar model(Schmidt [60]) and similar model of Johnson [61] that changes the production term in a $k-\epsilon$ formulation to better simulate the transition region. Their results are cut short when they discover a problem that the Chien low Reynolds number $k-\epsilon$ model [62] faces when used in transitional flow. The Chien model with the Schmidt modifications does not predict the transition region heat transfer well and, more importantly, does not result in fully turbulent flow at the end of transition. A thorough investigation reveals that the f_μ function for the Chien model is not valid for laminar or transitional flows. A strength of this paper is a thorough literature search that includes transition region models as well as transitional experimental data.

Singer, Dinavahi, and Iyer [4] and Singer [5] are two excellent transition region

model papers which form the foundation of this work. Complete descriptions are provided in both papers of Narasimha's linear combination model and Arnal's algebraic transition region model. The linear combination model combines a turbulent flow field and a laminar flow field to form the transition region. The algebraic transition region model proportions the amount of eddy viscosity added to the molecular viscosity (Both models will be discussed further later). "Modeling the Transition Region" [5] presents an overview of the current methods that can be used to simulate or predict the transition region. Equally valuable is a section that discusses the effect of flow features such as pressure gradients and compressibility on transition. "Testing of Transition-Region Models: Test Cases and Data" [4] compares the previously mentioned linear combination and algebraic transition region models with over a dozen experimental cases. The same authors have combined for a number of other articles reviewing and testing transition region models [63, 64, 65, 66].

1.3.2 Overview of Experimental Studies

The goal of the experimental literature search is to find papers that will either provide insight into the mechanisms of the transition region, or more importantly, provide a test case with some experimental data for comparison with the transition region models. The papers are listed in chronological order.

In one of the classic transition papers, Schubauer and Klebanoff [18] investigate the transition region in detail. Their test case consists of a flat plate at incompressible speeds. One part consists of a roughness element that is used to generate a turbulent wedge in the laminar flow, the growth of the wedge is investigated. Small sparks are used to generate turbulent spots. The geometry and growth rate of these spots is investigated. Their overall conclusions about transition support the work of Emmon's [17] turbulent spot theory and disprove the old theory that transition occurs in a non-stationary line. Graphs presented include mean velocity profiles through the transition region that are clearly laminar at the beginning and clearly turbulent at the end with smooth changes in the in between stations. A graph of the intermittency is also presented showing that is a Gaussian distribution. Even though this paper is over 40 years old, it is still one of the best available.

Chen and Thyson [13] expand on the work of Emmons [17] and Dhawan and Narasimha [30] to develop their own intermittency function. They start with the triangular spot geometry and the source rate density of the spot formation. The resulting function is for axisymmetric bodies with zero angle of attack and it reduces to the form of Dhawan and Narasimha for a flat plate. The problem with the formula that makes it difficult for implementation in CFD codes is that it involves integrals that depend on the geometry. Chen and Thyson go on to investigate the correlations between transition length and the starting point of transition in terms of Reynolds numbers. Mach number is shown to have a big effect. These results are applied to develop a formula for the spot formation rate. The frequency of Tollmein-Schlichting waves and their effect on the spot formation rate is also investigated.

Stainback, Fisher, and Wagner [67] study the effect of disturbances on the transition of supersonic cones. Figures 3 and 13 in this paper show typical heat transfer results for a Mach 6 cone. The plots feature a very distinct transition region that is very well resolved, providing a good experimental comparison for CFD results even though the purpose of the paper was not to present heat transfer data in the transition region. Stainback, Fisher and Wagner's real purpose was to investigate the pressure fluctuations and their effect on transitional Reynolds number.

Abu-Ghannam and Shaw [1] investigate transition from laminar to turbulent flow from an engineering point of view, in that their main concern is the end results, not the physics of stability that cause transition. They work to develop empirical correlations for the starting and ending points of transition as functions of free stream turbulent kinetic energy and pressure gradient for incompressible flow. They present correlations and graphs from their own experiments and from experiments in the literature for the starting and ending points of transition in terms of Reynolds number based on momentum thickness. They finalize their correlation and then use it to compute transitional boundary layers by bridging classic methods of computing laminar and turbulent flow. Results using this method are presented for several flows with promising results.

Daniels and Browne [7] compare five different boundary layer codes to experimental data on gas turbine blades. The five codes include a program by Cebeci and

Smith[68], a program by Patankar and Spalding [26], the Cebeci and Smith program with the McDonald and Fish turbulence model [23], Wilcox's EDDYBL program [69], and Wilcox's program where the eddy viscosity is inputed. None of these are described in great detail in the paper because they are referenced. The experimental turbine blade data is presented at two different Reynolds numbers. The heat transfer on the suction side for both Reynolds numbers show a distinct transition region. The plots are busy and are hard to read. Good agreement is shown for the fully laminar and fully turbulent region but not for the transition region.

Fisher and Dougherty [70] present a very thorough and complete study of transition on a 10° cone in flight tests. The focus is on the starting and ending points of transition, not on variation of skin friction or heat transfer through the transition region. This paper is excellent for anyone looking to develop a correlation for the starting and ending points of transition versus any number of variables.

Hylton, Mihelc, Turner, Nealy, and York [71] presents an in depth study into turbine blades using experimental and computational results. While transition is not the main focus of the paper, because of its occurrence on the turbine blades, it becomes very important to the paper. The computation methods are aimed more at practical everyday models and methods rather than research tools but a lot of good information is presented with a large number of references. The real strength of the paper is the experimental results presented. Several other turbine blade experiments are referenced, but the ones presented in this paper are the best as they feature distinct transition effects and are presented well.

Wang, Simon, and Buddhavarapu [72] present an experimental study into the effect of free stream turbulence on transition. A laminar baseline case and a low and high free stream turbulence case are run on a flat plate at low speeds. Stanton number and skin friction for all three cases are shown on the same plot which is an excellent example of the effect of transition. Mean temperature and velocity profiles are given at five stations for each flow.

Supersonic, transitional, heat transfer data isolating the effect of pressure gradients is presented by Kimmel [2, 73]. The experiment consists of a half meter forecone followed by one of several different flared sections used to create constant pressure

gradients, both favorable and adverse. Kimmel notes that the original purpose of his work was to study the effect of second mode instabilities on transition, not to generate heat transfer profiles in the transition region. For this reason, the experiment has not been optimized to measure heat transfer data and the result is that the number of data points at the beginning of the transition region is sparse for some of the cases. However, Kimmel notes the paucity of hypersonic transitional heat transfer data available in the literature so this data is published on its own merits for whatever it is worth to the research community. Despite the limitations, this work is one of the best experimental data cases available.

It seems that few papers exist that investigate transitional boundary layers and, specifically, measure the heat transfer through the transition region. An exception to this is the work of Holden and Chadwick [74]. They measure the transitional heat transfer on a compression ramp at Mach numbers of 10, 11 and 12. The varying Mach numbers and Reynolds numbers enable them to have transition occur on different parts of the ramp which means transition is occurring at different parts of the pressure gradient. This enables an investigation of the effect of an adverse pressure gradient on transition. The experimental measurements are presented in graphs and tables for all 18 test cases, which makes this an excellent paper to use for computation comparisons. Holden and Chadwick do their own computational comparisons using the Reynolds averaged Navier-Stokes code GASP. The laminar parts agree well but for some of the cases, the turbulent results from the Baldwin and Lomax algebraic turbulence model and the Chien $k - \epsilon$ model give results different from each other and from the experimental data. Their only attempt at transition region modeling was running laminar flow up to the transition point and then switching to a turbulent calculation. Results using this method were disappointing.

1.3.3 Overview of Theoretical Studies

This section features papers that present theoretical insight into the transition region. The papers are listed in chronological order.

The classical description of laminar to turbulent transition is of small disturbances that become amplified in the flow field in the form of Tollmien-Schlichting waves which

break down in a series of events. Turbulent spots form which coalesce downstream and form fully turbulent flow. Lin [75] provides a summary of the classical transition process.

Mack [21, 22] has studied the use of linear stability theory in supersonic conditions. Mack [21] shows that second mode disturbances are dominant for Mach numbers of 4 and above. Increasing Mach number makes the inviscid mechanisms more unstable and the viscous mechanisms more stable. It is shown that the upper instability modes occur where there is a area of supersonic flow relative to the phase velocity of the disturbances [21]. Mack [22] examines the stability of cones compared to flat plates at hypersonic speeds. Comparison with experiment shows that since the wave length of the disturbance is twice the boundary layer thickness, the disturbance is the second mode. The most unstable modes grow as much or more on cones as they do on flat plates.

Boundary layers with strong disturbances bypass the classical steps of transition. This is called bypass transition. Morkovin [16] qualitatively discusses the physics and issues of bypass transition which becomes very valuable when trying to model these types of flows.

Madavan and Rai [76] expand on the previous work of Rai and Moin [77] and perform Direct Numerical Simulation (DNS) of transition on flat plates. The evolution of each of the fluctuating components of velocity as well as the Reynolds stress is shown through the transition region. Temperature fluctuations and turbulent heat flux distributions are also presented. Results for skin friction and Stanton number are compared against experimental results [78, 79, 80]. Computations of the turbulent Prandtl number are provided. This paper provides an excellent insight into the transition region.

1.3.4 Summary

There is a large body of work on transition. Most of the theoretical work has been done in the field of linear stability theory and trying to determine the start of transition. Similarly, much of the experimental work is concerned with developing correlations for the starting and ending points of transition. As will be discussed later, neither of

these subjects are important to this work.

A majority of the experimental studies that measure the skin friction or heat transfer in the transition region are for incompressible flow. The limited number of supersonic cases are sometimes just a byproduct of other research and are not optimized to present heat transfer data in the transition region.

A significant number of transition region models exist in the literature. Most are originally designed for incompressible flow and are later extended to compressible flow.

1.4 Purpose of the Investigation

The preceding literature search has shown the body of work that has been done by the research community in transition region modeling. The focus of the experimental work has been mostly for incompressible flow. The focus of the transition region model research has been mostly with boundary layer codes. The goal of the current work is to take the most promising transition region models out of the literature search and implement them in a Reynolds averaged Navier-Stokes code and apply them to high speed flow. The current definitive reviews of transition region models in the literature are by Singer *et al.* [4, 5] which test two transition region models in a boundary layer code. The current work will test six models in a Navier-Stokes code for high Mach number flows and compare the results to detailed experimental test cases. The ability of each model to simulate the transition region will be addressed as well as the ease of use and implementation of the model. In addition, modifications will be made to some of the models to improve their performance. Clearly, the current work goes beyond any existing paper to completely define the current state of transition region modeling in a Reynolds averaged Navier-Stokes code for high speed flow and improve on it.

Chapter 2

A look at Turbulence

2.1 Overview

This dissertation is a study of transition region models, not turbulence or turbulence models. Turbulence models are used, but their ability to simulate turbulence is not addressed, only their ability in simulating the transition region is discussed. That being said, the field of transition region models has deep roots in turbulence modeling and a brief study into the theory behind turbulence models is necessary. The following study is by no means complete or exhaustive. It is meant as a review or reference for those who are familiar with turbulence, not as an introductory text. Many of the missing details can be found in Wilcox [38] and Liou and Shih [81].

2.2 Reynolds and Favre averaging

The birth of turbulence modeling came with the Reynolds-averaged Navier-Stokes equations. The idea behind Reynolds averaging is that any time varying quantity, such as the velocity, can be broken up into a mean part and a fluctuating part:

$$u_i = U_i + u_i^{'} \tag{2.1}$$

The mean part is defined to be

$$U_i = \frac{1}{T}\int_t^{t+T} u(x,y,z,t)dt \tag{2.2}$$

T is a time scale that is long relative to the fluctuations of the flow but is short compared to the time variations not related to the turbulence. In other words, U_i is a function of time. The above decomposition is performed on the quantities in the Navier-Stokes equations and then the time or Reynolds average is taken which eliminates the simple fluctuating terms and leaves the steady state terms and products of the fluctuating components which are called velocity correlations. For incompressible flow, the resulting continuity and momentum equations are

$$\frac{\partial \rho}{\partial t} + \frac{\partial}{\partial x_i}\left(\rho U_i\right) = 0 \tag{2.3}$$

$$\frac{\partial}{\partial t}\left(\rho U_i\right) + \frac{\partial}{\partial x_j}\left(\rho U_j U_i\right) = -\frac{\partial p}{\partial x_i} + \frac{\partial}{\partial x_j}\left[\tau_{ij} - \rho\overline{u_j^{'} u_i^{'}}\right] \tag{2.4}$$

These are known as the Reynolds averaged Navier-Stokes equations. When comparing the above equations to the instantaneous Navier-Stokes equations, the Reynolds averaging has produced velocity correlations known as the Reynolds stresses. Simply stated, the goal of turbulence modeling is to compute the Reynolds stress.

Now for compressible flow, when the density is decomposed and Reynolds averaging is performed, the Navier-Stokes equations are littered with multiple velocity fluctuation terms (See Liou and Shih [81]). Each of these new correlations would require modeling in addition to modeling the Reynolds stress which is clearly an undesirable situation. Favre [82] averaging, also called mass-weighted averaging, decomposes a given quantity, such as the velocity, into a mass average and its associated fluctuating part

$$u_i = \tilde{u_i} + u_i^{''} \tag{2.5}$$

where

$$\tilde{u_i} = \frac{\overline{\rho u_i}}{\bar{\rho}} \tag{2.6}$$

Applying this decomposition and averaging to the continuity, momentum and energy equations results in the Favre averaged Navier-Stokes equations.

$$\frac{\partial \bar{\rho}}{\partial t} + \frac{\partial}{\partial x_i}\left(\bar{\rho}\tilde{u}_i\right) = 0 \tag{2.7}$$

$$\frac{\partial}{\partial t}\left(\bar{\rho}\tilde{u}_i\right) + \frac{\partial}{\partial x_j}\left(\bar{\rho}\tilde{u}_j\tilde{u}_i\right) = -\frac{\partial p}{\partial x_i} + \frac{\partial}{\partial x_j}\left[\tau_{ij} - \overline{\rho u_j^{''} u_i^{''}}\right] \tag{2.8}$$

$$\frac{\partial}{\partial t}\left[\bar{\rho}\bar{e}_o + \frac{\overline{\rho u_i'' u_i''}}{2}\right] + \frac{\partial}{\partial x_j}\left[\bar{\rho}\tilde{u}_j\tilde{h}_o + \tilde{u}_j\frac{\overline{\rho u_i'' u_i''}}{2}\right]$$
$$= \frac{\partial}{\partial x_j}\left[-qL_j - qT_j + \overline{\tau_{ij}u_i''} - \overline{\rho u_j''\frac{1}{2}u_i''u_i''}\right]$$
$$+\frac{\partial}{\partial x_j}\left[\tilde{u}_i\left(\bar{\tau}_{ij} - \overline{\rho u_j'' u_i''}\right)\right] \tag{2.9}$$

The Favre averaged Navier-Stokes equations appear identical to the incompressible Reynolds averaged Navier-Stokes equations and that is the intention. Again, the object of turbulence modeling is to model the Reynolds stress tensor, denoted by

$$\tau_{ij}^T = -\overline{\rho u_j'' u_i''} \tag{2.10}$$

2.3 The Eddy Viscosity

We need some way to model the Reynolds stress. Looking at the momentum equation (2.8), the Reynolds stress seems to play a similar role to the viscous stress. We will attempt to model the Reynolds stress in analogy to the viscous stress [83]. This is the Boussinesq eddy-viscosity approximation.

$$\tau_{ij}^T = 2\mu_T\left(\frac{1}{2}\left(\frac{\partial U_i}{\partial x_j} + \frac{\partial U_j}{\partial x_i}\right) - \frac{1}{3}\frac{\partial \tilde{u}_k}{\partial x_k}\delta_{ij}\right) - \frac{2}{3}\bar{\rho}k\delta_{ij} \tag{2.11}$$

where μ_T is the eddy viscosity. It is important to note that the trace of τ_{ij} must be $-2\bar{\rho}k$ [38] by definition of the compressible TKE.

Now the problem of modeling the Reynolds stress has been transferred to computing the eddy viscosity. Dimensional analysis and analogy to the viscous stress shows that the eddy viscosity is a function of a velocity scale, v, and a length scale, l, and the density, viz.

$$\mu_T = \rho v l \tag{2.12}$$

Now the problem of modeling turbulence has been transferred to computing the velocity scale and length scale. Many different models use many different methods to determine these scales, that will not be discussed here. The interested reader is once again referred to Wilcox's book [38].

2.4 Derivation of TKE Equation

We will now take a step forward to the derivation of the turbulent kinetic energy equation. $k-\epsilon$ turbulence models have become very popular. Knowledge of where the TKE equation comes from is essential for a good understanding of the $k-\epsilon$ model. The following derivation is largely from Wilcox's book [38].

For simplicity, the derivation will be performed for incompressible flow. The purpose of this section is to understand where the terms in the TKE equation come from. Deriving the equation using Favre averaging, while basically the same, would only add confusion. Reynolds averaging is the basis of turbulence modeling. The instantaneous quantity will be broken up into its mean and fluctuating components

$$x = X + x^{'} \tag{2.13}$$

where x is any quantity and X is the mean value and $x^{'}$ is the instantaneous value. An overbar will denote taking the Reynolds average. See section 2.2 or [83] for a discussion of Reynolds averaging. We will define the incompressible turbulent kinetic energy as

$$k = \frac{1}{2}\overline{u_i^{'}u_i^{'}} \tag{2.14}$$

The derivation starts with the instantaneous Navier-Stokes momentum equation.

$$\rho u_{i,t} + \rho u_k u_{i,k} + p_i - \mu u_{i,kk} = 0 \tag{2.15}$$

Multiply (2.15) by the fluctuating component of velocity, $u_i^{'}$

$$\overbrace{u_i^{'}\rho u_{i,t}}^{1} + \overbrace{u_i^{'}\rho u_k u_{i,k}}^{2} + \overbrace{u_i^{'}p_i}^{3} - \overbrace{u_i^{'}\mu u_{i,kk}}^{4} = 0 \tag{2.16}$$

Look at each individual term and take the Reynolds average.

Term 1

$$\begin{aligned}\overline{u_i^{'}\rho\left(U_{i,t} + u_{i,t}^{'}\right)} & \\ \overline{\rho u_i^{'}U_{i,t}} &+ \overline{\rho u_i^{'}u_{i,t}^{'}} \\ 0 &+ \overline{\rho\frac{\partial \frac{1}{2}u_i^{'}u_i^{'}}{\partial t}} \\ & \rho k_{,t}\end{aligned} \tag{2.17}$$

Term 2

$$\begin{aligned}
&\overline{\rho u_i^{'}\left(U_k+u_k^{'}\right)\left(U_{i,k}+u_{i,k}^{'}\right)}\\
&\underbrace{\overline{\rho u_i^{'}U_kU_{i,k}}}_{0}+\overline{\rho u_i^{'}U_ku_{i,k}^{'}}+\overline{\rho u_i^{'}u_k^{'}\left(U_{i,k}+u_{i,k}^{'}\right)}\\
&\rho U_k\overline{\left(\frac{1}{2}u_i^{'}u_i^{'}\right)_{,k}}+\overline{\rho u_i^{'}u_k^{'}}U_{i,k}+\overline{\rho u_k^{'}\left(\frac{1}{2}u_i^{'}u_i^{'}\right)_{,k}}\\
&\rho U_kk_{,k}-\tau_{i,k}^{T}U_{i,k}+\overline{\rho\left(u_k^{'}u_i^{'}u_i^{'}\frac{1}{2}\right)_{,k}}-\overline{\frac{1}{2}\rho u_i^{'}u_i^{'}\underbrace{u_{k,k}^{'}}_{0}}\\
&\rho U_kk_{,k}-\tau_{i,k}^{T}U_{i,k}+\overline{\rho\left(u_k^{'}u_i^{'}u_i^{'}\frac{1}{2}\right)_{,k}}
\end{aligned}\tag{2.18}$$

Term 3

$$\begin{aligned}
&\overline{u_i^{'}\left(P_{,i}+p^{'}{}_{,i}\right)}\\
&\underbrace{\overline{u_i^{'}P}}_{0}+\overline{p^{'}{}_{,i}\,u_i^{'}}\\
&\overline{p^{'}{}_{,i}\,u_i^{'}}
\end{aligned}\tag{2.19}$$

Term 4

$$\begin{aligned}
&\overline{\mu u_i^{'}\left(U_i+u_i^{'}\right)_{,kk}}\\
&\underbrace{\overline{\mu u_i^{'}U_{,kk}}}_{0}+\overline{\mu u_i^{'}u_{i,kk}^{'}}\\
&\overline{\mu\left(u_i^{'}u_{i,k}^{'}\right)_{,k}}-\overline{\mu u_{i,k}^{'}u_{i,k}^{'}}\\
&\overline{\mu\left(\frac{1}{2}u_i^{'}u_i^{'}\right)_{,kk}}-\mu\overline{u_{i,k}^{'}u_{i,k}^{'}}\\
&\mu k_{,kk}-\mu\overline{u_{i,k}^{'}u_{i,k}^{'}}
\end{aligned}\tag{2.20}$$

Combine all terms 1-4 and rearrange notation:

$$\overbrace{\rho\frac{\partial k}{\partial t}}^{\substack{\text{Unsteady}\\(\text{exact})}} + \overbrace{\rho u_j\frac{\partial k}{\partial x_j}}^{\substack{\text{Convection}\\(\text{exact})}} = \overbrace{\tau_{ij}^T\frac{\partial U_i}{\partial x_j}}^{\substack{\text{Production}\\(\tau_{ij}^T\ \text{modeled})}} - \overbrace{\rho\epsilon}^{\substack{\text{Dissipation}\\(\text{Modeled})}} + \frac{\partial}{\partial x_j}\Bigg[\overbrace{\mu\frac{\partial k}{\partial x_j}}^{\substack{\text{Molecular}\\\text{Diffusion}\\(\text{exact})}} - \overbrace{\overline{\frac{1}{2}\rho u_i' u_i' u_j'}}^{\substack{\text{Turbulent}\\\text{Transport}\\(\text{modeled})}} - \overbrace{\overline{p' u_j'}}^{\substack{\text{Pressure}\\\text{Diffusion}\\(\text{modeled})}}\Bigg] \tag{2.21}$$

Some terms have introduced even higher correlations. Thus, these terms must be modeled. We will start with the Dissipation term where ϵ has been defined:

$$\epsilon = \nu\overline{\frac{\partial u_i'}{\partial x_k}\frac{\partial u_i'}{\partial x_k}} \tag{2.22}$$

Different types of turbulence models deal with ϵ different ways. One equation models use an algebraic length scale with the turbulent kinetic energy. Two equation models use another equation to find ϵ.

In the production term, τ_{ij}^T is modeled with equation (2.11).

The turbulent transport and pressure diffusion terms are usually lumped together in a gradient-diffusion term.

$$\frac{1}{2}\rho\overline{u_i' u_i' u_j'} + \overline{p' u_j'} = \frac{\mu_T}{\sigma_k}\frac{\partial k}{\partial x_j} \tag{2.23}$$

where σ_k is simply a closure coefficient. Launder, Reece and Rodi [84] model these two terms differently. The pressure diffusion term is dropped and the turbulent transport term is modeled from a simplification of the exact turbulent transport equation which is a gradient diffusion term which has a tensor coefficient instead of a scalar one like above. These modeled terms are not included here because they are not used often.

The final modeled form of the incompressible turbulent kinetic energy equation is [38]:

$$\rho\frac{\partial k}{\partial t} + \rho U_j\frac{\partial k}{\partial x_j} = \tau_{ij}^T\frac{\partial U_i}{\partial x_j} - \rho\epsilon + \frac{\partial}{\partial x_j}\left[\left(\mu + \frac{\mu_T}{\sigma_k}\right)\frac{\partial k}{\partial x_j}\right] \tag{2.24}$$

For comparison, here is the final modeled form of the Favre averaged turbulent kinetic energy equation [38]:

$$\bar{\rho}\frac{\partial k}{\partial t} + \bar{\rho}\tilde{u}_j\frac{\partial k}{\partial x_j} = \tau_{ij}^T\frac{\partial \tilde{u}_i}{\partial x_j} - \rho\epsilon + \frac{\partial}{\partial x_j}\left[\left(\mu + \frac{\mu_T}{\sigma_k}\right)\frac{\partial k}{\partial x_j}\right] \tag{2.25}$$

The pressure work and pressure dilation terms have been neglected. The two equations are for all purposes identical, and that is the intention of Favre averaging.

2.5 Derivation of the ϵ equation

As was mentioned above, one of the terms in the turbulent kinetic energy equation(equation (2.24)) that must be modeled is the dissipation term, ϵ. Currently, a very popular method is to use another partial differential equation to find ϵ. The derivation of the ϵ equation provides a necessary insight into workings of the two equation $k-\epsilon$ model. It is important to note that for simplicity, incompressible flow will be assumed. Again, these derivations are being done to study turbulence. Using the Favre averaged form, while essentially identical except for notation, might confuse the turbulence issues.

The transport equation for the dissipation is found, similar to the derivation of the TKE equation, by manipulating the Navier-Stokes momentum equation.

$$\overline{2\nu\frac{\partial u_i'}{\partial x_j}\frac{\partial}{\partial x_j}\left[\text{Equation:2.8}\right]} = 0 \tag{2.26}$$

Multiplying out and switching to indicial notation gives:

$$\overbrace{\overline{2\nu u_{i,j}'\rho u_{i,tj}}}^{1} + \overbrace{\overline{2\nu u_{i,j}'\rho(u_k u_{i,k})_{,j}}}^{2} + \overbrace{\overline{2\nu u_{i,j}' p_{,ij}}}^{3} + \overbrace{\overline{2\nu u_{i,j}'\mu u_{i,kkj}}}^{4} = 0 \tag{2.27}$$

Look at each individual term

Term 1

$$\begin{aligned}
&\overline{2\nu u_{i,j}'\rho(U_i + u_i')_{,tj}} \\
&\overline{2\nu u_{i,j}'\rho u_{i,tj}'} \\
&\overline{\rho(\nu u_{i,j}' u_{i,j}')_t} \\
&\rho\epsilon_{,t}
\end{aligned} \tag{2.28}$$

Term 2

$$\overline{2\nu u'_{i,j}\rho\left[(U_k+u'_k)(U_i+u'_i)\right]}$$
$$\overbrace{\overline{2\nu u'_{i,j}\rho(u'_kU_{i,k})_{,j}}}^{2.1} \quad \overbrace{+\overline{2\nu u'_{i,j}\rho(U_ku'_{i,k})_{,j}}}^{2.2} \quad \overbrace{+\overline{2\nu u'_{i,j}\rho(u'_ku'_{i,k})_{,j}}}^{2.3} \tag{2.29}$$

Again, look at each individual term

Term 2.1

$$\overline{2\nu u'_{i,j}\rho(u'_kU_{i,k})_{,j}}$$
$$\overline{2\nu u'_{i,j}\rho u'_kU_{i,kj}}+\overline{2\nu u'_{i,j}\rho u'_{k,j}U_{i,k}} \tag{2.30}$$

Term 2.2

$$\overline{2\nu u'_{i,j}\rho(U_ku'_{i,k})_{,j}}$$
$$\overline{2\nu u'_{i,j}\rho U_{k,j}u'_{i,k}}+\overline{2\nu u'_{i,j}\rho U_ku'_{i,kj}}$$
$$\overline{2\nu u'_{i,j}\rho U_{k,j}u'_{i,k}}+\overline{\nu\rho U_k(u'_{i,j}u'_{i,j})_{,k}}$$
$$\overline{2\nu u'_{i,j}\rho U_{k,j}u'_{i,k}}+\rho U_k\epsilon_{,k} \tag{2.31}$$

Term 2.3

$$\overline{2\nu u'_{i,j}\rho(u'_ku'_{i,k})_{,j}}$$
$$\overline{2\nu u'_{i,j}\rho u'_{k,j}u'_{i,k}}+\overline{2\nu u'_{i,j}\rho u'_ku'_{i,kj}}$$
$$\overline{2\rho\nu u'_{i,j}u'_{k,j}u'_{i,k}}+\overline{\rho\nu u'_k(u'_{i,j}u'_{i,j}),,k}$$
$$\overline{2\rho\nu u'_{i,j}u'_{k,j}u'_{i,k}}+\overline{\mu(u'_ku'_{i,j}u'_{i,j})_{,k}} \tag{2.32}$$

Term 3

$$\overline{2\nu u'_{i,j}p_{,ij}}$$
$$\overline{2\nu u'_{i,j}(P+p')_{,ij}}$$
$$\overline{2\nu u'_{i,j}p'_{,ij}}$$
$$\overline{(2\nu u'_{i,j}p'_{,j})_{,i}} \tag{2.33}$$

Term 4

$$\begin{aligned} & \overline{2\nu u_{i,j}^{'} \mu u_{i,kkj}} \\ \overline{\nu\mu(u_{i,j}^{'}(u_{i,j}^{'})_{,kk}} & - \overline{2\nu\mu u_{i,jk}^{'} u_{i,jk}^{'}} \\ \mu\epsilon_{,kk} & - \overline{2\nu\mu u_{i,jk}^{'} u_{i,jk}^{'}} \end{aligned} \tag{2.34}$$

Recombine

$$\begin{aligned} & \overbrace{\rho\epsilon_{,t}}^{1} + \overbrace{\overline{2\nu u_{i,j}^{'} \rho u_k^{'} U_{i,kj}} + \overline{2\nu u_{i,j}^{'} \rho u_{k,j}^{'} U_{i,k}}}^{2.1} \\ & \overbrace{\overline{2\nu u_{i,j}^{'} \rho U_{k,j} u_{i,k}^{'}} + \rho U_k \epsilon_{,k}}^{2.2} \\ & \overbrace{\overline{2\rho\nu u_{i,j}^{'} u_{k,j}^{'} u_{i,k}^{'}} + \overline{\mu(u_k^{'} u_{i,j}^{'} u_{i,j}^{'})_{,k}}}^{2.3} \\ & \overbrace{\overline{(2\nu u_{i,j}^{'} p^{'}{}_{,j})_{,i}}}^{3} + \overbrace{\mu\epsilon_{,kk} - \overline{2\nu\mu u_{i,jk}^{'} u_{i,jk}^{'}}}^{4} = 0 \end{aligned} \tag{2.35}$$

Rearrange equation and switch some indices

$$\begin{aligned} \rho\frac{\partial\epsilon}{\partial t} + \rho U_j \frac{\partial\epsilon}{\partial x_j} = & -2\mu\left[\overline{u_{i,k}^{'} u_{j,k}^{'}} + \overline{u_{k,i}^{'} u_{k,j}^{'}}\right]\frac{\partial U_i}{\partial x_j} \\ & -2\mu\overline{u_k^{'} u_{i,j}^{'}}\frac{\partial^2 U_i}{\partial x_k \partial x_j} - 2\mu\overline{u_{i,k}^{'} u_{i,m}^{'} u_{k,m}^{'}} - 2\mu\nu\overline{u_{i,km}^{'} u_{i,km}^{'}} \\ & +\frac{\partial}{\partial x_j}\left[\mu\epsilon_{,j} - \mu\overline{u_j^{'} u_{i,m}^{'} u_{i,m}^{'}} - 2\nu p^{'}_{,m} u^{'}_{j,m}\right] \end{aligned} \tag{2.36}$$

This is the exact transport equation for the dissipation as found in [38]. It is very complicated. Drastic modeling of some of the terms, which will not be discussed here, results in the following standard incompressible, Reynolds averaged equation for ϵ from Wilcox's book [38].

$$\rho\frac{\partial\epsilon}{\partial t} + \rho U_j \frac{\partial\epsilon}{\partial x_j} = C_{\epsilon 1}\frac{\epsilon}{k}\tau_{ij}\frac{\partial U_i}{\partial x_j} - C_{\epsilon 2}\rho\frac{\epsilon^2}{k} + \frac{\partial}{\partial x_j}\left[(\mu + \mu/\sigma_e)\frac{\partial\epsilon}{\partial x_j}\right] \tag{2.37}$$

The two equations bear little resemblance.

The Favre averaged form of the dissipation equation is

$$\bar{\rho}\frac{\partial\epsilon}{\partial t} + \rho\tilde{u}_j \frac{\partial\epsilon}{\partial x_j} = C_{\epsilon 1}\frac{\epsilon}{k}\tau_{ij}\frac{\partial\tilde{u}_i}{\partial x_j} - C_{\epsilon 2}\bar{\rho}\frac{\epsilon^2}{k} + \frac{\partial}{\partial x_j}\left[(\mu + \mu/\sigma_e)\frac{\partial\epsilon}{\partial x_j}\right] \tag{2.38}$$

Chapter 3

Transition Region Models

3.1 Introduction to Transition Region Modeling

Six transition region models were chosen from the literature to be implemented and tested. Before these models are discussed, the goal and purpose of transition region modeling must be defined. This dissertation defines the goal of transition region modeling to be:

> Assuming the starting location of transition will be given or will be found with another method, model the effect of the transition region on such quantities as skin friction and heat transfer.

This stated goal must be analyzed to understand what is trying to be done. The first part states that the transition region model will not be used to find the location of transition. Predicting the location of transition is a complicated problem which is dependent on quantities such as the frequency of the disturbances which are not going to be computed in a Reynolds averaged Navier-Stokes code. Most of the transition region models found in the literature had to be given the location of transition. The models that were designed to predict the location of transition were found to be grossly inaccurate. For these reasons, it was determined that the burden of locating transition would be lifted from these models so that their ability to model the effect of the transition region on skin friction and heat transfer could be better studied,

which is the second part of the stated goal. A typical transition profile was shown in figure 1.1. The purpose of the transition region model is to make the computed skin friction or heat transfer display the smooth curve between the laminar value and the fully turbulent value with the peak near the end of transition.

Section 1.2 gave a brief description of the physics of the transition region. As was stated above, the purpose of transition region modeling is to simulate the effect that transition has on the flow. Ideally, the models should include as much as the physics of the flow as possible for accuracy. However, that is difficult due to the Favre averaged or Reynolds averaged codes used. The transition region is an unsteady phenomena where spots form and coalesce downstream to form the turbulent flow. A given location in the transition region will appear to be turbulent for a fraction of the time and laminar for the other part. The percentage of time that the flow is turbulent at a given location is defined to be the intermittency which starts at 0 at the beginning of the transition region and ideally smoothly reaches a value of 1 at the turbulent region. The Favre and Reynolds averaged equations cannot account for the small time scale by definition. So the actual flow field cannot be described. Attempts at modeling the physics of the problem must be done in the time averaged domain of the Favre or Reynolds averaged equation which includes such definitions as the intermittency and turbulent kinetic energy. It can be argued that the physics of transition cannot be modeled in the time averaged domain. Because of this, transition region models are very empirical, similar to turbulence models.

The transition region models found in the literature can be broadly classified as one of two methods. The first method is to use a turbulence model or changes to a turbulence model that can simulate the effect of the transition region, i.e. the transition region is simulated by directly changing how the eddy viscosity is computed. The second method is to use a pure transition region model that is independent of the origin of eddy viscosity, i.e. as far as the model is concerned, the eddy viscosity comes from a black box. Four of the transition region models presented, the Baldwin-Lomax algebraic model, Wilcox $k - \omega$ model, Schmidt-Patankar production term modifications, and Warren-Harris-Hassan one equation model, are turbulence models or modifications for turbulence models that mimic the transition region. Two of the

models, algebraic and linear combination, are transition region models that can be used with theoretically any turbulence model.

All six models will now be presented now in a logical order of three pairs. The Baldwin-Lomax followed by the Wilcox $k-\omega$ model will be presented first. These are turbulence models that have minor modifications to account for the transition region, Next will be the Schmidt and Patankar Production Term Modification(PTM) model and the Warren, Harris and Hassan model. These are turbulence models with more severe modifications for the transition region. Last will be the algebraic transition model and the linear combination transition region model. They are pure transition region models which are theoretically independent of the origin of the eddy viscosity. This logical ordering will be followed in subsequent chapters also.

3.2 Baldwin-Lomax Turbulence Model

The well known Baldwin-Lomax turbulence model can be used to simulate the transition region. The Baldwin-Lomax and the Wilcox $k-\omega$ turbulence models both make the Bousinessq assumption of an eddy viscosity which results in an effective viscosity.

$$\mu_{eff} = \mu_{mol} + \mu_t \tag{3.1}$$

The Baldwin-Lomax[24] turbulence model is called an algebraic turbulence model because no differential equations are used to determine the eddy viscosity. Instead, the model uses a two layer approach where

$$\mu_t = \begin{cases} (\mu_t)_{inner} & y \leq y_c \\ (\mu_t)_{outer} & y_c < y \end{cases} \tag{3.2}$$

and y_c is the minimum value of y where the two eddy viscosities are equal.

The inner viscosity is defined by

$$(\mu_t)_{inner} = \rho l^2 |\omega| \tag{3.3}$$

where $|\omega|$ is the magnitude of the vorticity and

$$l = \kappa y[1 - \exp(-y^+/A^+)] \tag{3.4}$$

The viscosity in the outer region is defined by

$$(\mu_t)_{outer} = \rho K C_{cp} F_{wake} F_{kleb}(y) \tag{3.5}$$

and

$$F_{wake} = min \left\{ \begin{array}{c} y_{max} F_{max} \\ C_{wk} y_{max} U_{diff}^2 / F_{max} \end{array} \right\} \tag{3.6}$$

where U_{diff} is the difference between the maximum and minimum total velocity for the given profile.

The function

$$F(y) = y|\omega|[1 - \exp(-y^+/A^+)] \tag{3.7}$$

is used to determine F_{max} and y_{max}. F_{max} is the maximum value of $F(y)$ which occurs at the y value of y_{max}. The last term in the equation for the outer viscosity is the Klebanoff intermittency function:

$$F_{kleb}(y) = \left[1 + 5.5 \left(\frac{C_{kleb} y}{y_{max}} \right)^6 \right]^{-1} \tag{3.8}$$

This is a popular model because it does not require finding the edge of the boundary layer, δ_t .

Baldwin and Lomax predict transition by setting the eddy viscosity to zero at a given station if the maximum eddy viscosity in a profile is not above a certain tolerance. Their relation for transition is

$$\mu_t = 0 \quad if \ (\mu_t)_{max \ in \ profile} < C_{mutm} \ \mu_\infty \tag{3.9}$$

where C_{mutm} is 14 and μ_∞ is the free stream viscosity. For the cases here, it was found that this value did not predict transition in the correct location. Also, this work stipulates that the transition location will be found independently of the transition model so this criteria for transition is unnecessary. Instead the eddy viscosity was set to zero for all profiles ahead of the given location of transition. This turns out to be a very simple transition region model. It is basically just an on/off switch. The turbulence model is turned off for the laminar region and then is just turned on for the transition and turbulent regions. Despite the simplicity, the results from this model have some satisfactory points.

3.3 Wilcox $k-\omega$ Turbulence Model

Low-Reynolds number two equation turbulence models, including the Wilcox low Reynolds number $k-\omega$ model, can be used to simulate the transition region. An initially low TKE results in laminar flow at the beginning of the domain. Downstream, a point will be reached where the production exceeds the destruction in the TKE equation. The TKE begins to grow until a balance in the TKE equation is reached between production and destruction resulting in fully turbulent flow.

The Wilcox[38] $k-\omega$ turbulence model uses two partial differential equations to determine k and ω which are used to determine μ_t from:

$$\mu_t = \alpha^* \frac{\rho\ k}{\omega} \tag{3.10}$$

$$\begin{aligned} \frac{\partial}{\partial t}(\rho k) + \frac{\partial}{\partial x_j}(\rho u_j k) &= \tau_{ij}^T \frac{\partial u_i}{\partial x_j} - \beta^* \rho \omega k \\ &+ \frac{\partial}{\partial x_j}\left[(\mu + \sigma^* \mu_t)\frac{\partial k}{\partial x_j}\right] \end{aligned} \tag{3.11}$$

$$\begin{aligned} \frac{\partial}{\partial t}(\rho \omega) + \frac{\partial}{\partial x_j}(\rho u_j \omega) &= \alpha \frac{\omega}{k} \tau_{ij}^T \frac{\partial u_i}{\partial x_j} - \beta \rho \omega^2 \\ &+ \frac{\partial}{\partial x_j}\left[(\mu + \sigma \mu_t)\frac{\partial \omega}{\partial x_j}\right] \end{aligned} \tag{3.12}$$

To improve on the near wall behavior of the model and to help model the transition region, Wilcox developed damping terms for these three equations by making α^*, α and β^* functions of the turbulent Reynolds number Re_T

$$\alpha^* = \frac{\alpha_0^* + \frac{Re_T}{R_k}}{1 + \frac{Re_T}{R_k}} \tag{3.13}$$

$$\alpha = \frac{1}{2}\frac{\alpha_0 + \frac{Re_T}{R_\omega}}{1 + \frac{Re_T}{R_\omega}}(\alpha^*)^{-1} \tag{3.14}$$

$$\beta^* = \frac{9}{100}\frac{5/18 + \left(\frac{Re_T}{R_\beta}\right)^4}{1 + \left(\frac{Re_T}{R_\beta}\right)^4} \tag{3.15}$$

where

$$Re_T = \frac{\rho\ k}{\omega\mu} \tag{3.16}$$

The constants α_0^* and α_0 were originally chosen to predict correct transition for the Blasius boundary layer. In order to correctly predict transition for other flows, these constants would have to be recalibrated, which is an unrealistic requirement on the model. It is also unnecessary for the calculations performed here since the transition point is given.

Wilcox [39] uses the roughness boundary condition on ω to make a roughness strip to trip the boundary layer at a desired location. The roughness boundary condition on the wall for ω is given by

$$\omega = \frac{u_\tau^2}{\nu} S_R \tag{3.17}$$

where S_R is defined by

$$S_R = \begin{cases} \left(\frac{50}{k_R^+}\right)^2, & k_R^+ < 25 \\ \\ \frac{100}{k_R^+}, & k_R^+ \geq 25 \end{cases} \tag{3.18}$$

$k_R^+ = 1$ is used for hydraulically smooth walls. Wilcox states that increasing the surface roughness height will lower ω which in turn lowers the dissipation or destruction of k in the boundary layer. Placing a roughness strip in the flow will tend to destabilize it and start transition which is analogous to the use of roughness strips in wind tunnel tests. The boundary layer is tripped using the roughness strip. The question then is how long is the roughness strip, Δs, and what surface roughness height, k_R, should be used? Wilcox presents the following relationships:

$$\frac{k_R}{\delta_t} = \max\left\{\frac{5000}{\sqrt{Re_{s_t}}}, 3\right\} \tag{3.19}$$

$$\frac{\Delta s}{\delta_t} = 0.015\sqrt{Re_{s_t}} \tag{3.20}$$

Wilcox states that the values for k_R and Δs from these equations form an upper bound for the cases he considered and that lower values can be used. For some of the cases presented in this work, the suggested values did not work and larger values had to be used.

Wilcox[38] states that the near-wall solution for ω is given by

$$\omega = \frac{\omega_w}{\left(1 + \sqrt{\frac{\omega_w \beta^*}{2\nu_w}}\, y\right)^2}, \qquad y^+ < 2.5 \tag{3.21}$$

For a smooth wall, the near wall solution produced by the model is correct. But when the value of ω is lowered for the roughness strip, this no longer holds. In fact, the value of ω goes up from the wall which can hamper the designed effect of the roughness strip. The above equation was implemented in the code so that the near-wall behavior of ω could be controlled. Specifying ω was not done for all cases, its use was investigated for some cases that could not be made to transition using just the roughness strip.

3.4 Schmidt and Patankar PTM Model

Low Reynolds number two equation turbulence models, like the very popular $k - \epsilon$ models, seem to have their own built in transition simulation. The right choice of initial conditions starts the domain with a low turbulent kinetic energy which produces laminar flow. As the solution marches downstream, the turbulent kinetic energy begins to grow and the production exceeds the destruction in the k equation. Transition has started. Eventually destruction equals production in the k equation and the flow is fully turbulent, [38]. The problem with using these methods is that transition is predicted too early and the transition length is too short.

Schmidt and Patankar [34] have developed modifications for low Reynolds number $k - \epsilon$ models that overcome the standard model's inherent problems with modeling the transition region mentioned above. These modifications have been developed for the Lam and Bremhorst [35] $k - \epsilon$ model, but they can theoretically be used with any low Reynolds number $k - \epsilon$ model. Their approach consists of a production term modification(PTM) for the TKE equation. At the beginning of the domain, the production term in the k equation is set to zero. With no production term and a destruction term that is still intact, k is forced to zero in the boundary layer which results in laminar flow. In the next part of the domain, the production of k is limited

by the following formula:

$$\frac{dP_{k_{max}}}{dt} = A * P_k + B \tag{3.22}$$

where P_k is the production term in the k equation. Schmidt and Patankar calibrate the empirical functions A and B using the work of Abu-Ghannam and Shaw [1], which present empirical functions for the start and ending points of transition correlated with the free stream turbulent kinetic energy for incompressible flow. The resulting values for A and B are shown in figure 3.1 in non-dimensional form which is

$$A_0 = \frac{A\mu_e}{\rho_e U_e^2} \tag{3.23}$$

$$B_0 = \frac{B\mu_e}{\rho_e^3 U_e^6} \tag{3.24}$$

The form of equation (3.24) for B is different than the one presented in [34] which appears to have an error in the power of ρ_e based on dimensional analysis. Stephens and Crawford [9] non-dimensionalize B the same as equation (3.24).

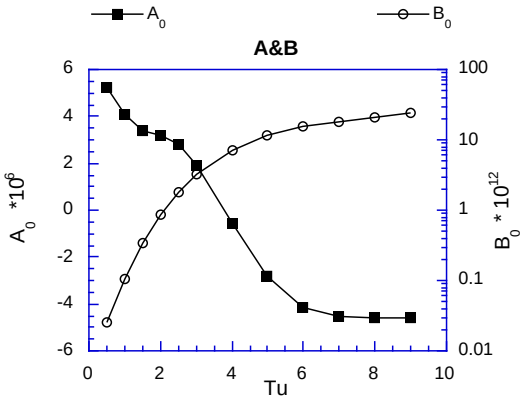

Figure 3.1: Non-Dimensional A and B versus free-stream turbulence intensity

Schmidt and Patankar [34] specify that the model should be initiated at a critical Reynolds number based on momentum thickness, Re_θ, of 125 which enables the model to predict the start and length of transition in accordance to the Abu-Ghannam and Shaw relations without sensitivity to the starting profiles of k and ϵ. Several problems emerge. This starting criterion and the Abu-Ghannam and Shaw relations used for calibration are for incompressible flow so they are not accurate for the high speed cases

presented in this work. Also, this work assumes that the starting point of transition is given or will be found using another method. So the problem emerges of how to make the model "predict" transition where we want it to. All the cases featured in this work are supersonic which means that the governing Navier-Stokes equations become parabolic and can be space marched. Space marching entails iterating solely on the first plane of the domain until it is converged and then moving onto the next plane downstream, converging it and moving on to the next plane. The whole domain is solved then by marching down it. When the Schmidt and Patankar model is space marched, a trial and error method must be used to force transition to occur in the desired location. Initial conditions are chosen and the solution is marched downstream. The location that the model predicts transition is noted and the initial conditions are changed in an effort to force the model's transition point closer to the desired transition point.

In terms of implementing the model, Schmidt and Patankar present a pseudo-Fortran implementation of equation (3.22) which helps clear up how the model works. The time derivative is discretized into a spatial derivative using the local velocity

$$\begin{aligned} \frac{dx}{dt} &= U_j \\ \rightarrow dt &= \frac{dx}{U_j} \end{aligned} \tag{3.25}$$

where U is the local stream velocity and j is the coordinate direction normal to the flow. The governing equation becomes

$$P_{k,max,i+1,j} - P_{k,i,j} = \left(A * P_{k,i,j} + B\right) \frac{dx}{U_j} \tag{3.26}$$

where i is the stream wise coordinate. This ultimately leads to the relationship

$$P_{k,i+1,j} = \min \left[P_{k,max,i+1,j} \quad , \quad P_{k,i+1,j} \right] \tag{3.27}$$

where $P_{k,i+1,j}$ on the right hand side is the production of k computed from the original governing equation and $P_{k,i+1,j}$ on the left hand side is the value used for the production term in the k equation.

Schmidt and Patankar also make a small change to the Lam and Bremhorst model to make it more accurate for transitional flows with low free stream turbulent kinetic

energy. f_μ from Lam and Bremhorst [35] is

$$f_{\mu,LB} = \left(1 - e^{-0.0165R_y}\right)^2 (1 + 20.5/Re_t) \tag{3.28}$$

Schmidt and Patankar limit the value of this function for low turbulent Reynolds number

$$f_\mu = \min\left[f_{\mu,LB}, 1.0, 0.5 + 0.0025Re_t\right] \tag{3.29}$$

Schmidt and Patankar maintain this will only affect transitional calculations, not the fully turbulent calculations.

3.5 Warren, Harris, and Hassan Transition Region Model

Transition from laminar to turbulent flow is initiated and dominated by first and second mode instabilities. Most transition modelers ignore the effect of these modes on the mean flow. Warren, Harris, and Hassan [3] account for this effect by writing the transitional stress as a function of turbulent and non-turbulent contributions using the intermittency:

$$\overline{(u_i' u_j')_r} = \Gamma\overline{(u_i' u_j')_t} + (1 - \Gamma)\overline{(u_i' u_j')_l} \tag{3.30}$$

where the "laminar" contribution, $\overline{(u_i' u_j')_l}$, is due to the aforementioned first and second mode disturbances. The turbulent contribution is simply the Reynolds stress and it is found using a one-equation turbulence model first presented in Micheltree, Salas and Hassan [52]. The one equation used is the turbulent kinetic energy originally from Launder, Reece and Rodi that has been converted to a Favre averaged compressible form.

$$\frac{\partial}{\partial t}(\bar{\rho}k) + \frac{\partial}{\partial x_j}(\bar{\rho}\tilde{u}_j k) = \tau_{ij}^T \frac{\partial \tilde{u}_i}{\partial x_j} - \bar{\rho}\epsilon + \frac{\partial}{\partial x_j}\left[\nu\frac{\partial \bar{\rho}k}{\partial x_j} - C_k \frac{k}{\bar{\rho}\epsilon}\tau_{ij}^T \frac{\partial \bar{\rho}k}{\partial x_i}\right] \tag{3.31}$$

A major difference between this turbulent kinetic energy equation and the more common form from Wilcox's book [38]

$$\frac{\partial}{\partial t}(\bar{\rho}k) + \frac{\partial}{\partial x_j}(\bar{\rho}\tilde{u}_j k) = \tau_{ij}^T \frac{\partial \tilde{u}_i}{\partial x_j} - \bar{\rho}\epsilon + \frac{\partial}{\partial x_j}\left[\left(\mu + \frac{\mu_T}{\sigma_k}\right)\frac{\partial k}{\partial x_j}\right] \tag{3.32}$$

is the modeling of the turbulent transport and pressure diffusion which appears as the last terms in each equation. Launder neglects the pressure diffusion and models the turbulent transport diffusion using a gradient-driven diffusion term with a tensor diffusion coefficient. The more common approach is to model the turbulent transport using a gradient-diffusion with a scalar coefficient and to lump in the pressure diffusion with the turbulent transport through the constant σ_k. Theoretically, both approaches are modeling the same term, so their modeled terms should be about the same. Considering the popularity of the scalar coefficient approach, the more common form of the turbulent kinetic energy equation (3.32) was used instead of the Launder version (3.31).

Because this is a one equation turbulence model, algebraic length scales must be defined for the dissipation and the eddy viscosity

$$\epsilon = \frac{k^{3/2}}{l_\epsilon} \tag{3.33}$$

$$\mu_t = \rho C_\mu \sqrt{k} l_\mu \tag{3.34}$$

The form for the length scales originates from Chen and Patel [85]

$$l_\mu^t = (0.3)^{-3/2} \kappa y \left[1 - \exp\left(\frac{\sqrt{k} y}{70.0 \sqrt{\frac{T_w}{T_{aw}}} \nu} \right) \right] \tag{3.35}$$

$$l_\epsilon = \kappa C_\mu^{-3/4} y \left[1 - \exp\left(\frac{-Re\sqrt{k} y}{2\kappa C_\mu^{-3/4}} \right) \right] \tag{3.36}$$

The $\frac{T_w}{T_{aw}}$ is a compressibility correction for high speed flows with cooled walls. Both length scales are limited to a maximum value of y_{max} which is the y value where the Baldwin and Lomax function

$$F(y) = |\omega| y \tag{3.37}$$

is a maximum.

Focusing back on transition, computation of the transitional stress, equation (3.30), is implemented by combining different length scales for the eddy viscosity

$$l_\mu = (1 - \Gamma)[l_{TS} + l_{SM}] + \Gamma l_\mu^t \tag{3.38}$$

where l_μ is the length scale for the eddy viscosity (3.34), l_μ^t is the turbulent length scale(3.35) and l_{TS}, l_{SM} are the length scale contributions from the first and second mode disturbances, to be defined in equations (3.41),(3.42). The intermittency, Γ, is from Dhawan and Narasimha[30], which is defined in this chapter for use in the linear combination transition region model, section 3.7.

The first mode disturbance is commonly known as the Tollmein-Schlichting waves. They are dominant for Mach numbers less than about four[3]. Walker [86] presents a correlation for the frequency, ω, of the first mode disturbance

$$\frac{\omega\nu}{U_e^2} = 3.2 Re_{\delta^*}^{-3/2}. \tag{3.39}$$

The problem is this formula is valid for only incompressible flow. Warren*et al.*[3] overcomes this by using the fact that a compressible flow can be computed using incompressible formulas at some reference temperature [87]. Using a formula for the reference temperature from [88],

$$\frac{T^*}{T_e} = 1 + 0.032 M_e^2 + 0.58\left(\frac{T_w}{T_e} - 1\right) \tag{3.40}$$

the length scale for the first mode disturbances becomes

$$l_{TS} = .05 \frac{\sqrt{k}\ \nu^*}{3.2 U_e^2 {Re_{\delta^*}^*}^{-3/2}} \tag{3.41}$$

where all $*$ed quantities are evaluated at the reference temperature.

The second mode disturbances dominate the transition process for Mach numbers greater than four [3]. The length scale for the second mode disturbances is

$$l_{SM} = \left(\frac{0.23}{0.94 U_e}\right) M_e^2 \sqrt{\frac{kx}{Re}} \tag{3.42}$$

The paper makes it unclear as to when these first and second mode disturbances should be turned on. Since these are transitional effects, one may argue that they should be turned on at the transition point. In reality, because of their small effect (which will be discussed later) it did not really matter where they were turned on.

3.6 Algebraic Transition Region Model

The algebraic transition region model was developed at ONERA/CERT and is described in Arnal[89, 10]. The form of the model presented is from Singer *et al.*[4, 5]. The algebraic transition region model simulates transition by multiplying the eddy viscosity produced by any given turbulence model by a transition function before it is added to the molecular viscosity to form the effective viscosity

$$\mu_{eff} = \mu_{mol} + \epsilon_t \mu_t \tag{3.43}$$

The transition function ϵ_t effectively proportions the amount of eddy viscosity that is added to produce the smooth transition region profile. Note that the transition function ϵ_t is not the intermittency of the flow. Instead, it is defined by the fact that the momentum thickness grows significantly during transition. It is governed by the parameter

$$\chi_1 = \frac{\frac{\theta}{\theta_{t0}} - 1 + 0.005M_e^2}{1 + 0.02M_e^2} \tag{3.44}$$

Once χ_1 is determined, the transition function is computed from the following empirical relations:

For $0 < \chi_1 \leq 0.25$,

$$\epsilon_t = 1 - \exp\left\{-4.5\left[\chi_1\left(1 + 0.02M_e^2\right) - 0.005M_e^2\right]^2\right\}$$

For $0.25 < \chi_1 \leq 0.75$,

$$\epsilon_t = 18.628\chi_1^4 - 55.388\chi_1^3 + 52.369\chi_1^2 - 16.501\chi_1 + 1.893$$

For $0.75 < \chi_1 \leq 3$,

$$\epsilon_t = 1.25 - 0.25\sin\left[\pi\left(0.444\chi_1 - 0.833\right)\right]$$

For $\chi_1 > 3$,

$$\epsilon_t = 1 \tag{3.45}$$

Looking more closely at the parameter χ_1 (equation 3.44), it is seen to be a function of the growth of the momentum thickness with the term $\frac{\theta}{\theta_{t0}}$. The Mach

number terms are present for compressibility effects. Figure 3.2 shows a plot of the transition function ignoring the compressibility effects. It was mentioned previously that the transition function is not the intermittency. That can be clearly seen by the fact that ϵ_t reaches values above unity while the intermittency is bounded between zero and unity. This overshoot of unity is done in an attempt to model the peak above the nominal turbulent value in skin friction and heat transfer at the end of transition.

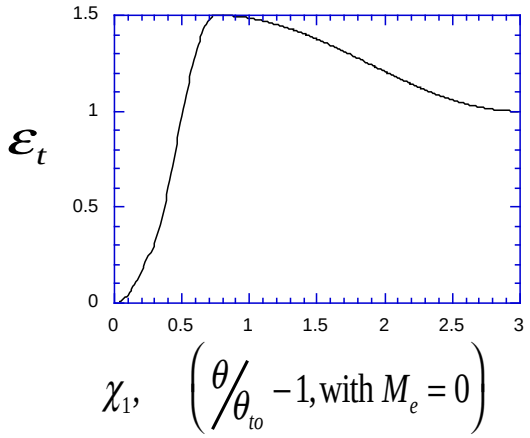

Figure 3.2: Algebraic Model Transition function ignoring compressibility effects

Theoretically, any turbulence model can be used to compute the eddy viscosity for this transition region model, but in reality this was not true. The transition region model at times performed poorly when a two equation $k-\epsilon$ model was used, this will be discussed further in the Summary chapter, section 5.6. Therefore, the Baldwin and Lomax algebraic turbulence model was used to compute the eddy viscosity for the cases featured later in this paper.

3.7 Linear Combination Transition Region Model

The idea behind the model of Dey and Narasimha[31] described in Singer *et al.* [4, 5] is that transitional flow can be represented by the linear combination of laminar and

turbulent flow fields through the intermittency

$$\vec{V}_{trans} = (1-\gamma)\ \vec{V}_{lam} + \gamma \vec{V}_{turb} \tag{3.46}$$

where $\vec{V}$ is a vector representing the respective flow field and γ is the intermittency which is defined to be the percentage of time that the flow is turbulent at a given station. γ is found by

$$\gamma = 1 - \exp\left[-0.411\left(\frac{x - x_{t0}}{\lambda}\right)^2\right] \tag{3.47}$$

x_{t0} is the starting location of transition that will either be given or found with another method as discussed in the introduction. λ is defined to be the stream-wise distance between the points where $\gamma = 0.25$ and $\gamma = 0.75$. This distance is obtained by

$$\lambda = \left[0.411\frac{Re_\theta^3(x_{t2})}{N_2}\right]^{\frac{1}{2}} \frac{\nu}{U_e(x_{t2})} \tag{3.48}$$

x_{t2} is the location of the subtransition which is used to model the effect of pressure gradients on the intermittency profile (See Dey and Narasimha [31] for more details). Unfortunately, no relation is given for finding x_{t2}, so it is just set equal to x_{t0}. N_2 is determined from

$$N_2 = \begin{cases} N_o(M,q) + 0.24L_{t2}^2 & (L_{t2} > 0) \\ N_o(M,q) - 323.0L_{t2}^3 & (L_{t2} < 0) \end{cases} \tag{3.49}$$

where L_{t2} incorporates the effects of pressure gradients and is defined by

$$L_{t2} = \frac{dU_e}{dx}\frac{\theta_{lam}^2}{\nu} \tag{3.50}$$

For incompressible flows $N_o = 0.7 \times 10^{-3}$. The compressible effect on N_o is shown in a graph in Narasimha[12] which shows a tentative relationship between N_o and Mach number where N_o dips down after a Mach number 4 to a value of $N_o = 0.2\times10^{-3}$. This will be discussed more in later sections. For flows where the free-stream turbulence level is very low ($q < 0.2\%$), N_o takes on a new value

$$N_o = -1.453 \times 10^{-3}\log(q) - 1.61 \times 10^{-3} \quad (q < 0.2\%) \tag{3.51}$$

It should be noted that the turbulent flow field used for this model has a boundary layer that originates at x_{t0}.

Implementation of the model consisted of a program separate from GASP that uses the restart file from a fully laminar flow and a restart file from a turbulent flow. It was noted above that boundary layer for the turbulent flow field begins at the starting point of transition. In order to produce a turbulent flow field with the boundary layer starting at the transition point, the tangency boundary condition is used from the beginning of the domain up to the transition point and then the no-slip boundary condition is used until the end of the domain. The tangency boundary condition forces the flow to be parallel to the body but does not limit the velocity, so no boundary layer is generated. A third restart file is generated from the laminar and turbulent restart files that contains the the transition region solution.

The implementation and basic theory of this model is often misinterpreted. Many people working on transition, such as Abid [90], have implemented this model as an algebraic transition region model in that the intermittency is used to proportion the amount of eddy viscosity added. What this implies is that linearly combining two flows is the same as linearly combining the viscosity, which may seem like an innocent assumption but this does lead to different answers. Dinavahi [66] uses Narasimha's intermittency for an algebraic transition region model, but emphasizes the fact that the method is not a linear combination model. Computations will be presented using the intermittency of the linear combination model as an algebraic transition region model for two reasons. First, the two methods are not the same and that will be proven through the results. Second, this must be evaluated as a transition region model because so many people are using it.

3.8 Summary

In summary, the six models that have been implemented into the GASP code and compared to experiment are listed in table 3.1 with brief descriptions of the models. It is important to note that the first four models listed are turbulence models or modifications of turbulence models that mimic the transition region. The last two models listed are pure transition region models and are theoretically independent of the origin of the eddy viscosity.

Table 3.1: Summary of Transition Region Models

Name	Description
Baldwin and Lomax	Algebraic Turbulence Model
Wilcox $k-\omega$	Two Equation Turbulence Model
Warren, Harris and Hassan	One Equation turbulence model with Intermittency applied to Length Scale
Schmidt and Patankar PTM	Modification for two-equation turbulence model
Algebraic Transition	Proportions amount of Eddy Viscosity added to Molecular viscosity
Linear Combination Transition	Combines Laminar and Turbulent Flow field using Intermittency

Chapter 4

Results

4.1 Introduction

With all six models implemented, it is time to check them using some experimental results to validate the models. The literature search from section 1.3 has revealed several experimental transitional test cases. However, since GASP Version 2 [14] is a compressible Navier-Stokes code with a practical lower limit in Mach number of 0.1, many of the test cases found could not be used ([18, 91, 78]) because they were below this Mach number limit. The paucity of experimental results for transitional flow cases for high speed flow quickly became very evident. Still, several cases were found and will be presented now.

The starting point of each model will be chosen in order to optimize the accuracy of the computed solution with the experimental solution. The experimental data can best be used to judge the transition region models when the both the transition region model and the experiment start transition in the same region. It would be difficult to judge the accuracy of the model if it starts to transition at a location away from the experimental transition region. Optimizing the starting location of the model consists of triggering the model at several points in the domain and comparing these solutions with the experimental solution. The profile that best fits the data is then picked. For models that tend to predict an almost instantaneous solution, they are often started in the middle of the experimental transition region to cut through the

middle of the experimental profile to minimize the error. It can be difficult to force transition to occur in a desired location for some of the models and in this case, when a run finally results in the transition point occurring anywhere in the experimental transition region it will be chosen. It is a goal of this work to find the relationship between where the model is started and where the profile begins. Some models will have a lag between the starting point of the model and the point where transition begins. Given the knowledge gained from this chapter, recommendations will be made of where the model should be started for cases where experimental data is unavailable and there is not the luxury of picking the best solution.

All experimental data is subjected to some uncertainty and some scatter, the following cases are no exception. It is acknowledged that in some cases the resulting predicted heat transfer might not appear satisfactory, but might be within any experimental error bands.

For each of the three test cases, the results are featured on separate graphs. It was originally desired to show all six models on the same graph. However, the resulting graph was too clustered and it was too difficult to evaluate the individual models. For that reason, it was determined to put each individual solution on a different graph.

The transition region model's heat transfer results will be judged against the experimental data under several criteria. One of them is the length of the transition region. The transition length will be measured as the distance between the local maximum and minimum in heat transfer, though Narasimha [12] shows that the transition region extends slightly in front and beyond these boundaries. Another criteria is the peak in heat transfer that occurs near the end of the transition region. These two criterias will be quantified as the ratio of the model's result to the experimental data. Due to the scatter in the experimental data, the experimental transition length and peak in heat transfer are subject to high uncertainty. The last criteria, which cannot be quantified, is the shape of the profile. The transition region model should produce a smooth curve in the heat transfer.

4.2 Stainback, Fischer, and Wagner

Stainback, Fischer, and Wagner [67] examine the effect of wind tunnel disturbances on the starting point and length of the transition region. Most of the graphs presented show pressure fluctuations and transitional Reynolds numbers, but two of the graphs, figures 3 and 13 in [67], show typical transition region heat transfer results on a supersonic cone. While the purpose of this paper was not to present heat transfer results in the transition region, these two graphs show crisp and distinct profiles with a generous amount of experimental data points so they will be used for a comparison. The two graphs agree well with each other in the laminar region and at the beginning of transition, but they differ greatly at the end of transition and for the turbulent region. While this is disturbing, it illustrates the uncertainty involved with all experimental data. The test case is a supersonic cone, the free stream conditions are shown in table 4.1.

Table 4.1: Test Conditions for Stainback case

Test Gas	Air
Mach Number	6
Cone Half Angle	10°
$T_\circ$	500 K
Wall Temperature	300 K

The transition length is estimated as the distance between the local minimum and maximum in heat transfer. Looking at the experimental data shows a transition length of roughly 10cm for this case which is 20% of the total domain. The transition length predicted by the models will also be computed from the local minimum to maximum in heat transfer. The transition length computed by the model will be divided by the experimental length to normalize it. Likewise, the peak value computed by the models will be normalized by the peak value from the experiment. The peak of heat transfer from the experiment is taken as the average of the peak of the two data runs which turns out to be $Ch = 1.55 \times 10^{-3}$. Both the normalized length and peak are highly subject to error.

Ideally, since this problem is an axisymmetric cone, the grid used should be itself

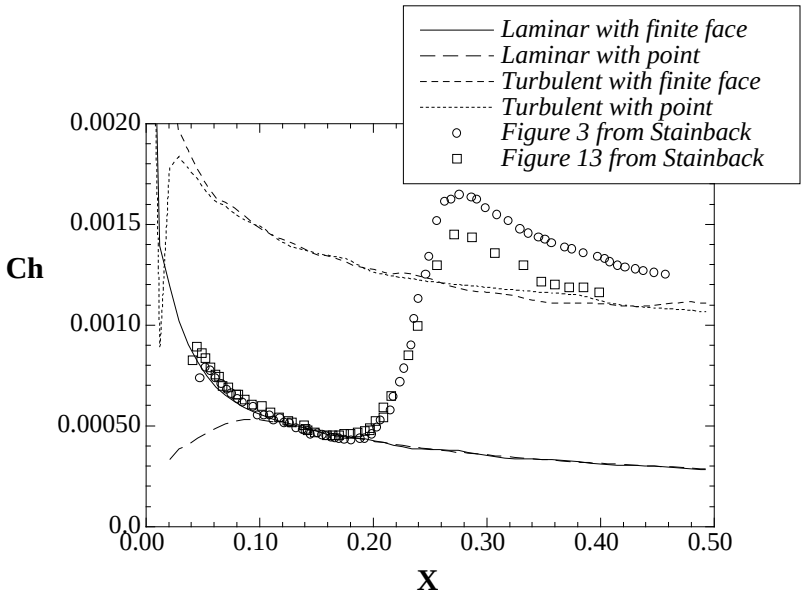

Figure 4.1: Grid Comparison on Stainback Cone

a cone, starting from a single point at the beginning of the domain so that the grid lines will form rays that will have constant properties. However, because this is a viscous problem, a finite face is needed at the beginning of the domain in order to set up the viscous effects at the beginning of the domain. Figure 4.1 shows the solution as computed by two different grids, one starting from a point and the other from a finite face. The grid starting from a point does not adequately predict the heat transfer at the beginning of the domain, so it was determined that a grid with a finite face must be used.

Figure 4.2 shows the 61x61 grid used for the Stainback case with the axisymmetric boundary conditions available in GASP. The first grid point off of the wall is at $y^+ \approx 0.1$. The grid is generated by a modification to the GASP flat plate grid generator program. The back face is generated using the flat plate relations and grid stretching, the grid is then built back to front going down to a single point that extends beyond the beginning of the grid which is then chopped off to form the finite face. The grid is then rotated back at the desired cone half angle. The two dimensional grid is converted to an axisymmetric slice by rotating it out of plane by $\pm\frac{\pi}{80}$.

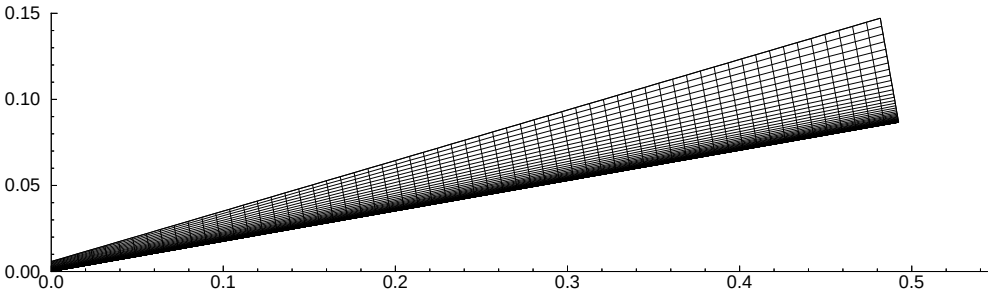

Figure 4.2: Grid for Stainback Cone

In the graphs presented, there are two dotted lines on the graphs used for comparison. The lower dotted line is the fully laminar solution. The upper dotted line is the fully turbulent solution computed using the Baldwin-Lomax turbulence model, for reference. These lines are shown as guides to help understand the transitional profile.

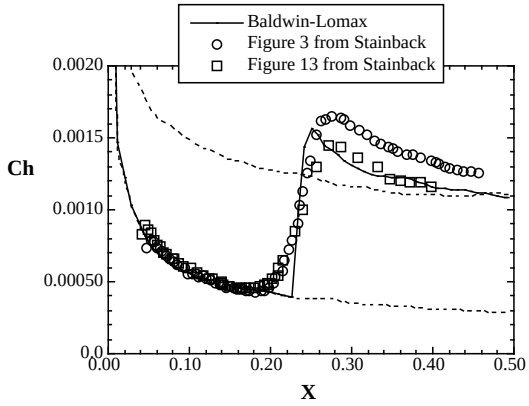

Figure 4.3: Baldwin-Lomax model on Stainback Cone

Figure 4.3 shows the results for the Baldwin and Lomax model on the Stainback supersonic cone. The transition length predicted is less than 25% of the experimental transition length but that is to be expected from this on/off type of model. The model does predict the peak in heat transfer at the end of transition within 2%. The model also does a satisfactory job of predicting the heat transfer in the turbulent region. Because the resulting transition length is underpredicted, the starting point

was chosen 6cm downstream of the experimental transition point so that the instantaneous profile would pass through the middle of the experimental transition region. Some other starting locations resulted in the computed profile not passing through the experimental transition region which was felt to be of less interest.

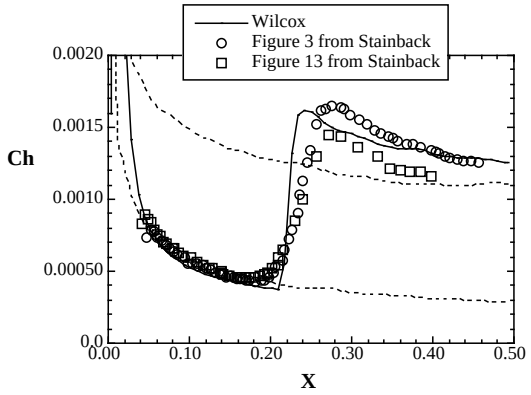

Figure 4.4: Wilcox model on Stainback Cone

The results for the Wilcox $k-\omega$ low-Reynolds number model are shown in figure 4.4. The transition length predicted is 32% of the experimental length. However, the peak in heat transfer is predicted within 5% of the experimental peak. The near wall behavior of ω was not specified but the roughness factor used was ten times greater than recommended by Wilcox and the roughness strip was three times longer than recommended. Transition did not occur when the values suggested by Wilcox were used, the entire domain remained laminar. Over 10 runs were made before a correct combination of parameters could be found to force transition in acceptable location where the short transition profile would occur in the middle of the longer experimental profile. The stiffness of the two equation model coupled with the number of runs results in high computational costs for using the model.

The results for the one equation turbulence/transition region model of Warren, Harris, and Hassan are shown in figure 4.5. The computations with and without the first and second mode contributions are almost identical. The computed profile is satisfactory at the beginning of the transition region but the peak is not resolved and the model has a wavy profile in the turbulent region. Since the peak is not predicted and the curve is wavy, a minimum to maximum distance will not give an

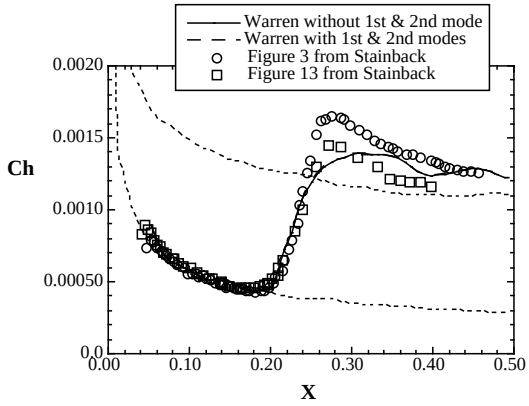

Figure 4.5: Warren, Harris and Hassan model on Stainback Cone

accurate account of the transition length, so the transition length is not computed. This model requires the specification of the transition point and starts to transition from the given point. The model was started at the experimental transition point.

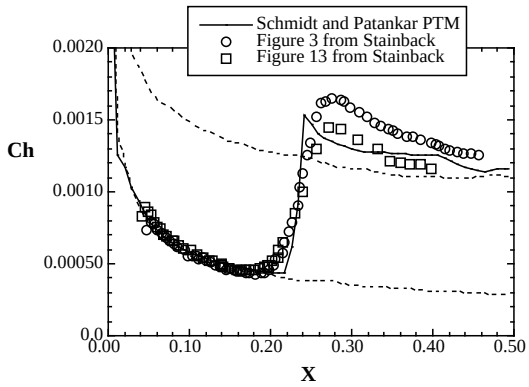

Figure 4.6: Schmidt and Patankar PTM model on Stainback Cone

The Schmidt and Patankar PTM model, shown in figure 4.6, produces a transition length 25% of the experimental length. The slope is discontinuous at the beginning and end of transition. On the plus side, the peak in heat transfer at the end of transition is predicted within 1%. The heat transfer level in the turbulent region is predicted well, but the solution is too wavy.

Over 15 attempts were made with the model until the correct combination of initial conditions could be found to produce the start of transition in the experimental

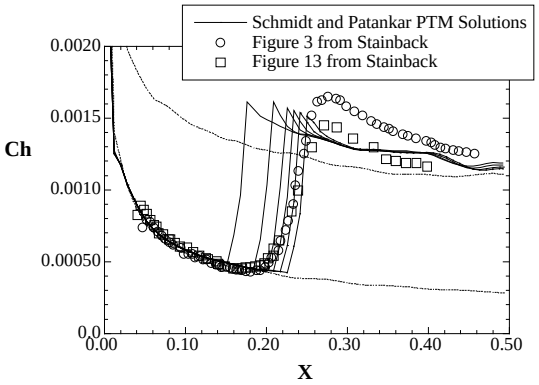

Figure 4.7: Schmidt and Patankar PTM model triggered at different locations on Stainback Cone

transition region. The free stream turbulence intensity, Tu, was 1.1% and the reference TKE length, l_{TKE} was 5.0×10^{-3}. The model was started 5cm from the leading edge. Considering the long run times associated with running this stiff two equation model and the number of runs, this model is very computationally expensive. Figure 4.7 shows several of the runs and the effect on the accuracy of the profile when transition starts at different locations. The transition point was varied by using different values of the free stream turbulence intensity from 1% to 5%. The most accurate profile was chosen to be the one that passes through the most points in the middle of the transition region.

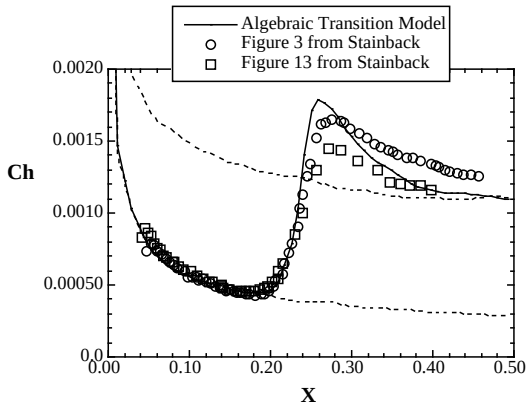

Figure 4.8: Algebraic Transition model on Stainback Cone

Figure 4.8 features the results for the algebraic transition region model for the

Stainback cone. The curve is smooth at all points, most notably at the beginning of transition where most models tend to have a discontinuous slope. The peak in heat transfer is predicted 15% higher than the experimental value. The predicted transition length is 75% as long as the experiment. The location to start the model was chosen in order to obtain satisfactory agreement at the beginning of the transition region. Triggering the model at the experimental start of transition produced the most accurate results.

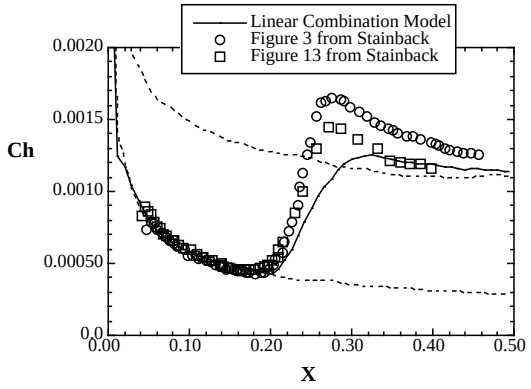

Figure 4.9: Linear Combination model with $N_o = 0.2 \times 10^{-3}$ on Stainback Cone

Figure 4.9 shows the results for the linear combination model on the Stainback supersonic cone. The location to start the model was chosen 3cm downstream of the experimental transition point to obtain satisfactory agreement in the middle of the transition region. The transition length is 25% too long and the peak is not predicted. The effect of compressibility is introduced by using different values of N_o. The relationship given between N_o and Mach number is very tentative, it is only presented on a graph. When a value of $N_o = 0.5 \times 10^{-3}$ is used instead of the value suggested of $N_o = 0.2 \times 10^{-3}$ for this case, the solution looks much better, see figure 4.10. The transition length is satisfactory, about 85% of the experimental value, but the peak is still not predicted. The overall agreement is satisfactory.

Using the linear combination model as an algebraic transition region model (See Section 3.7) on the supersonic cone, shown in figure 4.11, predicts a transition length that is slightly shorter than before. The heat transfer levels are about the same at the end of transition and through the turbulent region.

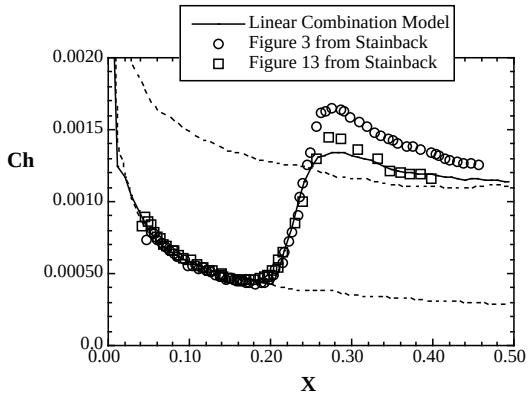

Figure 4.10: Linear Combination model with $N_o = 0.5 \times 10^{-3}$ on Stainback Cone

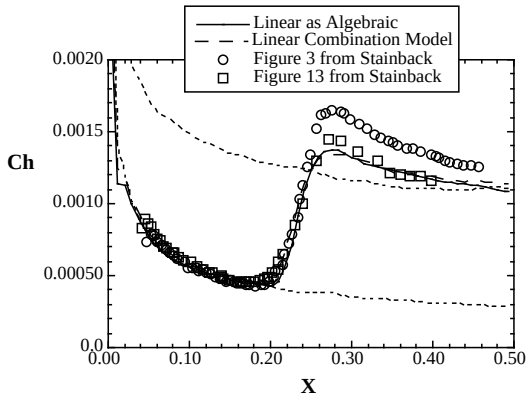

Figure 4.11: Linear Combination Model as Algebraic Transition Model on Stainback Cone

Table 4.2 provides a summary of how each model performed on the Stainback *et al.* supersonic cone. L_{model}/L_{exper} provides a comparison of the length of the transition region, measured from the minimum to maximum heat transfer, computed by the model to that of the experiment. The peak ratio column presents a comparison of the peak value from the model to an average of the two peak values from the experiment. Both ratios are highly subject to error and the first digit is the only true significant figure. The ratios can be interpreted as normalized peak and length numbers used for comparison between models. It should be noted that the transition length for the Warren, Harris and Hassan model was a not computed because the profile was unsatisfactory. This is the simplest test case possible. Cone flows are analogous to flat plate flows. So the results for this case should be satisfactory. The Warren, Harris and Hassan model and the two pure transition region models do an adequate job predicting the transition length but the peak in heat transfer is poorly predicted. The other models predict the peak in heat transfer adequately but underpredict the transition length. Note that when the values from the table are compared against the graphs, good agreement in the numbers does not always correspond to good profiles. The numbers do not reflect how smooth the profile is.

Table 4.2: Model Performance Summary for Stainback case.

Model	L_{model}/L_{exper}	Peak Ratio
Baldwin and Lomax	.25	1.01
Wilcox $K-\omega$	.32	1.04
Warren, Harris, and Hassan	-	.86
Schmidt and Patankar PTM	.25	.99
Algebraic Transition Model	.75	1.15
Linear Combination with $N_o = 0.5 \times 10^{-3}$	.85	.86

4.3 Holden and Chadwick Compression Ramp

The quality of Holden and Chadwick [74] experiment for this work stems from the fact that their goal was to measure heat transfer in the transitional region. Their test cases consists of a 5° ramp followed by curved compression surface going into a

10° ramp. The curved compression surface creates the very severe adverse pressure gradient. Figure 4.12 shows the geometry of the ramp and the corresponding pressure.

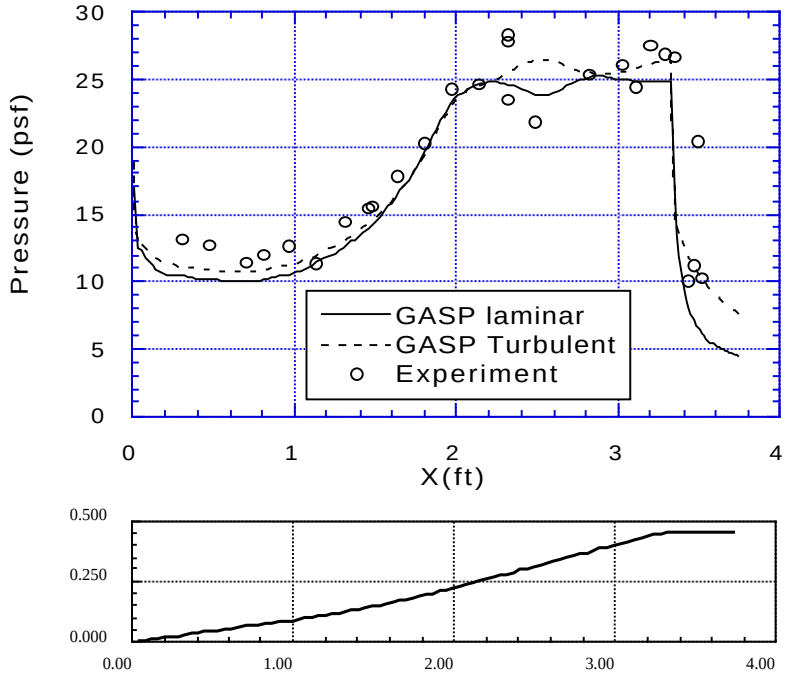

Figure 4.12: Compression Ramp of Holden and Chadwick

18 different test conditions were used that created a transition point on different parts of the ramp to examine the effect of pressure gradients on transition. Test case run 14 was chosen after communication with Dr. Ken Chadwick because the simple pressure calculations agreed satisfactorily for this case whereas for other cases there was some discrepancy between the computed and experimental pressure. Considering it is more difficult to match heat transfer calculations then pressure calculations, cases where the pressure could not be matched were dismissed from consideration. The test conditions for run 14 are featured in table 4.3.

Heat transfer data is presented in both graphs and tabular form. It will be used for comparison with the computational results. The uncertainty in the experimental heat transfer measurements is given as ±5%.

Another advantage of using the Holden and Chadwick paper for this work is that GASP was used in the original paper to help validate the measurements. The

Table 4.3: Test Conditions for Holden and Chadwick Run 14

Test Gas	Nitrogen
Mach Number	10.08
Reynolds Number	5.713×10^5 1/ft
Pressure	2.152×10^{-2} PSIA
Wall Temperature	526.20 R

experimental results are presented in a form conducive to using GASP, which means there is less chance of misinterpreting the experimental data. Dr. Ken Chadwick provided the grid generating program he used to generate grids for his results. A grid convergence study, shown in figure 4.13, was done to determine how clustered the grid should be. β is the stretching parameter, the closer it is to unity, the more clustered the grid is. The different grids had little affect on the heat transfer level for the laminar solution but differed for the turbulent solution. The grid with the least clustering, $\beta = 1.005$, predicts a heat transfer well below the other two grids. $\beta = 1.0005, 1.0001$ produced similar results with the difference most likely being due to problems with running a high clustered grid which results in a wavy profile. $\beta = 1.0005$ was used and the grid it produced is shown in figure 4.14. The first grid line above the wall is located at $y^+ \approx 0.1$.

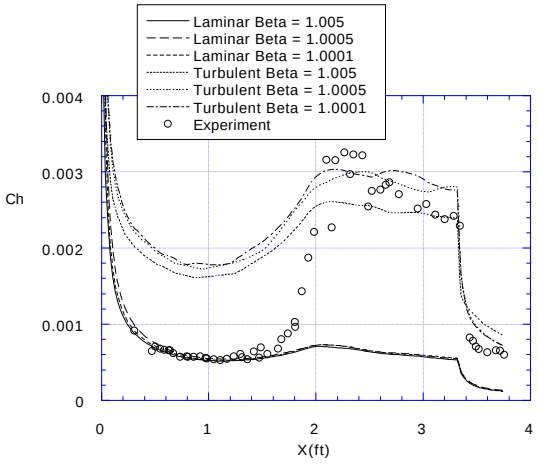

Figure 4.13: Grid Convergence study for compression ramp

Examining the experimental data points (shown on all solution plots) shows that

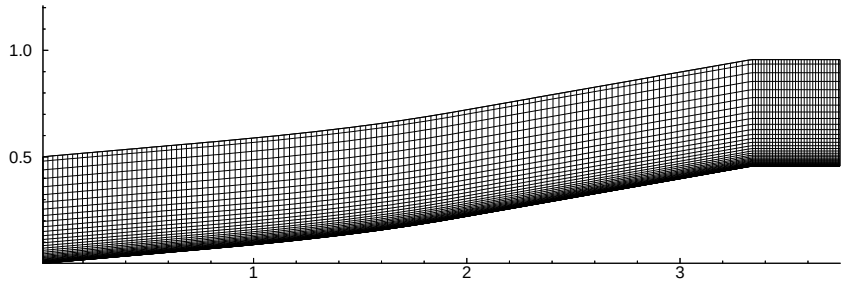

Figure 4.14: Grid for compression ramp

there is some slight scatter to the data, but in general the transitional heat transfer profile is well represented. Measuring from the local minimum to the maximum in heat transfer produces a transition length of about .72 feet which is about 20% of the total domain. It should be noted that due to the scatter in the experimental data, this value is subject to some error. Computing the transition length using other possible data points has shown the estimated experimental transition length is subject to roughly $\pm 15\%$ uncertainty.

All the graphs presented feature a lower dotted line representing the fully laminar solution and an upper line which is the fully turbulent solution generated with the Baldwin and Lomax algebraic turbulence model for reference. Some transitional solutions presented use a turbulence model other than Baldwin-Lomax and that is a possible explanation of any lack of agreement in the turbulent region.

Figure 4.15 shows the results for the Baldwin and Lomax model on the compression ramp. The transition length is about 74% too short but that is to be expected considering the on/off nature of this model. The heat transfer prediction for the end of transition and the fully turbulent region is too high. The starting point for the model of 1.95ft was chosen in order to make the instantaneous profile cross the experimental profile in the middle of the transition region. Figure 4.15 here agrees with Figure 20 in Holden and Chadwick [74] which was computed using GASP by starting with fully laminar flow and then switching zones to a fully turbulent solution generated with the Baldwin and Lomax turbulence model, which is basically the same as the Baldwin and Lomax turbulence/transition region model used here.

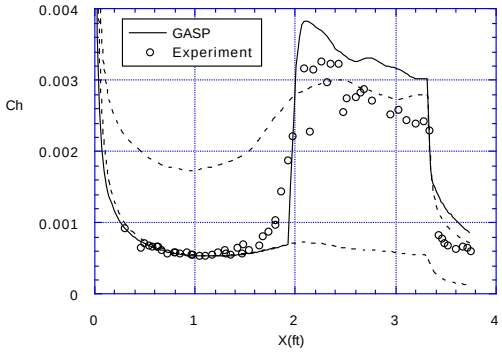

Figure 4.15: Baldwin-Lomax model on Compression Ramp

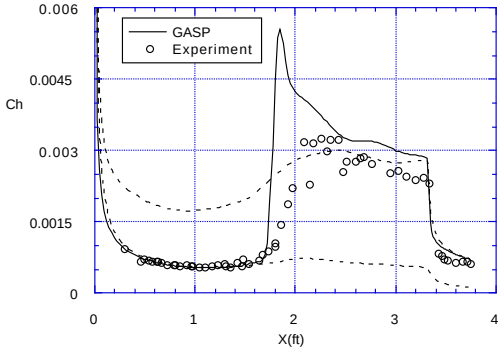

Figure 4.16: Wilcox $k - \omega$ model on Compression Ramp

Figure 4.16 shows the results for the Wilcox $k-\omega$ model on the compression ramp. There is a spike overshoot which leads to overprediction of the heat transfer as well as a transition length that is 75% too short. The roughness value and roughness strip length used were the values suggested by Wilcox. However, the free stream TKE was $10^{-10}U_\infty^2$ instead of $10^{-16}U_\infty^2$ suggested by Wilcox. For this case, the value of ω was specified with equation 3.21 to the 25th cell off of the wall which is a y^+ of about 500. This is obviously out of the defined range of equation 3.21 but when this was not used, the pressure gradient killed the production of k so that transition never started. This was true even for long roughness strips with a high value of roughness. Many sets of roughness strip length and roughness factors had to be used before transition was forced to occur in a location close to the experimental transition region without crashing which resulted in high computational costs.

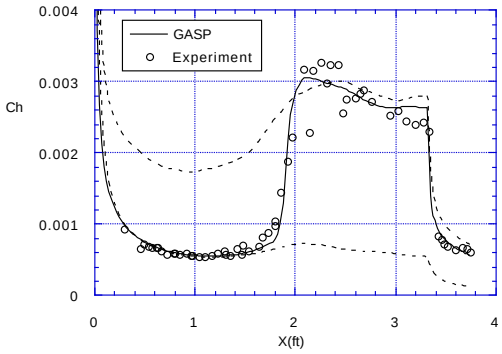

Figure 4.17: Schmidt and Patankar PTM on Compression Ramp

Figure 4.17 presents the Schmidt and Patankar PTM for the Calspan compression ramp. The free stream turbulence intensity was 5% and the free stream TKE length was 5.4×10^{-3}. The model was started at .54ft. This model produced the best results for this test case. The transition length is only 55% of the experimental transition length, but when comparing the lengths by looking at the graphs, the computed transition length looks acceptable. Good agreement between the computed solution and experiment is found at all points, but it comes at great expense. The problem was space marched and as was mentioned above, that requires using trial and error

to force the model to predict transition at the correct location. The case had to be run about a dozen times before the correct combination of initial conditions was found that resulted in the model transitioning in the experimental transition region. Coupling the number of runs made with the long run times associated with two equation turbulence models leads to a high computational cost for this model.

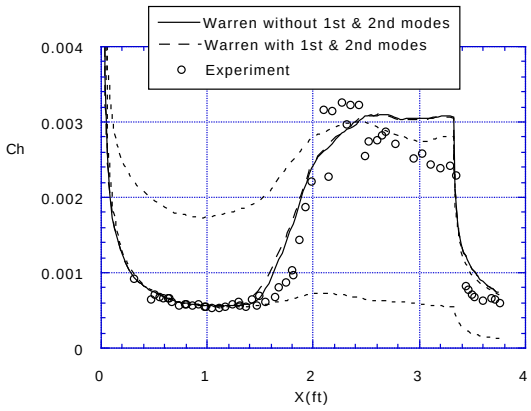

Figure 4.18: Warren, Harris and Hassan Model with $N_o = 0.2 \times 10^{-3}$ on Compression Ramp

Figure 4.18 shows the Warren, Harris and Hassan model on the compression ramp with and without the first and second mode contributions. The model was started 6 inches upstream of the experimental transition point. The first and second mode contributions are seen to have little effect. Without the laminar contributions to the Reynolds stress, this model is basically just using the intermittency relations from Narasimha as an algebraic turbulence mode, i.e. proportioning the eddy viscosity with it. The intermittency relations from Narasimha seem to have the wrong compressibility effect for this test case, if a value of $N_o = 0.5 \times 10^{-3}$ is used instead of $N_o = 0.2 \times 10^{-3}$ the predictions look much better, see figure 4.19. The more accurate transition length allows the model to be started at the experimental transition point. While the transition region is predicted well, the turbulent region is overpredicted.

Figure 4.20 shows the algebraic transition region model on the compression ramp. The results are unsatisfactory. The model transitions very late in the domain. The reason for this is interesting. Looking back at the description of the algebraic transition region model in section 3.6 on page 38, the model is based on the fact that the

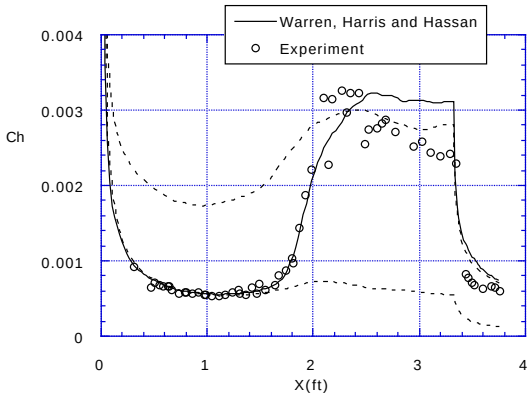

Figure 4.19: Warren, Harris and Hassan Model with $N_o = 0.5 \times 10^{-3}$ on Compression Ramp

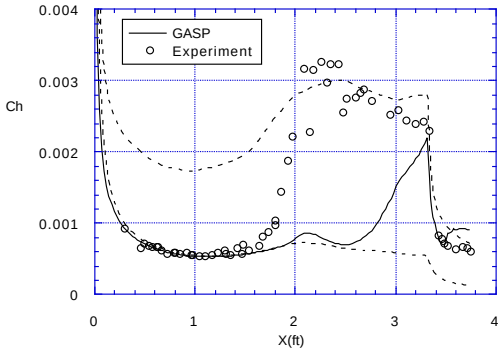

Figure 4.20: Algebraic Transition Model on Compression Ramp

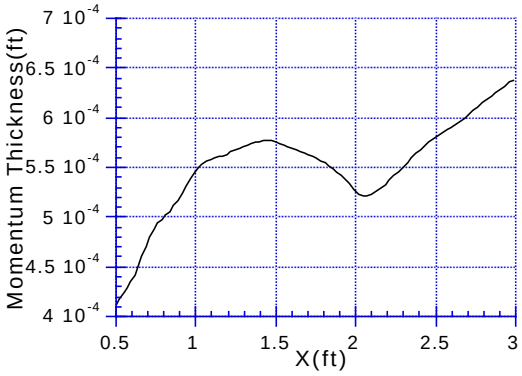

Figure 4.21: Momentum Thickness on Compression Ramp

momentum thickness grows significantly during the transition process. For this case, there is a severe adverse pressure gradient which causes the computed momentum thickness to actually decrease. No experimental data is available on the momentum thickness. Figure 4.21 shows the momentum thickness computed for a laminar flow on the compression ramp using GASP, the momentum thickness decreases from a station of 1.5 ft to 2.0 ft. Looking back at the graph of the pressure, figure 4.12, it is seen that this is the region where the pressure gradient is most severe. In this severe pressure gradient region, the factor χ_1 does not grow because the momentum thickness does not grow which means that the model is not adding in more of the eddy viscosity. Later in the domain, the momentum thickness does begin to grow and the model does start to transition, but by that time, it is too late. It was attempted to start the model at several different locations in the domain to circumvent the severe adverse pressure gradient but the length of the pressure gradient was too large and this method was unable to produce a satisfactory profile.

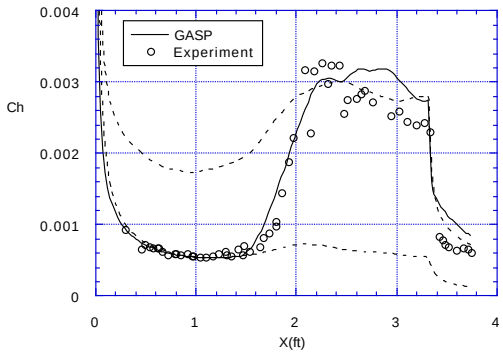

Figure 4.22: Linear Transition Model with $N_o = 0.5 \times 10^{-3}$ on Compression Ramp

Figure 4.22 presents the results for the linear combination transition region model for the compression ramp and figure 4.23 shows how the model combines the different parts into the transitional solution. The partial turbulent solution is zero from the beginning of the domain up until the transition point because the tangency boundary condition is used in this region. When the no-slip condition is turned on to start the boundary layer, the heat transfer spikes up and gradually comes down. The

transitional solution is made by combining the partial turbulent solution and the laminar solution. The graph in Narasimha [12] gives a value of $N_o = 0.2 \times 10^{-3}$ but this value was fond to yield transition lengths that were entirely too long. Instead, a value of $N_o = 0.5 \times 10^{-3}$ was used and even with this value the transition length was predicted 25% too long. Overall, agreement is satisfactory. The transition region looks especially good. The only noticeable downside is that the model overpredicts the last part of the turbulent region.

Because the predicted transition length was longer than the experimental transition length, the model was started around 2 inches upstream of the experimental transition point in an effort to achieve better agreement.

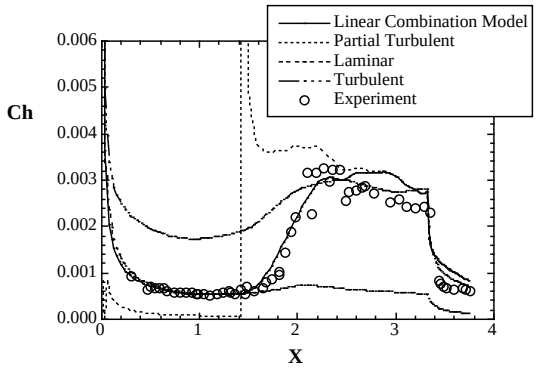

Figure 4.23: Linear Transition Model with contributing parts on Compression Ramp

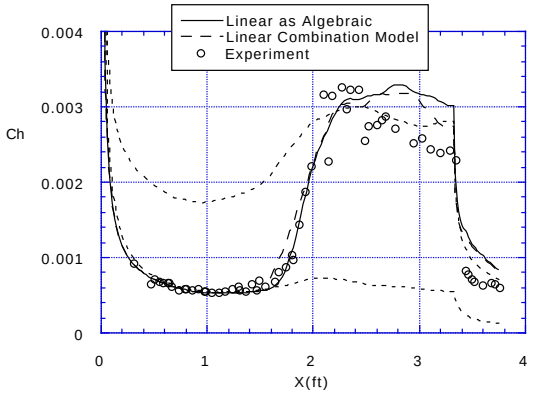

Figure 4.24: Linear Transition Model as an Algebraic Transition Model on Compression Ramp

The results using the linear combination model as an algebraic transition region model are shown in figure 4.24. The length of the transition region is predicted shorter for this method which is more accurate for this flow. The peak is predicted well but the turbulent region is overpredicted.

Table 4.4: Model Performance Summary for compression ramp

Model	L_{model}/L_{exper}	Peak Ratio
Baldwin and Lomax	.27	1.17
Wilcox $K-\omega$	.25	1.71
Warren, Harris, and Hassan $N_o = 0.5 \times 10^{-3}$	1.31	.99
Schmidt and Patankar PTM	.55	.94
Algebraic Transition Model	-	-
Linear Combination with $N_o = 0.5 \times 10^{-3}$	1.25	.94

Table 4.4 presents a summary of how the models performed on the compression ramp. The data point with the highest Ch (3.25369×10^{-3}) was used as the peak value. There are four other data points around this one, all within 3%, which leads to high certainty that this is a representative peak value and not data scatter. It must be noted that both of the presented ratios are highly subject to error due to the data scatter as well as experimental uncertainty. The first digit is the only true significant digit. The entries for the algebraic transition region model are blank because the model transitioned very late. Clearly, at times these numbers do not reflect the accuracy of the solution. The numbers do not reflect how smooth the profile is or how the model performs in the turbulent region.

4.4 Kimmel Supersonic Flared Cones

Kimmel [2, 73] examines the effect of pressure gradients on hypersonic transition. The test case consists of 5 different flared cones. The first part of the domain is a straight 7° half angle cone .475m in length. The next part of the domain is flared either in or out to produce constant pressure gradients. There are two adverse pressure gradient cases, two favorable pressure gradient cases, and a non-flared, no pressure gradient case for comparison. Kimmel labels each flared cone using a DPDX notation where

DPDX = 1 means that the pressure gradient would produce a 100% increase in the cone pressure coefficient over the models total length. Since the flared part is about half of the model length, DPDX = 1 produces about a 50% rise in the cone pressure coefficient. Figure 4.25 shows the geometry of the flared cones where each cone is labeled with the DPDX notation. The flared sections were designed to produce a constant pressure gradient. Figure 4.26 shows the resulting pressure distributions computed by GASP and shows that the pressure gradients are indeed constant.

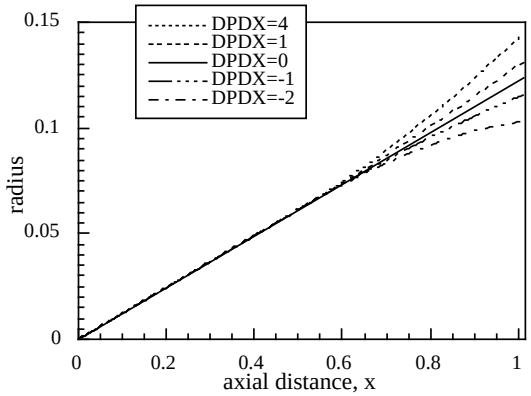

Figure 4.25: Kimmel Flared cones

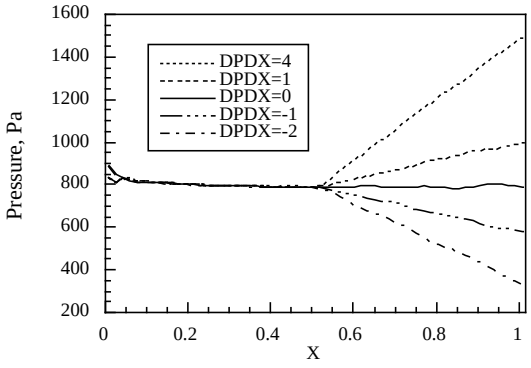

Figure 4.26: Pressure on flared cones

The free stream conditions for these test cases are shown in table 4.5. These initial conditions lead to transition starting on the straight cone part of the domain and finishing in the flared or pressure gradient part. So these cases really isolate

the effect of pressure gradients on the middle to end of transition, not on the whole process.

Table 4.5: Test Conditions for Kimmel

Mach Number	7.93
Reynolds Number	$6.6 \times 10^6 m^{-1}$
Total Temperature	722 K
Wall Temperature	303.24 K

The original purpose of Kimmel's work was to look at the effect of pressure gradients on second mode disturbances, not to measure and present transitional heat transfer data. But Kimmel notes the paucity of hypersonic transitional heat transfer data, so the heat transfer data is presented for whatever it is worth to the research community.. Because this data has not been optimized for this purpose, there is not enough data points at the beginning of the domain for some of the cases. Even with that shortcoming, this data set is one of the best around.

For all cases, transition starts on the cone and finishes on the flared pressure gradient part. Ideally since the free stream conditions are the same, transition should start on the same point of the cone for all cases. But because transition is so complicated and is dependent on so many different variables, the starting point is slightly different for each of the cases. For each of the models, the initial conditions and starting point used for the zero pressure gradient case (DPDX=0) will be initially used on each pressure gradient case to see what effect the pressure gradient has on the model. For most cases, the model will perform about the same, but because the transition point is different for the some of the different cases, the results will not be acceptable because the profile looks shifted. In other cases, the pressure gradient and the resulting different grid used will drastically affect the model.

The grids used for each of the cases were 61x81 grids generated using Gridgen2D. The spacing at the wall was constrained to be 1.0×10^{-5} at the grid edges in an effort to produce a $y^+ = 0.1$. However, because some of these grids are flared, the spacing at the wall in the interior of the grid may be slightly different than the edges.

Kimmel [73] reports the heat gauges used have an accuracy of $\pm 5\%$. Some data

points fall outside this band. Therefore, Kimmel presents a more conservative uncertainty of the heat transfer data at ±10%.

4.4.1 Kimmel DPDX=0

The first case to be presented is the zero pressure gradient case, the case of just a plain cone with no flaring. This case is presented first so it can be used for comparisons with the subsequent cases featuring pressure gradients. We want to know if the effects seen are due to the pressure gradient or not. In addition, the zero pressure gradient case has more experimental data points than the pressure gradient cases. There is slight scatter in the points, but in general, the shape of the transition profile is represented well. The transition length is roughly 31 cm. The experimental peak value was $Ch = 1.556 \times 10^{-3}$. Again, due to the scatter in the data, both values are subject to error. The results found for this case should be similar to the results for the supersonic cone case of Stainback [67] shown in section 4.2.

Figure 4.27 shows the 61x81 grid used for the current case. Gridgen2D was used to generate the grid. The first grid line off of the wall was spaced roughly 1.0×10^{-5}m which produced a $y^+ \approx 0.1$.

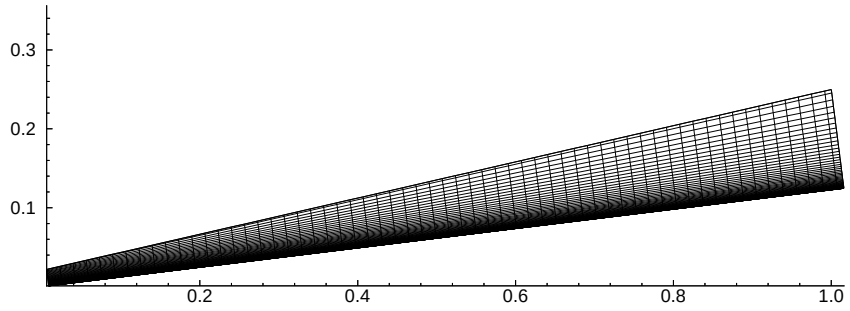

Figure 4.27: Grid for Kimmel DPDX=0

An 81x101 grid was run in comparison to the 61x81 grid to verify that the 61x81 mesh was grid converged for this problem. Figure 4.28 shows that both meshes do produce similar heat transfer levels for fully laminar and fully turbulent flow.

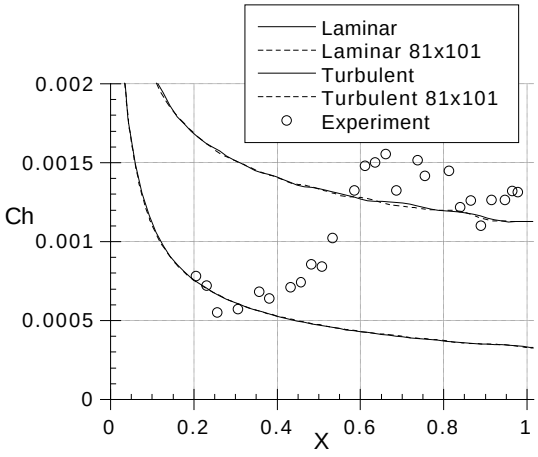

Figure 4.28: Grid convergence study for Kimmel DPDX=0

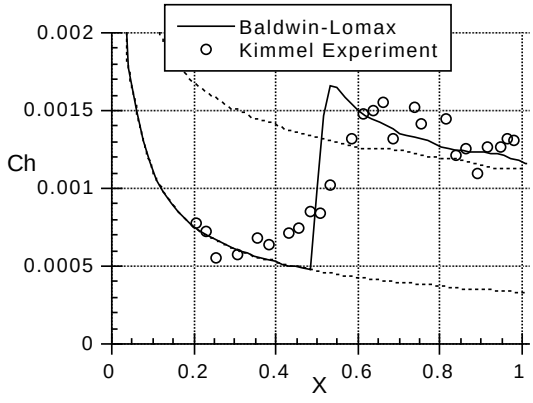

Figure 4.29: Baldwin-Lomax results on Kimmel DPDX=0

Figure 4.29 presents results for the Baldwin and Lomax model for this cone. The transition length is less than 17% of the experimental length. The computed peak in heat transfer is 7% higher than the experimental value. The turbulent region is resolved adequately. The starting point of the model was chosen 15cm downstream of the experimental starting point because the predicted transition length is shorter than the experimental transition length. By starting the model in the middle of the experimental transition region the discrepancy between the computed and experimental results is minimized. As was stated previously, this method only works because the experimental solution is known. The purpose of the current work is to understand exactly how the models work so they can be better applied to cases with unknown solutions.

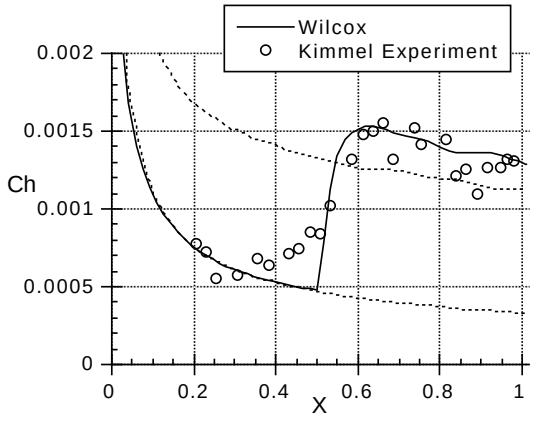

Figure 4.30: Wilcox results on Kimmel DPDX=0

The results for the Wilcox model, shown in figure 4.30, predict a transition length too short but the turbulent region is well within the data scatter. ω near the wall was not specified for this case. The roughness strip length and roughness factor were chosen in order to make transition occur in the middle of the experimental transition region. The roughness factor used was that given by Wilcox's relations but the roughness strip used was almost 5 times longer than Wilcox recommended. The initial free stream TKE was $10^{-6}U_\infty^2$ instead of $10^{-15}U_\infty^2$ recommended by Wilcox. A lower free stream TKE resulted in a totally laminar flow.

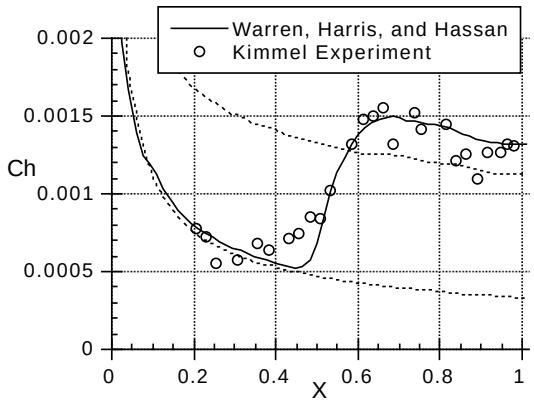

Figure 4.31: Warren, Harris and Hassan results on Kimmel DPDX=0

The Warren, Harris and Hassan model, shown in figure 4.31, predicts the transition length within 25% of the experimental length though that is slightly misleading because the shape of the profile gives it the appearance of a shorter length. The profile is smooth at the beginning and end of transition where some models have discontinuous slopes. The heat transfer is predicted well at the end of transition. The first and second mode effects were used with this run, as was shown earlier, they make little affect on the profile. The starting point of the model was chosen 8cm downstream of the experimental point which results in the solution being inaccurate at the beginning of the transition region but satisfactory in the later stages of the experimental profile.

Figure 4.32 shows the results for the Schmidt and Patankar production term modification. The model pulls away from the laminar solution, stalls out before finally spiking up and finishing transition. While the solution is close to the data points, the shape of the profile is incorrect which makes this a poor solution. Measuring the transition length starting right before the heat transfer spikes up to the peak results in a short transition length that is 27% of the experimental length. The peak heat transfer is within 3% of the experimental value. This model was very expensive to run as it took over 30 tries before the correct combination of initial conditions was found to produce transition in the middle of the experimental transition profile. The free stream turbulence intensity was 6.5% and the free stream TKE length was 1.0×10^{-2}.

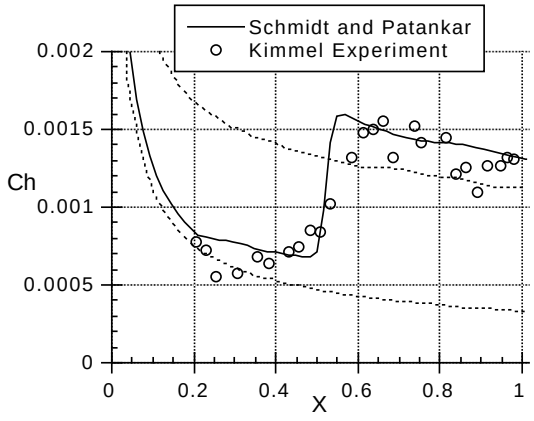

Figure 4.32: Schmidt and Patankar results on Kimmel DPDX=0

The model was started at 20 cm.

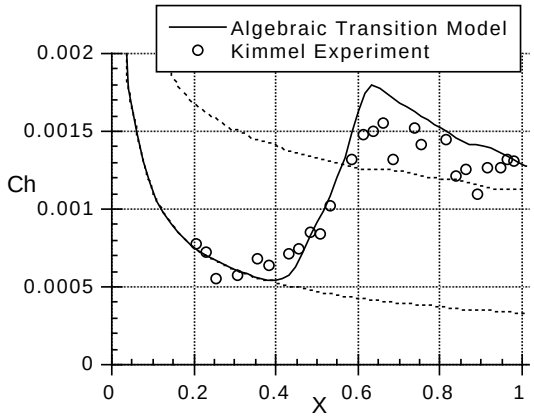

Figure 4.33: Algebraic Transition model results on Kimmel DPDX=0

The algebraic transition region model, shown in figure 4.33, produces a smooth curve, but the transition length is 24% shorter than the experimental length and the model overpredicts the heat transfer at the end of transition by 15%. The entire turbulent region is also overpredicted. This is a bit surprising considering how well the algebraic transition region model did for the other supersonic cone of Stainback shown in figure 4.8. A reason for this appears to be that the Stainback cone features a heat transfer at the end of transition much higher than the fully turbulent value when compared to the Kimmel case. The fully turbulent theoretical value used for

comparison and used for the transition region model is the Baldwin-Lomax turbulence model. Thus, the reason that the algebraic transition region model overshoots the turbulent region could be due to the turbulence model, not the transition region model. Though, considering when the Baldwin and Lomax turbulence model was used as a transition region model, the heat transfer was predicted well in the turbulent region, the overprediction of the turbulent region probably lies with the algebraic transition region model and not the turbulence model.

The model was started 3cm downstream of the experimental transition point because the predicted transition length is shorter than the experimental transition length.

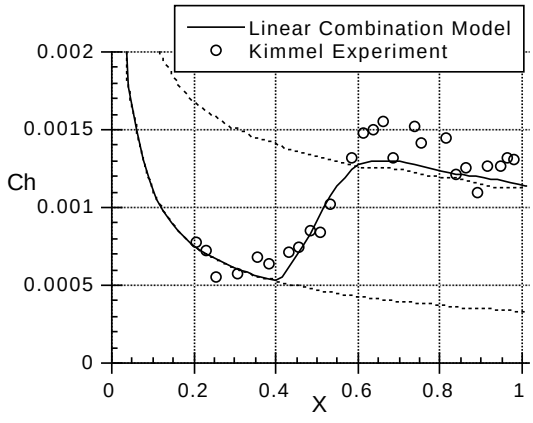

Figure 4.34: Linear Combination Transition model with $N_o = 0.2 \times 10^{-3}$ results on Kimmel DPDX=0

Figure 4.34 shows the results for the linear combination model on Kimmel's cone. The transition length is a bit short but is within 15% of the experimental value which is acceptable. The major problem is that the model does not predict the peak in heat transfer, the peak is underpredicted by over 15%. The two previous cases presented, Stainback's supersonic cone and the compression ramp of Holden and Chadwick, required raising the value of N_o otherwise the transition length was much too long. (The transition length is inversely proportional to N_o.) For this case, the value recommended of $N_o = 0.2 \times 10^{-3}$ was used that should predict a long transition length, but the transition length predicted is too short. Because the

transition length is too short, the model was started about 6cm downstream of the experimental transition point.

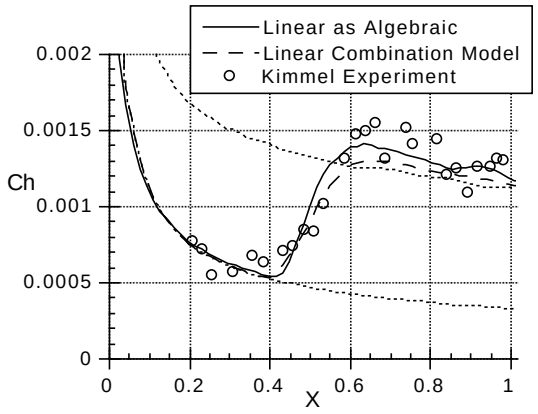

Figure 4.35: Linear Combination Transition model as an Algebraic transition model results on Kimmel DPDX=0

The results for the linear combination model used as an algebraic model are shown in figure 4.35, the results for the linear combination model are shown for comparison. Using this model as an algebraic transition region model creates a shorter transition length which is undesirable for this case but it does increase the heat transfer at the end of transition and the turbulent region, which is more accurate.

Table 4.6: Model Performance Summary for Kimmel DPDX=0 case.

Model	L_{model}/L_{exper}	Peak Ratio
Baldwin and Lomax	.16	1.07
Wilcox $K-\omega$	.44	.99
Warren, Harris and Hassan	.76	.96
Schmidt and Patankar PTM	.27	1.03
Algebraic Transition Model	.76	1.16
Linear Combination Model	.87	.84

Table 4.6 presents a summary of the performance of the models on the Kimmel DPDX = 0 case. Both ratios are highly subject to error and the first digit is the only true significant digit. More digits are shown in the table so that the ratios can be interpreted as the normalized length and peak for the models for comparison with

other models. Contributing to the error is the lack of data points which means the transition length can only be determined in the increments that the gauges are located at. The table shows that the Baldwin and Lomax model and the Wilcox $k-\omega$ model do a poor job of predicting the transition length but predict the peak in heat transfer well. The numbers for the Warren, Harris and Hassan model look good, but do not represent well the shape of the profile. The numbers in the graph clearly describe the results for the two pure transition region models. The algebraic model overpredicts the heat transfer while the linear combination model underpredicts the heat transfer, both by over 15%. However, both models predict the transition length well.

4.4.2 Kimmel DPDX=4

The Kimmel DPDX = 4 case features a strong adverse pressure gradient but it does not appear to be as strong as the pressure gradient from the Holden and Chadwick case. The experimental data does not have enough points at the start of transition. At the end of transition, there is some scatter of the data points (see figure 4.37). It will be tough to judge the performance of the models with the data points. A rough estimate of the transition length is obtained by using the first data point and the eighth data point which appears to be a peak, but could be due to the scatter of the data, the resulting length is 28cm. It should be noted that this is a very rough value and should only serve as an estimation of the transition length for comparison. The uncertainty of this value of the transition length can be roughly computed as $\pm 12\%$ by moving the start or end of transition to the right or left to the next data point. Again, using the eighth data point as a peak results in a experimental peak heat transfer of $Ch = 2.035 \times 10^{-3}$. The strong adverse pressure gradient forces the heat transfer to increase in the turbulent region after transition which will make determining the peak predicted by the model difficult. Where there is not a clear local maximum, the peak will be taken to be the value of the solution at the experimental transition point. As with all the Kimmel cases, transition starts on the cone and finishes on the flared section.

Figure 4.36 shows the 61x81 grid used for this case. Gridgen2D was used to generate the grid. The grid point closest to the wall was constrained at the boundaries

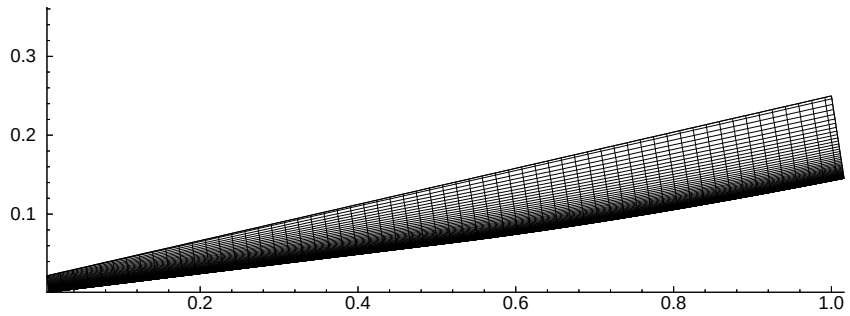

Figure 4.36: Grid for Kimmel DPDX = 4 case.

to be 1.0×10^{-5} which results in a $y^+ \approx 0.1$. It should be noted that because the grid curves upward and the elliptic solver was used, the grid spacing in the middle of the gird will be slightly different than the boundaries.

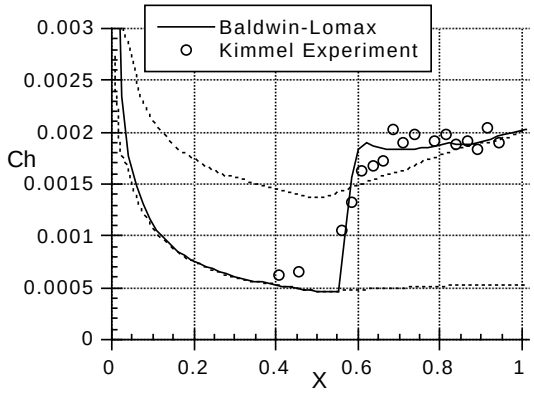

Figure 4.37: Baldwin-Lomax results on Kimmel DPDX=4

Figure 4.37 shows the results for the Baldwin-Lomax model. The transition length is almost 70% too short. The end of transition and the turbulent region are predicted well. The transition profile has discontinuous slope at the beginning of transition which is undesirable. The model was started 16cm downstream of the experimental transition point.

The Wilcox results, shown in figure 4.38, predict a transition length almost 40% too short. The agreement is good at the end of transition but the Wilcox model does not predict the heat transfer level going back to the fully turbulent level, it is too high

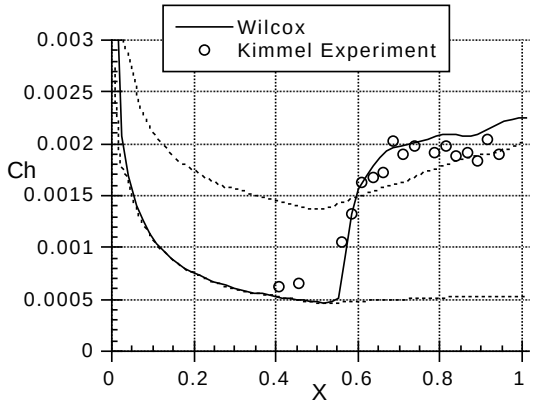

Figure 4.38: Wilcox results on Kimmel DPDX=4

in the fully turbulent region. The initial conditions used for the DPDX=0 case were initially attempted here, but that resulted in the transition point being slightly too far upstream. The free stream TKE was slightly reduced and the roughness strip was enlarged from the DPDX=0 initial conditions to make transition occur near the end of the experimental transition region in order to achieve better agreement with the data points in this region. The value of k_r used was that recommended by Wilcox, but the length of the roughness strip was 7 times greater. The initial free stream TKE was $8.1 \times 10^{-7} U_\infty^2$ instead of the $10^{-15} U_\infty^2$ recommended by Wilcox. The near wall behavior of ω was not specified.

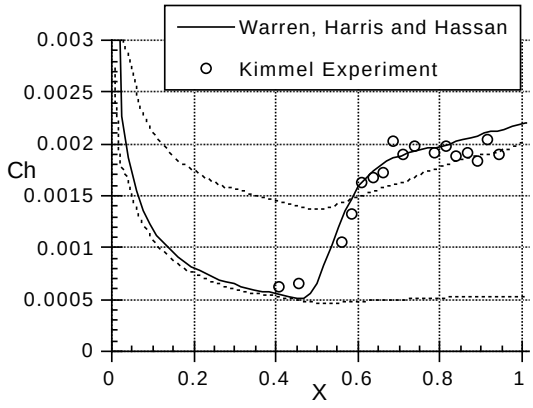

Figure 4.39: Warren, Harris and Hassan results on Kimmel DPDX=4

The results for the Warren, Harris and Hassan model are shown in figure 4.39. The

overall agreement is satisfactory. The transition length predicted is almost 80% of the experimental value which is acceptable. The peak in heat transfer is underpredicted by about 9%. The model was initiated at the experimental start of the transition region.

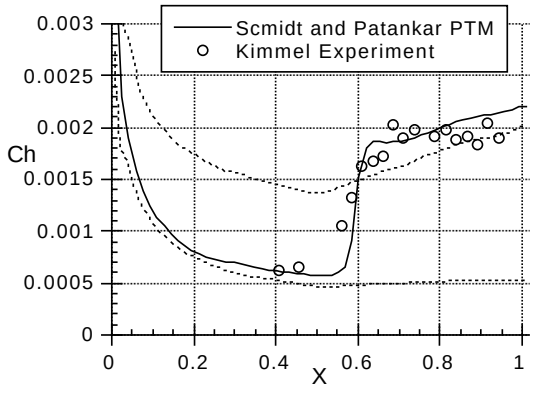

Figure 4.40: Schmidt and Patankar results on Kimmel DPDX=4

The results for the Schmidt and Patankar production term modifications are shown in figure 4.40. The transition length is again too short, over 55% too short. The peak is underpredicted. The agreement later in the domain is satisfactory, though slightly overpredicted. The free stream turbulence intensity was 5.0% and the free stream TKE length was .01. The model was started at 20cm.

The initial conditions used for the zero pressure gradient case were attempted on this case and they resulted in transition occurring far upstream on the cone. Considering that the beginning of transition is occurring on the cone ahead of the flared section, the shift upstream of the transition point is not due to the pressure gradient. The grid spacing at the wall for this case is about 15% greater than the grid spacing for the zero pressure gradient case due to the geometry of the problem and it is causing transition to occur too early. This dependence on the grid spacing of the model is undesirable. Fortunately, reducing the free stream turbulent kinetic energy moved the computed transition point back into the experimental transition region.

The algebraic transition region model, shown in figure 4.41, does a satisfactory job through the beginning of the transition with a smooth profile. The transition length is predicted within 3%. However, the end of the transition region and the

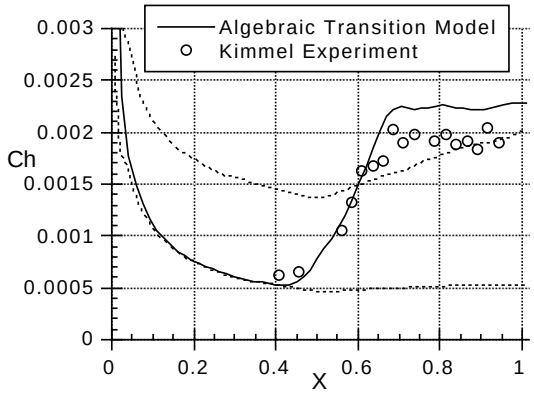

Figure 4.41: Algebraic Transition Model results on Kimmel DPDX=4

entire turbulent region are overpredicted by 10%. It is encouraging to see that the model does at least transition considering that it did not for the adverse pressure gradient from the Holden and Chadwick case. The model was started roughly at the beginning of the experimental transition region.

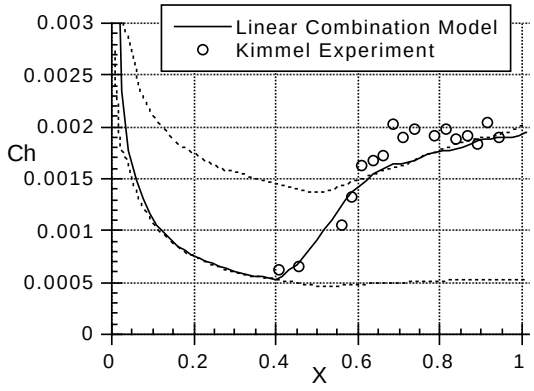

Figure 4.42: Linear Combination model results on Kimmel DPDX=4

Figure 4.42 shows the results for the linear combination model. The beginning of the transition region appears to be predicted well, but the peak at the end of transition is not found, the heat transfer level is almost 20% too low. The model was started approximately at the experimental transition point.

When the linear combination model is run as an algebraic transition region model, shown in figure 4.43, the transition length is shortened. But the heat transfer is

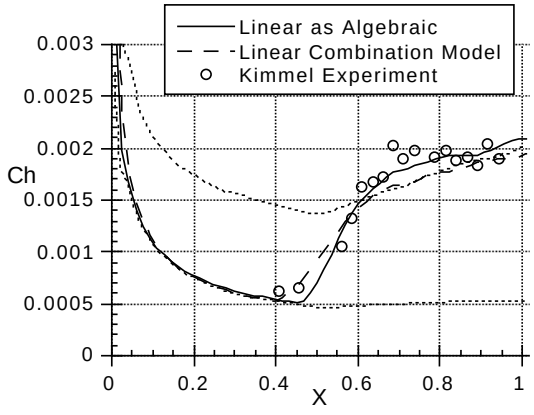

Figure 4.43: Linear Combination as Algebraic Model results on Kimmel DPDX=4

increased at the end of transition and for the turbulent region, which is desirable.

Table 4.7: Model Performance Summary for Kimmel DPDX=4 case

Model	L_{model}/L_{exper}	Peak Ratio
Baldwin and Lomax	.30	.93
Wilcox $K-\omega$	.61	.98
Warren, Harris, and Hassan	.79	.91
Schmidt and Patankar PTM	.42	.92
Algebraic Transition Model	1.03	1.10
Linear Combination	1.09	.82

Table 4.7 presents a summary of how each of the models performed on this case. Both ratios are highly subject to error due to the lack of data points and the scatter in the data. The first digit is the only true significant figure. Both ratios can be interpreted as normalized values of the length and peak used for comparison between models. The first four models listed are turbulence models or modifications to turbulence models and they all do a satisfactory job of predicting the peak in heat transfer, but the transition length at times is underpredicted. The last two listed are the pure transition region models. They do a satisfactory job of predicting the transition length, but the peak is not predicted well.

4.4.3 Kimmel DPDX=1

This case features a mild adverse pressure gradient. Looking at any of the solution plots (see figure 4.45 for example) shows that there is not enough experimental data points at the beginning of transition, but the points that are given do a sufficient job of representing the shape of the profile. Using the first point as the beginning of transition and the seventh point as the peak, a rough experimental transition length of 33cm is found which means about a third of the domain is the transition region. Due to the lack of data points, the uncertainty in this measurement is about ±15%. Using the seventh point again as the rough peak, the experimental peak heat transfer is $Ch = 1.631 \times 10^{-3}$. Both measurement are highly subject to error due to the lack of data points.

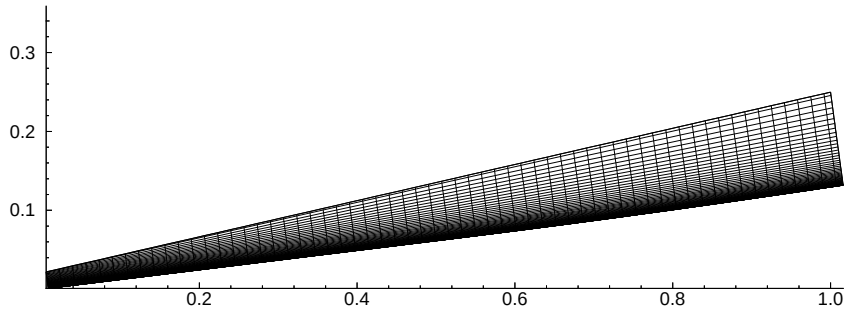

Figure 4.44: Grid for Kimmel DPDX = 1 case.

Figure 4.44 shows the 61x81 grid used for this case generated by Gridgen2D. The grid point closest to the wall was constrained at the boundaries to be 1.0×10^{-5} which results in a $y^+ \approx 0.1$. This cone is flared slightly upward, so the grid spacing in the middle of the grid will be slightly larger than the boundaries.

The Baldwin and Lomax model, shown in figure 4.45, predicts a transition length that is almost 80% too short. The slope is discontinuous at the beginning and ending of transition, which is undesirable. But the end of transition and the turbulent region are reproduced well. The model was started 20 cm downstream of the experimental transition point due to the underpredicted transition length.

The results for the Wilcox model are shown in figure 4.46. The transition length

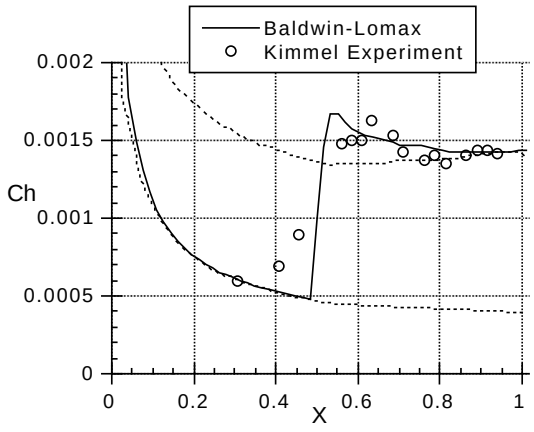

Figure 4.45: Baldwin-Lomax results on Kimmel DPDX=1

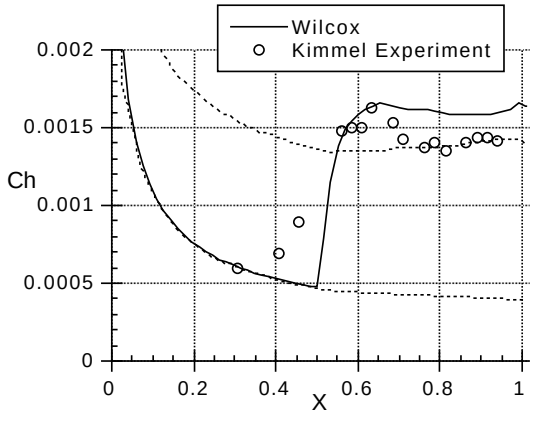

Figure 4.46: Wilcox results on Kimmel DPDX=1

is over 50% too short and while the peak at the end of transition is predicted well, the level of the heat transfer never comes down so the entire turbulent region is overpredicted.

Almost 10 runs were needed to make the model predict transition in the experimental transition region. The value of k_r used is that suggested by Wilcox but the roughness strip is more than 8 times longer than suggested. The initial free stream TKE was $10^{-6}U_\infty^2$. After these initial conditions were found, the initial conditions from the DPDX=0 case were used. The results were exactly the same. The largest difference between the two sets of initial conditions is a difference in the length of the roughness strip, implying the roughness strip does not have much of an effect.

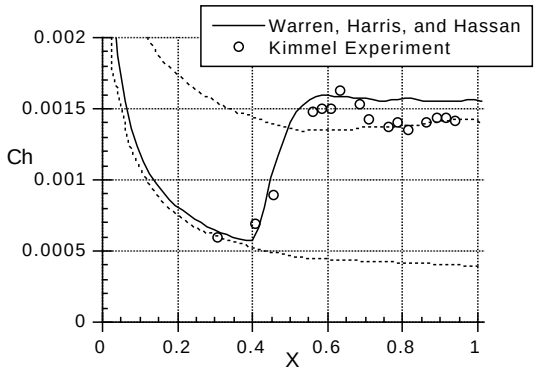

Figure 4.47: Warren, Harris, and Hassan results on Kimmel DPDX=1

The Warren, Harris, and Hassan model, shown in figure 4.47, predicts a transition length that is 38% too short but it does a satisfactory job of matching the few data points at the beginning of transition. The level of heat transfer is good at the end of transition but stays at that level and remains too high into the turbulent region, it should decrease to the fully turbulent value. The model was initiated slightly 6cm downstream of the experimental transition point.

The results for the Schmidt and Patankar production term modification model are shown in figure 4.48. The transition length is 74% too short. The heat transfer level is too high throughout the entire domain, including the laminar region. The reason is a very high free stream turbulent kinetic energy had to be used to get transition to occur in the experimental transition region. This problem was extremely difficult

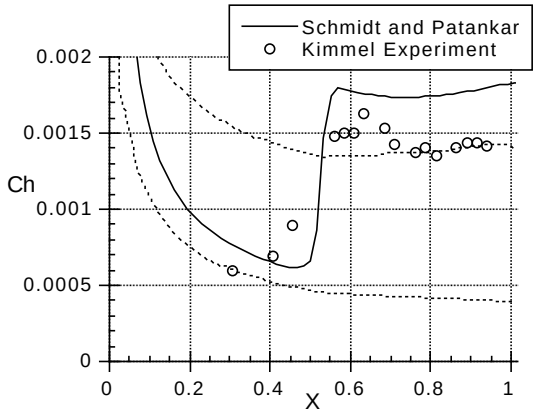

Figure 4.48: Schmidt and Patankar PTM results on Kimmel DPDX=1

to run. The initial conditions used for the zero pressure gradient case produced the similar results for this case as it did for the DPDX=4 case, transition occurs too early. What is disturbing is that the grid spacing difference normal to the wall between this grid and the DPDX=0 grid is less than 8%. The Schmidt and Patankar model is grid sensitive. Now for the DPDX=4 case, simply changing the free stream TKE produced transition in the correct point. However for this case, changing the free stream k and even ϵ could not move the transition point further downstream, the transition point would get stuck at a certain point in the domain. After almost 30 attempts, the best method found to force transition to occur at the correct location was to turn the model on 7 cm before the desired transition point with a high free stream k, 9.0%, and a low free stream ϵ. Unfortunately, this results in overprediction of the heat transfer throughout the domain.

The algebraic transition region model, shown in figure 4.49, matches the experimental data well at the beginning of transition, but it predicts the heat transfer entirely too high at the end of transition and for the turbulent region, the peak is overpredicted by over 20%. The model was started 6cm downstream of the experimental transition point because the transition length is slightly underpredicted.

Figure 4.50 shows the results for the linear combination model. The model is adequate at the beginning of transition as it passes through all 3 data points. It does not predict the peak in heat transfer at the end of transition, it is almost 15% too

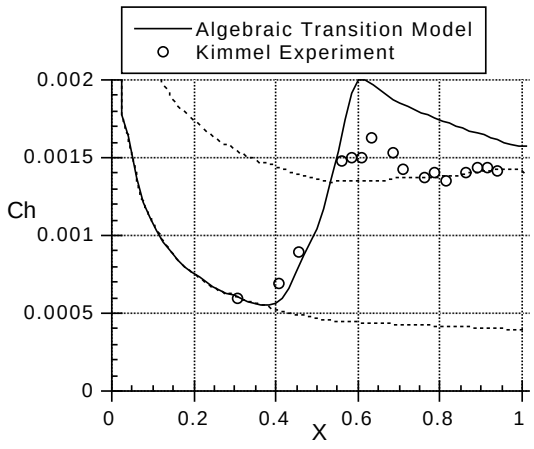

Figure 4.49: Algebraic Transition Model results on Kimmel DPDX=1

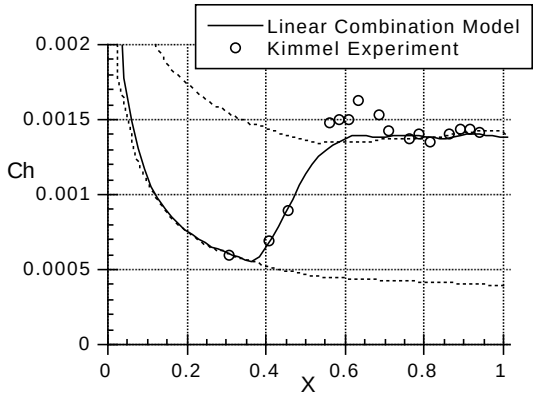

Figure 4.50: Linear Combination Model results on Kimmel DPDX=1

short. The model does predict the turbulent region well and the transition length is over 80% of the experimental length. The model was initiated at the approximate experimental transition point.

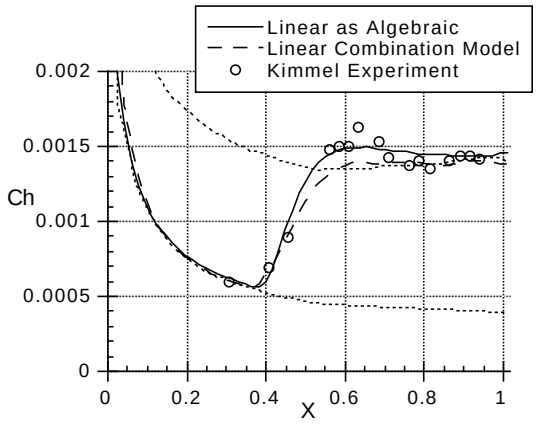

Figure 4.51: Linear Combination Model as Algebraic Transition Model results on Kimmel DPDX=1

Figure 4.51 shows the results for the linear combination model used as an algebraic transition region model. The length of the transition region has been reduced but the heat transfer has been raised to a value closer to the experimental values at the end of the transition region. Looking closely at this result, the computations pass through the first six data points which encompass almost all of the transition region.

Table 4.8: Model Performance Summary for Kimmel DPDX=1 case

Model	L_{model}/L_{exper}	Peak Ratio
Baldwin and Lomax	.21	1.02
Wilcox $K-\omega$	.46	1.02
Warren, Harris, and Hassan	.62	.98
Schmidt and Patankar PTM	.36	1.10
Algebraic Transition Model	.67	1.23
Linear Combination	.82	.86

Table 4.8 presents a summary of how the models performed on this case. Both ratios are prone to error as determining the peak value and the transition length for both the experimental and computed solutions is highly subjective. The first digit

may be the only significant digit. The Baldwin and Lomax model remains dismal at predicting the transition length but once again predicts the peak well, this time within 3%. The transition profile for with Wilcox $k-\omega$, the Warren, Harris and Hassan model, and the Schmidt and Patankar PTM transitions up to a peak but then never decrease down to the fully turbulent value. The two pure transition region models again predict the transition length well but the peak in heat transfer is mispredicted.

4.4.4 Kimmel DPDX=-1

This case and the case that follows (DPDX=-2) feature favorable pressure gradients. Considering all the cases presented before this one have been zero or adverse pressure gradients, this case is very important. The amount of data points at the beginning of transition is sparse (see figure 4.53), but it does manage to show the general shape of the transition region without much scatter. The data does not show a clear peak, but using the second data point as the beginning of transition and the eighth as the peak value produces an estimated transition length of 28cm. The peak heat transfer, taken as the eight data point, is $Ch = 1.35 \times 10^{-3}$.

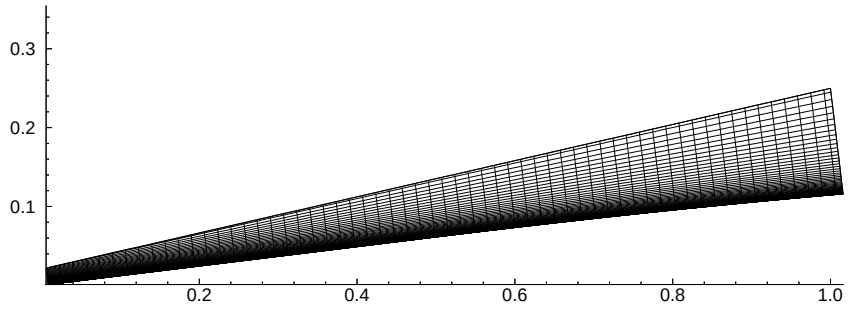

Figure 4.52: Grid for Kimmel DPDX = -1 case.

Figure 4.52 shows the 61x81 grid used for this case generated by Gridgen2D. The grid point closest to the wall was constrained at the boundaries to be 1.0×10^{-5} which results in a $y^+ \approx 0.1$. This cone is flared down, so the grid spacing at the middle of the grid will be slightly less than at the edges.

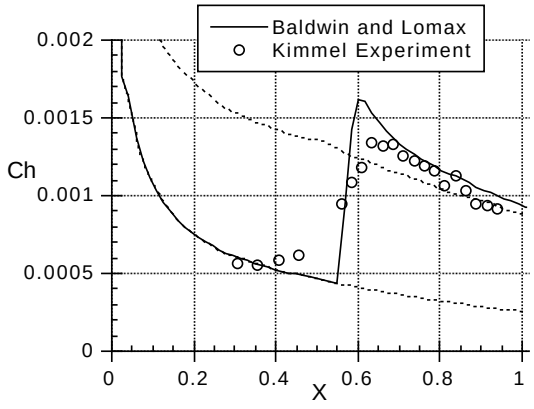

Figure 4.53: Baldwin-Lomax results on Kimmel DPDX=-1

Figure 4.53 shows the results for the Baldwin and Lomax model. The transition length is 82% too short which leads to an incorrect profile with a discontinuous slope at the beginning of transition. The peak is predicted 20% too high, but the turbulent region is predicted well. The overprediction of the peak in heat transfer could be due to where the model was initiated which was 15cm downstream of the experimental transition point. Starting the model further downstream might results in a lower peak heat transfer because the favorable pressure gradient causes the heat transfer to drop through the turbulent region. (See the results for the Baldwin-Lomax model on the DPDX=-2 case for a further discussion of this issue.)

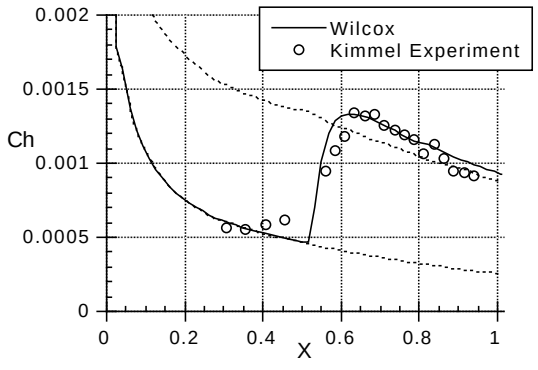

Figure 4.54: Wilcox result on Kimmel DPDX=-1

The Wilcox $k-\omega$ low Reynolds number results are shown in figure 4.54. The transition length predicted is only 36% of the experimental length. However, the

end of transition and the turbulent region are predicted well. The abrupt start of transition in the profile creates a discontinuous slope at the beginning of transition. The same initial conditions used for the zero pressure gradient case (DPDX=0) were used with this one and resulted in transition starting in the middle of the experimental transition region.

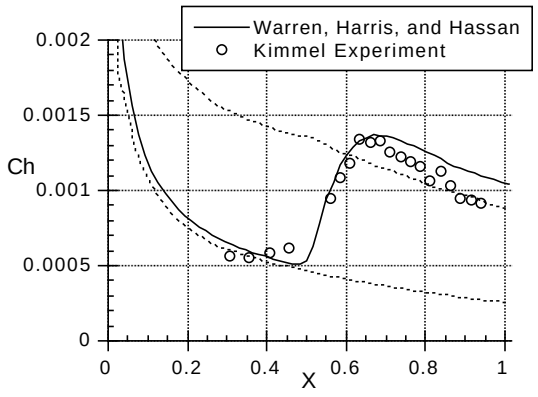

Figure 4.55: Warren, Harris, and Hassan results on Kimmel DPDX=-1

The Warren, Harris, and Hassan model, shown in figure 4.55, produces a smooth curve. However, the transition length is about 33% too short and the predicted heat transfer is slightly higher than experiment for the end of transition and the turbulent region. The peak is predicted but the heat transfer level never drops down to the fully turbulent values. The model was started 16cm downstream of the experimental start of transition.

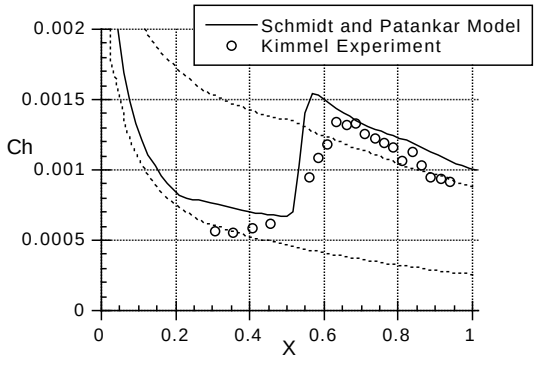

Figure 4.56: Schmidt and Patankar results on Kimmel DPDX=-1

Figure 4.56 shows the results for the Schmidt and Patankar model. The solution pulls away from the laminar boundary layer solution very early in the domain and stalls out there before finally transitioning to the fully turbulent value which leads to a predicted transition length 75% too short.

The initial conditions from the zero pressure gradient case (DPDX=0) were used with good success at forcing the transition point. It is notable that an 8% increase in the spacing of the grid at the wall drastically changed the way the model behaved but a 8% decrease had little effect.

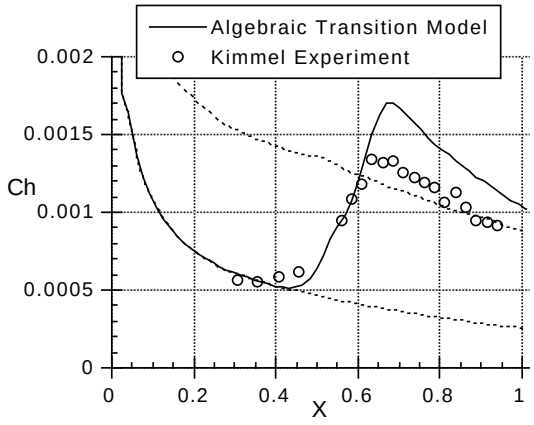

Figure 4.57: Algebraic Transition Model on Kimmel DPDX=-1

Figure 4.57 shows the results for the algebraic transition region model. The beginning of transition features a smooth curve but the end of transition and the turbulent regions are overpredicted by over 25%. The model was started 15cm downstream of the experimental start of transition.

The results for the linear combination model, shown in figure 4.58, are satisfactory. The transition length is predicted well, within about 15%. The turbulent region is computed correctly. Again, the only problem is the peak in heat transfer at the end of transition is not found. The model was started 18cm downstream of the experimental transition point.

Using the linear combination model as an algebraic transition region model, results shown in figure 4.59, produces a transition length that is too short. For the previous flows, higher heat transfer rates were found in the turbulent region, that is not true

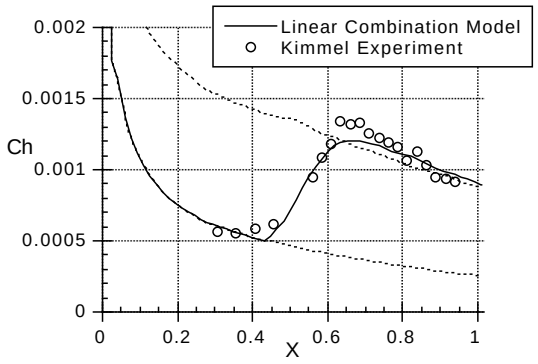

Figure 4.58: Linear Combination Model results on Kimmel DPDX=-1

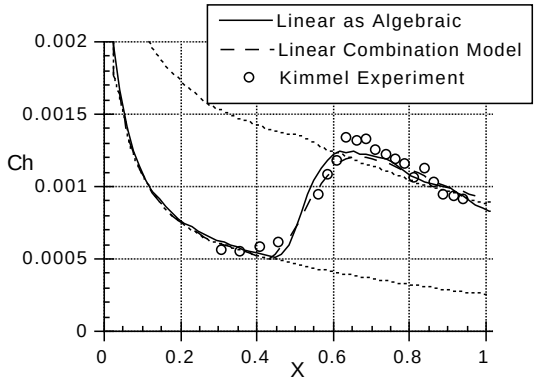

Figure 4.59: Linear Combination Model as an Algebraic Transition Model results on Kimmel DPDX=-1

for this case.

Table 4.9: Model Performance Summary for Kimmel DPDX=-1 case

Model	L_{model}/L_{exper}	Peak Ratio
Baldwin and Lomax	.18	1.20
Wilcox $K-\omega$	.36	.99
Warren, Harris, and Hassan	.67	1.02
Schmidt and Patankar PTM	.24	1.15
Algebraic Transition Model	.91	1.27
Linear Combination	.85	.90

Table 4.9 presents a summary of the models performance on the current DPDX=-1 case. Both ratios are prone to error as determining the experimental and computed peak values and transition lengths are highly subjective. These numbers should not be taken as hard facts, they merely are an attempt to quantify the accuracy of the profiles. The Baldwin and Lomax model suffers it worst outing so far as both the transition length and peak in heat transfer are poorly predicted. The Schmidt and Patankar PTM continues to feature irregular profiles. The last two models listed are the pure transition region models and they are able to adequately predict the length of transition but the peak in heat transfer is not predicted well.

4.4.5 Kimmel DPDX=-2

This case features a favorable pressure gradient that is stronger than the previous case (DPDX=-1). There are only 3 experimental data points for the beginning of the transition region (see figure 4.61), which does make it difficult to accurately determine how the models are performing at the beginning of the domain. The data points at the end of the transition region and the turbulent region provide a smooth curve showing the transitional profile with only a few instances of experimental data scatter. From the experimental data points, the transition length is estimated at roughly 25cm which is about 25% of the total domain.

Figure 4.60 shows the 61x81 grid used for this case generated by Gridgen2D. The grid point closest to the wall was constrained at the boundaries to be 1.0×10^{-5}

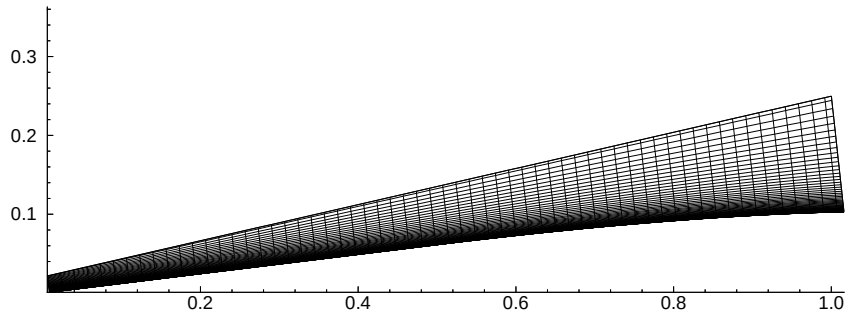

Figure 4.60: Grid for Kimmel DPDX = -2 case.

which produced a $y^+ \approx 0.1$. This cone is flared down to produce the favorable pressure gradient. Therefore, the grid spacing next to the wall at the center of the grid will be slightly less than at the edges.

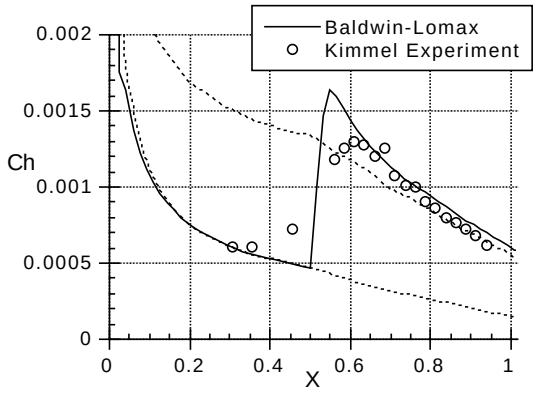

Figure 4.61: Baldwin and Lomax Model results on Kimmel DPDX=-2

The Baldwin and Lomax model, shown in figure 4.61, underpredicts the transition length by 80%. The transition profile is practically instantaneous. The peak in heat transfer at the end of transition is too high. But the heat transfer is predicted well in the turbulent region. As with the DPDX=-1 case, the overprediction of the peak in heat transfer could be due to where the model is triggered in the domain. Figure 4.62 shows the effect of triggering the model at different parts of the domain. The peak value is indeed a function of where the model is triggered, especially later in the domain where the fully turbulent heat transfer begins to severely drop because of the

pressure gradient. The heat transfer level in the turbulent region is also a function of where the model is triggered.

The "best" profile was chosen to be in the middle of the transition region, 15cm from the start of experimental start of transition. Since the transition length is almost instantaneous, it is desired to put it in the middle of experimental profile to slice through the experimental solution. A profile triggered later in the domain would have a more accurate peak value.

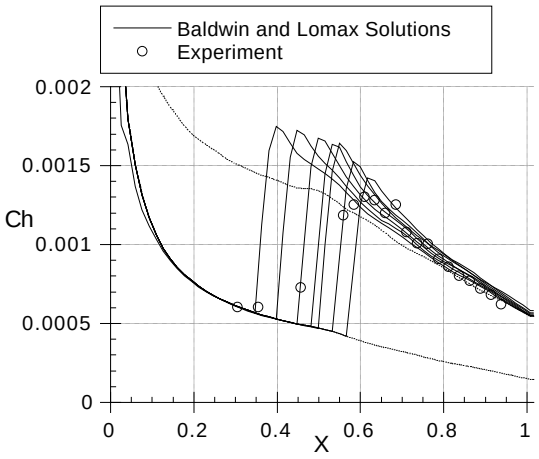

Figure 4.62: Baldwin and Lomax model triggered at different locations

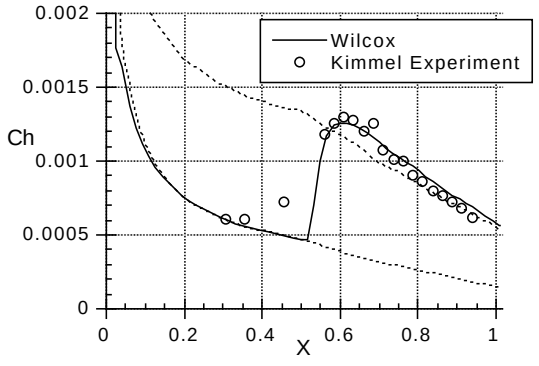

Figure 4.63: Wilcox results on Kimmel DPDX=-2

The Wilcox $k-\omega$ model, pictured in figure 4.63, predicts the transition length too short once again, about 66% short. The end of transition and the turbulent region

are predicted well but the transition profile does not have the correct shape. The same initial condition used for the zero pressure gradient case (DPDX=0) were used to trigger transition in the experimental transition region.

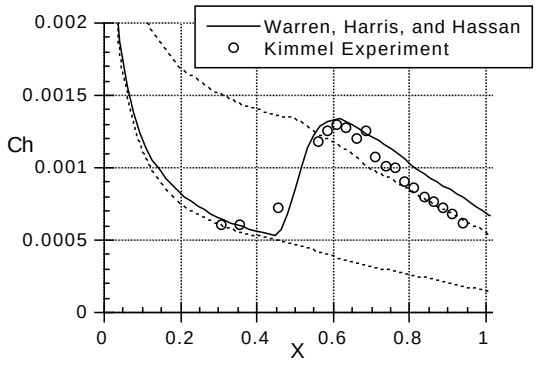

Figure 4.64: Warren, Harris and Hassan results on Kimmel DPDX=-2

The Warren, Harris, and Hassan model, featured in figure 4.64, underpredicts the transition length by about 33%, which is satisfactory. The heat transfer at the end of transition is satisfactory but the heat transfer is overpredicted for the turbulent region. The model was triggered 15cm downstream of the experimental start of transition.

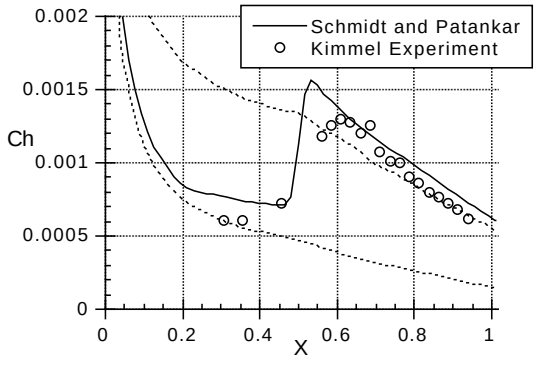

Figure 4.65: Schmidt and Patankar results on Kimmel DPDX=-2

The results for the Schmidt and Patankar model are shown in figure 4.65. The solutions pulls away from the laminar solution and stalls out before finally finishing transition leading to an undesirable transition profile with a transition region length of about 33% of the experimental length. The turbulent region is slightly overpredicted.

The initial conditions used for the zero pressure gradient case (DPDX=0) were used on this case. It was thought that the poor transition profile shape might be due to the set of initial conditions used. Other combinations of initial conditions were found that forced transition to occur in this location and they suffered similar problems.

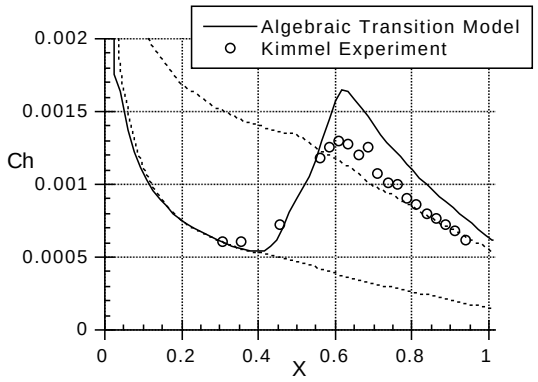

Figure 4.66: Algebraic Transition Model results on Kimmel DPDX=-2

Figure 4.66 shows the results for the algebraic transition region model. The beginning of transition seems to be modeled well, at least in terms of the limited data points. The transition length is even predicted within 15%. However, the heat transfer at the end of transition and in the turbulent region are badly overshot. The model was started 12cm downstream of the experimental start of transition.

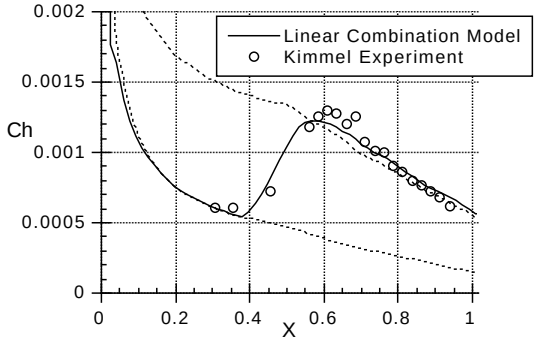

Figure 4.67: Linear Combination Transition Model results on Kimmel DPDX=-2

The linear combination model does a satisfactory job of predicting the transition

length within about 20%, see figure 4.67. Unfortunately, the peak in heat transfer is not resolved, though the heat transfer is low by only 7%. The heat transfer in the turbulent region is well predicted. The model was started 13cm downstream of the experimental start of transition.

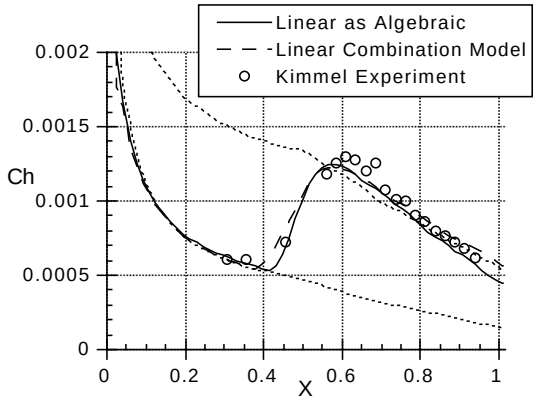

Figure 4.68: Linear Combination Transition Model as Algebraic Transition Model results on Kimmel DPDX=-2

Figure 4.68 shows the results computed by using the linear combination model as an algebraic transition region model. The transition length is once again too short. Surprisingly, the heat transfer in the turbulent region is predicted lower than using the model is it was intended.

Table 4.10: Model Performance Summary for Kimmel DPDX=-2 case

Model	L_{model}/L_{exper}	Peak Ratio
Baldwin and Lomax	.20	1.26
Wilcox $K-\omega$	.33	.97
Warren, Harris, and Hassan	.67	1.03
Schmidt and Patankar PTM	.33	1.20
Algebraic Transition Model	.87	1.27
Linear Combination	.80	.94

A summary of how the models performed on the current case is provided in table 4.10. Both ratios are prone to error as computing the transition length and peak value based on the experiment and computations is subjective. The ratios are an attempt

at quantitatively representing the profiles and only the first digit should be treated as significant. Three of the models severely overpredict the peak in heat transfer. Again, the Schmidt and Patankar PTM pulls away from the laminar solution too early. All the models underpredict the transition length with some being closer than others.

Chapter 5

Summary

5.1 Overview

This chapter provides a model by model summary of how each model performed. Addressed will be how the results looked, how easy the model was to run, and the computational expense of the model. Additionally, the convergence of the model to the steady state solution will be discussed. All the problems are space marched to the steady state solution, where the first plane is converged and then the next plane is converged. Slowly, the whole domain is converged using this process. The amount of orders that the residual was converged will be reported for each of the models.

In some ways this chapter will review what was stated in the previous results chapter. In other ways it will go more in depth and explore the usefulness of the model.

5.2 Baldwin and Lomax Model

The Baldwin and Lomax model was by far the simplest transition region model. The transition length was always predicted too short but that is to be expected considering this model is basically just an on/off switch. On the plus side, the peak in heat transfer in the transition region was usually predicted adequately. Another positive aspect of the model is that it is easy to use. The starting point of transition is implemented

into the model and transition occurs at that very point. The model will always transition, that is not a concern. The associated run times are very short because this is a simple algebraic turbulence model which can be converged relatively easily to the steady state. Each plane was converged four orders in under 250 iterations.

Another plus is the ease of implementation. The Baldwin and Lomax turbulence model is implemented in many CFD codes. To make the model simulate transition, all that is needed is a few lines of code setting the eddy viscosity to zero in the laminar region. Or if it is not desired to tamper with the code, the domain can be broken up into two different zones, the first laminar and the second turbulent much like Holden and Chadwick [74] did with GASP. The solutions generated with this model might not be as accurate as other models, but they are much more accurate than modeling the given domain as fully laminar or fully turbulent.

Because the predicted transition length was always underpredicted, the model was triggered downstream of the experimental transition point in roughly the middle of the experimental transition region. The resulting heat transfer profile would cut through the longer experimental transition profile which was judged to be the most accurate use of the model. For cases where the experimental data is not given, the model should be started downstream of the experimental transition point.

5.3 Wilcox Low-Reynolds number $k-\omega$ Model

It is notable that the Wilcox model did not require any modification to the turbulence model to simulate transition, only to the boundary condition. While almost all the other models had formulas to simulate the transition region, this model was assumed to have the capability of modeling the transition region built in to it. The concept of the roughness strip and its analogy to the use of roughness strips in experiments make the model seem very robust. The use of the roughness strip made implementation simple, no modifications are need to the turbulence model itself to simulate the transition region, only to the boundary conditions. As the computational domains evolve from simple cones and ramps to complicated configurations, the model would not require any changes whereas the other models would require severe modifications

for complicated geometries.

Unfortunately, the model was very hard to run. The values suggested by Wilcox for the roughness value and roughness strip length never resulted in transition. Specifying the near wall behavior of ω was tried with some limited success. Wilcox suggests that the initial TKE in the domain should be very small, $10^{-15}U_\infty^2$. When this value was used, it was extremely difficult to force transition to occur. A roughness value several orders of magnitude greater than suggested by Wilcox had to be used and usually the result was a crashed run on the roughness strip. Instead a much higher value of free stream TKE had to be used, sometimes as large as $10^{-4}U_\infty^2$. With the initial conditions used for the Kimmel case, the flow would transition even without the roughness strip, just later in the domain. While the designed function of the model was that the use of the roughness strip could force the flow to transition at any desired point, the reality is that the initial conditions were extremely important and the roughness strip only had a small affect.

Ideally, it was desired to run the model with transition occurring at several different points in the experimental transition region and then choose the most accurate one. However, due to the difficulty in running the model, great effort was required to get one run with transition occurring in the experimental transition region. Ten or more runs had to be done for most of the cases to produce a computed profile in the experimental transition region. Considering that this is a two equation model which is very stiff, the computational expense was very large.

The initial residual on each plane at times was very high, around 1.0×10^6 because ω can be very large near the wall. However, the residual would decrease by a 6 or 7 orders in the first 10 iterations. Using the convergence criterion from the algebraic turbulence models of converging each plane 4 orders results in each plane running less than 10 iterations and the true steady state values had not been reached. So the convergence criteria per plane was 8 or more orders.

The solutions featured transition lengths that were usually too short, some of the profiles were basically instantaneous. At times, the model predicted a peak entirely too high.

5.4 Schmidt and Patankar Production Term Modifications

Considering the popularity of two-equation turbulence models, the Schmidt and Patankar production term modifications have a lot of merit. They are addressing the problems usually found when using a two equation model to simulate the transition region, i.e. predicting transition too early and a length too short instead of ignoring those facts. The most severe problem was that this work is for compressible flow and the Schmidt and Patankar model has been calibrated for incompressible flows, so not only will the model not predict transition correctly, even the starting criterion given is invalid.

Considering that the parameters A and B are only functions of the free stream turbulent kinetic energy seems to imply that the free stream k uniquely determines the transition point. That is not true. The starting point of transition was found to be a function of a multitude of variables and flow conditions, which made this model extremely hard to run. A dozen or more runs had to be done until a correct combination was found to force transition to occur in a location that would maximizes the accuracy of the computed profile with the experimental data. Combining the number of runs with the long run times due to the fact that this is a stiff two equation turbulence model led to expensive computational costs.

Residual convergence to the steady state would frequently stall out. For the Kimmel and Stainback cases, the residual would only stall out in the laminar region and at the beginning of the transition region. At the end of the transition region and through the turbulent region, the residual would converge. For the Holden and Chadwick case, almost all the planes would stall out after about 3.5 orders, even in the fully turbulent region.

The resulting heat transfer plots for some of the cases were very good, this model produced the best results for the Holden and Chadwick Compression ramp case. However, for other cases, the solution is not satisfactory. For the Stainback *et al.* case, the solution was too wavy. For some of the Kimmel cases, the profiles do not look correct in that they peel away from the laminar solutions for a while before they

spike up into the turbulent value. The Kimmel cases also highlighted the models undesired sensitivity to the grid spacing at the wall.

5.5 Warren, Harris, and Hassan Model

The Warren, Harris, and Hassan model unique feature was incorporating the effect of first and second mode disturbances on the transition region. Unfortunately, the effect seen on the transitional heat transfer was negligible which reduced this model to an algebraic transition region model application of the intermittency model from the linear combination model using a one-equation turbulence model for the eddy viscosity. That being said, the results were usually quite satisfactory.

Considering the one governing equation used in this model was changed from the form presented in the paper, there was a definite concern about how this model would do on fully turbulent flow. Several fully turbulent cases were run and the modified one equation model performed well.

Converging the one equation model to the steady state was complicated by the fact that this was a one equation model implemented in a code for two equation models. The residual calculations included the second turbulence variable normally reserved for ϵ and ω, the resulting residual calculated reflected the fixed value of the second turbulence parameter. The residual would rarely change during the iteration process so it was impossible to see if the solution was converging on the given plane. Convergence studies were done where each plane was run 1000 iterations and 500 iterations and the resulting solutions looked identical which shows that 500 iterations provided enough time for each plane to converge to the steady state.

Forcing the model to predict transition in the correct location was simple. The transition point was inputed to the model and transition would usually start at the next cell downstream. For some of the cases, there was a slight lag of several cells. The transition point would be changed and the resulting profiles would be compared with the experimental profiles and the most accurate one is then chosen. Because the transition length is predicted adequately, the model can be triggered at the experimental transition point.

5.6 Algebraic Transition Region Model

The algebraic transition region model of ONERA/CERT performed well on the Stainback *et al.* supersonic cone case and that generated a lot of optimism about the model. The next case run was the Holden and Chadwick compression ramp and the model never transitioned which revealed the flaw of the model. The model is based on the growth in momentum thickness and for cases with severe pressure gradients where the momentum thickness decreases, the model does not transition.

The use of momentum thickness makes implementation and use of the model difficult. Finding the edge of the boundary layers is required which can be difficult for complicated geometries. On the positive side, this model is very easy to run since all it depends on is the starting point of transition.

For the calculations presented, the algebraic turbulence model of Baldwin and Lomax was used to generate the eddy viscosity which lead to inexpensive run times. The model was converged to four orders in less than 250 iterations per plane.

The Baldwin and Lomax model has been shown to be inaccurate for some types of flows, so inaccurate solutions by the algebraic transition region models can be linked to the choice of turbulence models.

Ideally this transition region model can be run with any turbulence model, but in reality that was not true. Originally, the transition function was implemented into the routine that adds the eddy viscosity with the molecular viscosity to form the effective viscosity and any two equation model used with the transition region model would result in the run crashing. The transition function was then moved into the routine that computes f_μ which multiplies the eddy viscosity and the Chien $k-\epsilon$ model was able to generate solutions. The Lam and Bremhorst $k-\epsilon$ model and the Wilcox $k-\omega$ model with and without the low-Reynolds number corrections all crashed when the flow would begin to transition. For the Kimmel case, the algebraic transition region model using Chien for the turbulence produced a satisfactory profile shown in figure 5.1. While the transition length is too short, the heat transfer level at the end of transition and in the turbulent region is predicted well. Unfortunately, using Chien with the algebraic transition region model does not always work well.

Figure 5.2 shows the results for the Stainback cone. At the beginning of transition, the profile spikes up before recovering to a normal profile. The underlying problem is that the $k - \epsilon$ model can qualitatively simulate the transition region. In the laminar region, the transition function is zero which forces the eddy viscosity to zero which lowers the TKE. At the start of transition, the transition function is some small finite value which causes the TKE to grow. The transition and turbulence model each want to simulate transition and the combination leads to inaccurate results.

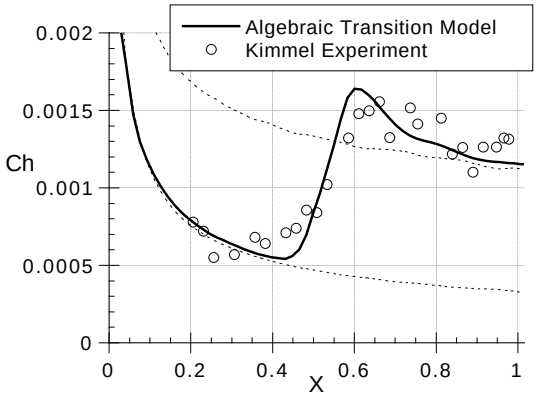

Figure 5.1: Algebraic Transition model using Chien on Kimmel DPDX=0

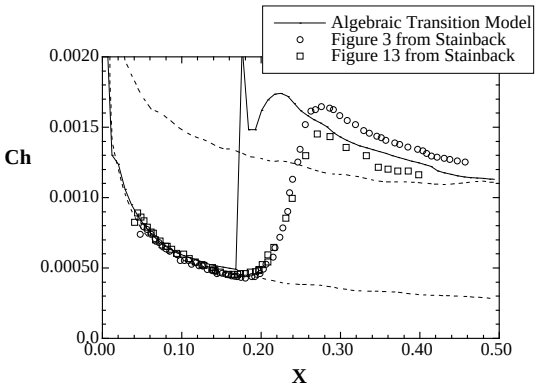

Figure 5.2: Algebraic Transition model using Chien on Stainback cone

5.7 Linear Combination Model

The linear combination model has the strongest physical basis of any model implemented. Unlike most other models which simply present empirical relations to mimic the transition region, the linear combination model presents a physical idea behind it. Since the transition region is sometimes laminar, sometimes turbulent, it can be represented as a combination of the two flows. People have argued that the transition region cannot be represented as a combination of laminar and turbulent regions, but the idea does have its merits. Nobody argues with the equations presented to determine the intermittency, they are very well respected in the literature.

Using two solutions, the laminar and the turbulent, to generate third solution at first appears to be expensive but it is not. After the laminar solution is generated, the turbulent solution must be generated with the boundary layer starting at the desired transition point. So really for each new transition point, only one solution had to be generated. The program that takes the two solutions and generates the transitional solution took under half a minute to run, it is not considered in the expense of using the model.

In terms of converging to the steady state, the fully laminar solution and fully turbulent solution starting at the transition point are standard type CFD solutions with simple convergence to the steady state.

The solutions in general were acceptable. The one consistent problem is that the peak is not predicted. That is to be expected considering the model cannot predict a value above the turbulent value that is used for the calculation. Because this turbulent value comes from a boundary layer that starts at the transition point, this turbulent value is higher at the beginning than the turbulent value computed from the beginning of the domain. Figure 4.23 shows the different parts that are combined to form the transitional solution. The turbulent contribution is seen to spike up at the beginning of transition and then gradually approach the fully turbulent value. For many of these cases, the predicted transition length is so long that by the time that significant parts of the turbulent contribution are being added in, the turbulent contribution is about the fully turbulent value, so the total transitional solution cannot rise above

the fully turbulent solution so the peak is not predicted.

Another problem addressed in the results section is the transition length. The compressibility correction for the model requires reading the value of N_o of a graph in [12]. The relationship between N_o and Mach number expressed in the graph is stated to be a tentative relationship. For the Stainback supersonic cone and the Holden and Chadwick Compression ramp, the value of $N_o = 0.2 \times 10^{-3}$ read off of the graph produces transition lengths that are too long, a more conservative value of $N_o = 0.5 \times 10^{-3}$ produces better results. However, for the Kimmel cases, a value of $N_o = 0.2 \times 10^{-3}$ produces an acceptable transition length that at times is too short.

The implementation of this model is confused by many authors, as highlighted in the transition region models section 3.7. Many people use the intermittency function from the linear combination model as an algebraic transition region function to proportion the amount of eddy viscosity added to the molecular viscosity. The results using this method turn out to be very similar to their linear combination counterparts but there are some noticeable differences. The transition length is always predicted shorter. For the cases with no pressure gradient and adverse pressure gradients, the heat transfer predicted now at the end of transition and through the turbulent region is significantly higher.

Chapter 6

Modifications

6.1 Introduction

The previous sections have presented some of the best transition region models found in the literature and tested them on several cases. Clearly, no one model is perfect. All the models have some sort of deficiency, many of which are due to the fact that the model is being used on high speed cases, instead of the incompressible cases the model was designed to run on. Other problems are because the models were implemented in a Navier-Stokes code instead of a boundary layer code like they were originally used.

One of the goals of this work set forth in the beginning of the introduction was to make modifications to the models. Here these are presented. Ideally, modifications to the models should reflect physical effects, they should improve the physics of the model. However, with the original models being largely empirical for incompressible flow, the most obvious course of action to improve the model is to recalibrate it for the hypersonic cases featured here. Other modifications do attempt to improve the physics of the model

6.2 Schmidt and Patankar PTM

The Schmidt and Patankar production term modifications showed great promise but had some severe problems that all seemed to be due to the model being empirically

calibrated for incompressible flow and being tested on compressible flow. Many, long expensive runs were necessary to find the right combination of initial conditions to produce transition in the desired location. The starting criterion was invalid. The model did not display the sole functionality to the free stream TKE. The resulting transitional profile was often too short.

The first problem to be addressed is running the model. The most efficient method for running the model would be to turn the model on at the transition point instead of turning the model on at the beginning of the domain and letting the initial conditions determine the starting point as it was intended. Looking at the physics of how transition starts, turbulent spots are formed which coalesce downstream and form the turbulent region. While this is very much a three dimensional unsteady phenomena, it will be attempted to simulate these physics in steady two dimensions by introducing a turbulent spot in one cell at $y^+ \approx 10$. The turbulent value will be the free stream TKE and it will be enforced as a minimum downstream of that point at the given y^+ location only. The choices of $y^+ \approx 10$ and the value of the TKE spot were a bit arbitrary. However, numerical experimentation showed that these values produced a minimal immediate effect on the heat transfer and the TKE was able to spread quickly from this spot into the whole boundary layer. This is how the modification allows the transition point to be picked. Originally the model would transition by having free stream TKE work its way down into the boundary layer which was a long process. Now the boundary layer starts off with a TKE spot which quickly grows which allows the flow to transition almost from the location that the model is started at, which was the desired outcome. While not rigorous, the physics of the model have been improved. Spot formation has been qualitatively reproduced in steady, two dimensions.

Figure 6.1 shows the first modified form of the model using the spot method to start transition on the Kimmel DPDX=0 case. Transition has started almost immediately downstream from where the model was started. However, the plot highlights the next problem that must be addressed with the model, the transition profile is too short.

As was mentioned in the beginning of the current section, the Schmidt and

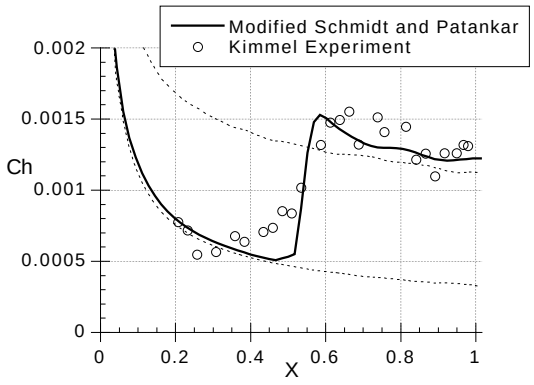

Figure 6.1: First modification of Schmidt and Patankar on Kimmel DPDX=0

Patankar PTM model was empirically calibrated for incompressible flow and is invalid for the compressible cases of this paper. The model is designed to limit the production of TKE but it was found that the limits were never enforced because they were always larger than the actual computed production. The limit needs to be decreased to be effective.

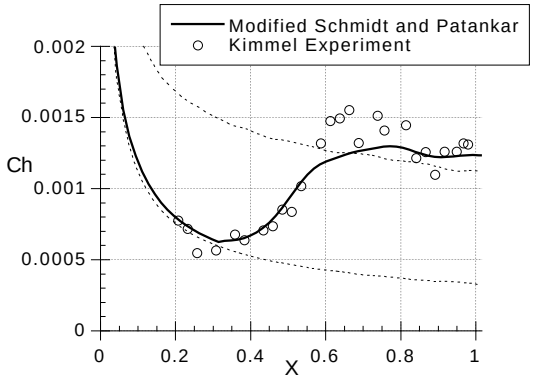

Figure 6.2: Second modification of Schmidt and Patankar on Kimmel DPDX=0

Figure 6.2 shows the results using the TKE spot procedure and multiplying the maximum production allowed by .001, which was found through numerical experimentation. The maximum production of TKE allowed has been reduced. The transition length has been dramatically increased. The solution does feature a discontinuous slope at the beginning of transition due to the TKE spot. While the beginning of transition is predicted well, the end of transition is not. The heat transfer is notably

too low, the peak is not predicted. The lower maximum production produces the correct curve at the beginning of transition but does not allow the production to grow fast enough at the end of transition to produce the peak. Therefore, the maximum production should be small at the beginning of transition and then be allowed to grow quickly for the end of transition. An exponential function was chosen for this purpose based on the stream wise distance over the Narasimha transition distance λ.

$$P_{k_{max}}^{new} = .0005 \times e^{\cdot 2\frac{x-xt}{\lambda}} \times P_{k_{max}}^{old} \tag{6.1}$$

x is the stream wise distance and xt is the stream wise location of the start of transition. $P_{k_{max}}^{old}$ is the value given by the formula from Schmidt and Patankar and $P_{k_{max}}^{new}$ is the value used. λ is defined in section 3.7 on the linear combination model. λ is a function on N_o which is a tentative function of the Mach Number, which has been discussed in the Results and Conclusion chapters. Unfortunately, the modification of the maximum production allowed is not based on any physical effects. However, the linear ramp function was empirical so modifying the ramp function to produce better results is justified.

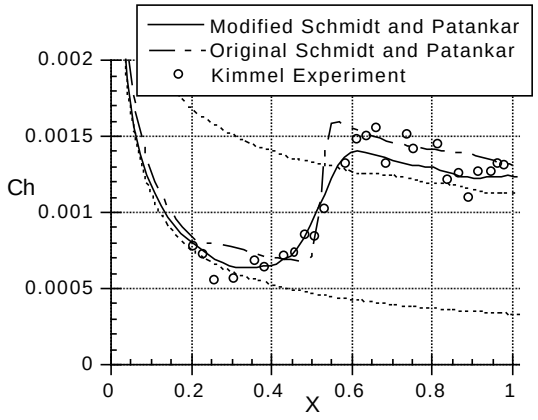

Figure 6.3: The modified Schmidt and Patankar PTM on Kimmel DPDX=0

Figure 6.3 shows the results for the final modified Schmidt and Patankar model on the Kimmel DPDX=0 cone. The transition length is accurately predicted within 2%. The peak in heat transfer at the end of transition is underpredicted by 10%. The turbulent region is predicted within the data scatter. Overall, the agreement

has been dramatically improved over the original version of the model, which is also shown. However, this is just for one of the cases. Results are shown for the modified model on all the cases.

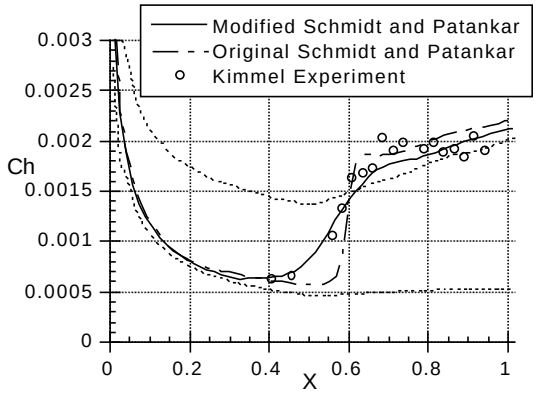

Figure 6.4: The modified Schmidt and Patankar PTM on Kimmel DPDX=4

Figure 6.4 shows the modified Schmidt and Patankar model on the Kimmel DPDX=4 flared cone. The transition length is overpredicted by 33% but looking at the solution, the model passes through the first four experimental data points. The peak is underpredicted by almost 15%. The overall agreement is satisfactory and is seen to be much more accurate than the original version of the model.

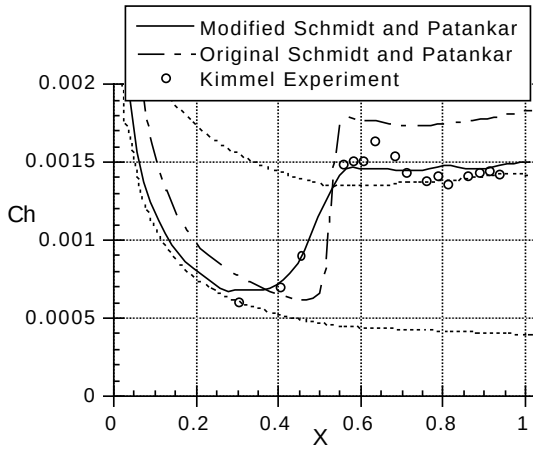

Figure 6.5: The modified Schmidt and Patankar PTM on Kimmel DPDX=1

Figure 6.5 shows the modified Schmidt and Patankar model on the Kimmel

DPDX=1 flared cone. The transition length is underpredicted by 23% but it should be noted that the lack of data points and the scatter in the data points that are given make determination of the experimental transition length prone to error. Clearly, the modified model is much more accurate than the original version model which overpredicts the heat transfer in the laminar, transition and turbulent regions due to problems with running the model (See section 4.4.3 for further explanation).

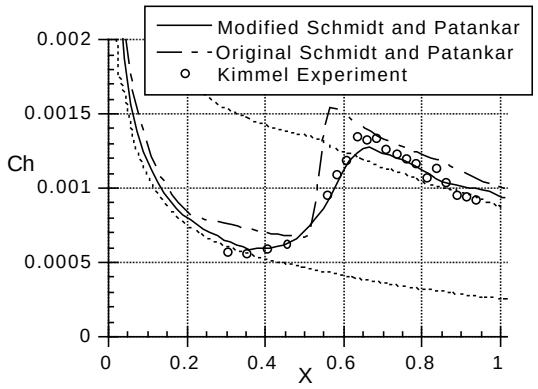

Figure 6.6: The modified Schmidt and Patankar PTM on Kimmel DPDX=-1

The results for the modified Schmidt and Patankar model on the Kimmel DPDX=-1 flared cone are shown in figure 6.6. This data case features good experimental data which makes determination of the experimental transition length more accurate. The model predicts a transition length within 10%, which is satisfactory. The entire domain is predicted within the slight experimental scatter. Again, the modified model is much more accurate than the original version, which is shown on the same plot.

Figure 6.7 shows the results for the modified Schmidt and Patankar model on the Kimmel DPDX=-2 case. The plot shows that the transition length is predicted well, but measuring from minimum to maximum heat transfer shows a transition length that is almost 20% too short which is not indicative of how well the model did. The peak is predicted within a couple percent. In general, the predicted heat transfer is always close to the experimental data points leading to an acceptable solution. In contrast, the original model only predicts the turbulent region well.

The results for the modified Schmidt and Patankar model on the Stainback cone case are shown in figure 6.8. $N_o = 0.5 \times 10^{-3}$ was used because this was found to

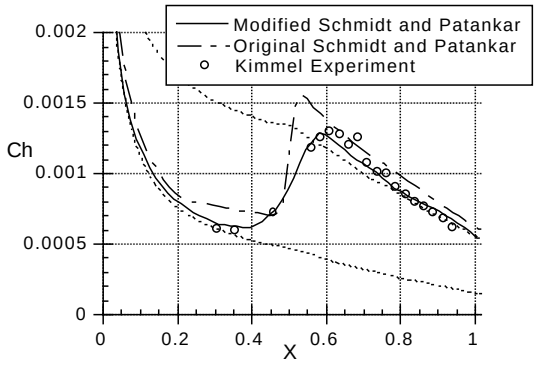

Figure 6.7: The modified Schmidt and Patankar PTM on Kimmel DPDX=-2

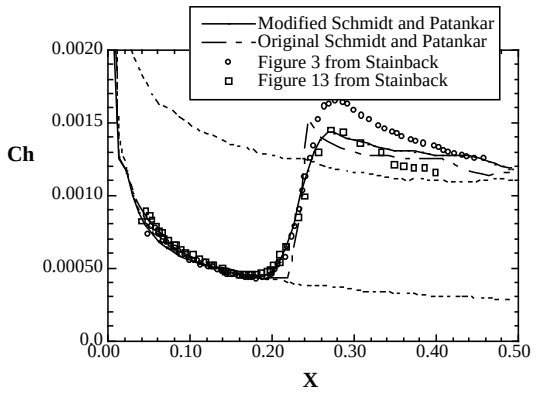

Figure 6.8: The modified Schmidt and Patankar PTM on Stainback case

produce the best results for the linear combination model. The transition length is underpredicted by 25% but looks acceptable on the plot. Overall, the results here are satisfactory. The heat transfer in the turbulent region is well within the experimental scatter.

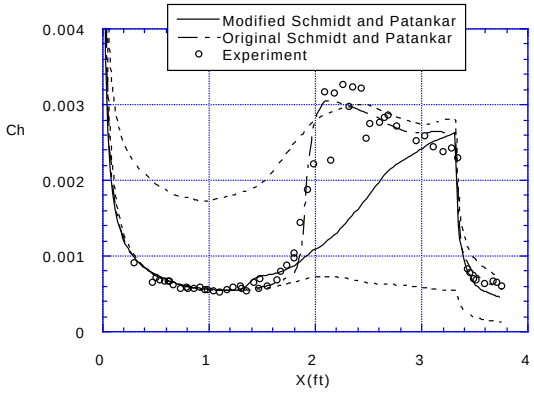

Figure 6.9: The modified Schmidt and Patankar PTM on Holden and Chadwick compression ramp

Figure 6.9 shows the results for the modified Schmidt and Patankar model on the Holden and Chadwick compression ramp. $N_o = 0.5 \times 10^{-3}$ was used because this was found to produce the best results for the linear combination model. The transition length is grossly overpredicted which makes the transition profile unsatisfactory. The unmodified Schmidt and Patankar model, also shown in the plot, performed very well for this case. Lowering the maximum production caused the transition length to dramatically increase to an undesirable length.

Table 6.1 presents a summary of the performance of the modified Schmidt and Patankar model versus the unmodified, original version. The modified version performs worse for the Holden and Chadwick but every other case feature dramatic improvements. The numbers in the graph reflect the improvement in transition length prediction. The original version does predict the peak slightly better than the modified version. However, that is far out weighed by the drastic improvement in the shape of the profile. What is not featured in the table is that the unmodified version is much simpler to run than the original version. The modified version required a handful of runs in order to place the transition point in the correct location while

Table 6.1: Modified Schmidt and Patankar Model Performance Summary

Test Case	Modified Model		Original Model	
	L_{model}/L_{exper}	Peak Ratio	L_{model}/L_{exper}	Peak Ratio
Kimmel DPDX=0	.983	.895	.272	1.027
Kimmel DPDX=4	1.333	.866	.424	.918
Kimmel DPDX=1	.770	.894	.360	1.100
Kimmel DPDX=-1	1.088	.942	.242	1.147
Kimmel DPDX=-2	.811	.981	.333	1.201
Stainback	.738	.927	.25	.992
Holden and Chadwick	2.775	-	.552	.938

the original version usually required 10 or more, which means huge savings in computational costs. The results for the Holden and Chadwick compression ramp are disappointing but more improvements to the model are currently being investigated.

In review, dramatic improvements are seen in most profiles. While it is true that the improvements are seen for only a limited number of cases and might not be valid for other cases like the Holden and Chadwick case, the method of the improvements is still valid. The turbulent spot method clearly enables the transition location to be input into the model and it is also seen that the maximum production allowed should grow by an exponential function instead of a linear profile. More work needs to be done to come up with modeling constants that are valid for a larger range of test cases.

6.3 Algebraic Transition Region Model

The algebraic transition region model performed well on the Stainback cone but showed problems with the rest of the test cases. The Holden and Chadwick test case featured a severe adverse pressure gradient which caused the momentum thickness to decrease which resulted in the model not transitioning. For the Kimmel cases, the model overpredicted the end of the transition region and the entire turbulent region.

The overprediction most likely results from the fact that the transition function is an empirical function originally calibrated for low speed flow. The high speed

corrections only address the change in transition length. The empirical transition function can be recalibrated for high speed flow by reducing the maximum value of the transition function ϵ_t. Looking at a graph of the transition function, figure 3.2, shows the current maximum is 1.5. It was found through numerical experimentation that reducing the maximum value to 1.1 will lower the predicted heat transfer to an adequate level for the cases presented here. While this solution is only valid for the cases shown here, it highlights the fact that the transition function formula is not valid for high speed flow. The resulting modified empirical equations for ϵ_t are:
For $0 < \chi_1 \leq 0.25$,

$$\epsilon_t = 1 - \exp\left\{-4.5\left[\chi_1\left(1 + 0.02M_e^2\right) - 0.005M_e^2\right]^2\right\} \tag{6.2}$$

For $0.25 < \chi_1 \leq 0.535$,

$$\epsilon_t = 18.628\chi_1^4 - 55.388\chi_1^3 + 52.369\chi_1^2 - 16.501\chi_1 + 1.893 \tag{6.3}$$

For $0.535 < \chi_1 \leq 2.785$,

$$\epsilon_t = 1.05 - 0.05\sin\left[\pi\left(0.444(\chi_1 + .215) - 0.833\right)\right] \tag{6.4}$$

For $\chi_1 > 2.785$,

$$\epsilon_t = 1 \tag{6.5}$$

The maximum value of ϵ_t is reached at the end of equation (6.3). Changing the limit in equations (6.3),(6.4) from 0.75 in the original set of equations (3.45) to a value of 0.535 reduces the maximum ϵ_t to 1.1. The value of χ_1 is offset in equation (6.4) to reflect the new limit and several coefficients have been changed for the new maximum value. In addition, since the peak now occurs at a χ_1 of 0.535 instead of 0.75, the growth of χ_1 will be limited by

$$\chi_1 = \frac{0.535}{0.75}\left(\chi_1 - \chi_0\right) + \chi_0 \tag{6.6}$$

where χ_1 is the same

$$\chi_1 = \frac{\frac{\theta}{\theta_{t0}} - 1 + 0.005M_e^2}{1 + 0.02M_e^2} \tag{6.7}$$

and χ_0 is the value of χ_1 at the beginning of the transition region where $\frac{\theta}{\theta_{t0}} = 1$ or

$$\chi_0 = \frac{0.005 M_e^2}{1 + 0.02 M_e^2} \tag{6.8}$$

Figure 6.10 shows the results for the modified algebraic model on the Kimmel DPDX=0 case. Clearly, the heat transfer has been reduced in the turbulent region resulting in a more accurate solution than the original model which is shown for comparison. The transition length is predicted 13% too short, which is an improvement over the original model. The solution is predicted well in the turbulent region.

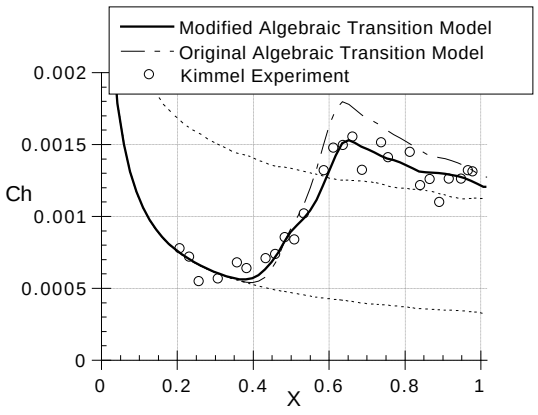

Figure 6.10: Modified Algebraic Transition Model on Kimmel DPDX=0

Figure 6.11 shows the results for the modified algebraic transition region model on the Kimmel DPDX=4 case. The transition length is predicted within 10%. The heat transfer in the turbulent region is predicted more accurately than before.

The results for the modified algebraic transition region model on the Kimmel DPDX=1 case are shown in figure 6.12. The transition length and peak heat transfer are both predicted within a few percent. Clearly, the model is much more accurate than the unmodified version.

Figure 6.13 shows the results for the modified algebraic transition region model on the Kimmel DPDX =-1 case. Again, the transition length and peak in heat transfer are predicted within 4% which is excellent. While the solution is much more accurate than the unmodified form, improvements could still be made. The transition profile

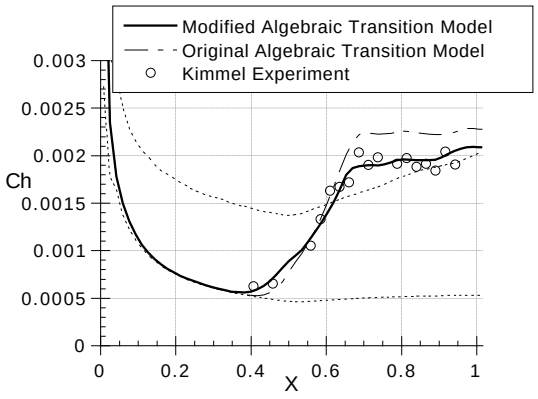

Figure 6.11: Modified Algebraic Transition Model on Kimmel DPDX=4

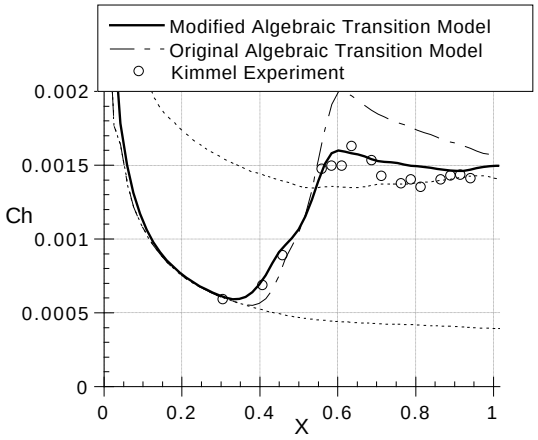

Figure 6.12: Modified Algebraic Transition Model on Kimmel DPDX=1

does have a slight wave in it and the heat transfer at the end of the turbulent region is slightly too high.

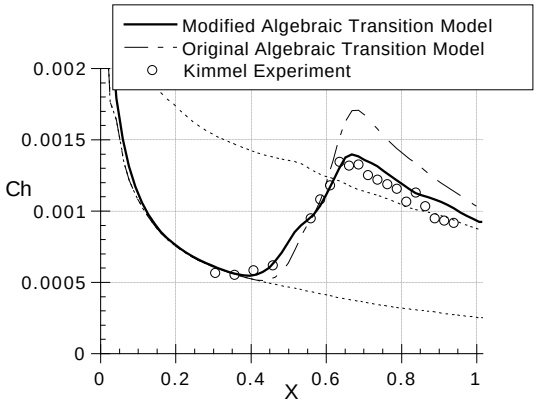

Figure 6.13: Modified Algebraic Transition Model on Kimmel DPDX=-1

Figure 6.14 presents the results for the modified algebraic transition region model on the Kimmel DPDX=-2 cone. The transition length and peak in heat transfer is within 6% of the experimental results. The predicted heat transfer is slightly above the data points in the turbulent region but very close. On the downside, the bend in the transition profile remains.

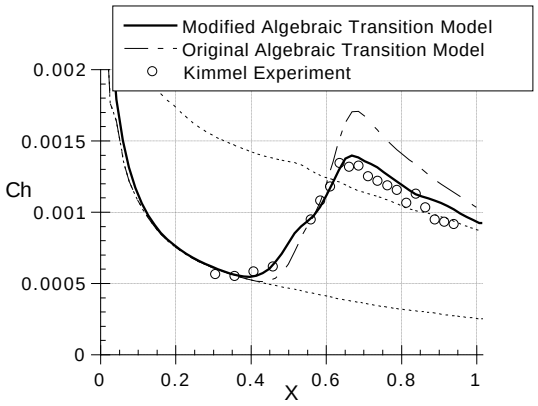

Figure 6.14: Modified Algebraic Transition Model on Kimmel DPDX=-2

The results for the modified algebraic transition region model on the Stainback cone are shown in figure 6.15. While the results for the original model were considered the best of any model for this case, the modified model performs even better. The

peak in heat transfer is predicted within 3% of the average of the two peaks. The transition length is within 2%. On the downside, there is a bubble in the solution in the turbulent region.

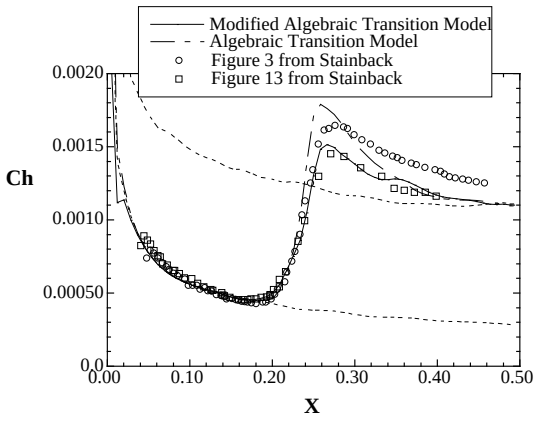

Figure 6.15: Modified Algebraic Transition Model on Stainback cone

Table 6.2: Modified Algebraic Transition Model Performance Summary

Test Case	Modified Model		Original Model	
	L_{model}/L_{exper}	Peak Ratio	L_{model}/L_{exper}	Peak Ratio
Kimmel DPDX=0	.872	.987	.761	1.155
Kimmel DPDX=4	1.090	.927	1.03	1.10
Kimmel DPDX=1	.968	.980	.667	1.225
Kimmel DPDX=-1	.967	1.038	.909	1.269
Kimmel DPDX=-2	.947	1.057	.865	1.266
Stainback	.985	1.024	.75	1.155
Holden and Chadwick	-	-	-	-

Table 6.2 presents a summary of the comparison between the original and modified algebraic transition region models. In almost every test case, the modified model performs better than the original model. The modified model is within 10% in all but one of the parameters. As was stated previously, the modifications made improve the prediction for the model for these cases, the modifications might harm the solution for other cases. What is important is that the empirical relations for the transition function were calibrated for incompressible flow. The compressibility corrections only

improve on the transition length. Compressibility corrections need to be made for the transition function. Unfortunately, this work does not include enough test cases to develop this compressibility correction.

The entries for the Holden and Chadwick case are left blank because the modifications in the model made no attempt to correct the problems with a decreasing momentum thickness so the model did not transition in this case, as shown in figure 6.16.

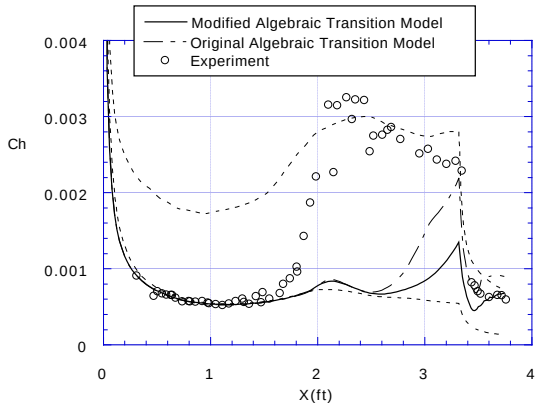

Figure 6.16: Modified Algebraic Transition Model on Holden and Chadwick case

Attempts were made at modifications that would make the model predict transition even when the momentum thickness is decreasing. What was found to be the most successful was to base χ_1 not on the growth in momentum thickness but on the stream wise distance normalized by Narasimha's transition length parameter, λ.

$$\chi_1 = 0.7\frac{x - xt}{2.5\ \lambda} \tag{6.9}$$

The modified form of the equations for the transition function, ϵ_t, are used. This model was called the combination model because it combines equations from the linear combination model with the algebraic transition region model. λ is not the length of the entire transition region, it is defined to be the length between where $\gamma = .25$ and $\gamma = .75$ and multiplying it by 2.5 results in roughly the length of the transition region. The factor of 0.7 has been found to optimize the predicted transition length for the Holden and Chadwick problem. The results for the new combination model

on the Calspan compression ramp are shown in figure 6.17. The transition length is predicted well, within 7%. However, the entire turbulent region is overpredicted which is due to the turbulence model used, the Baldwin and Lomax model. The only way to improve the prediction would be to use a more accurate turbulence model but it has already been shown that algebraic transition region models do not function well with two equation turbulence models.

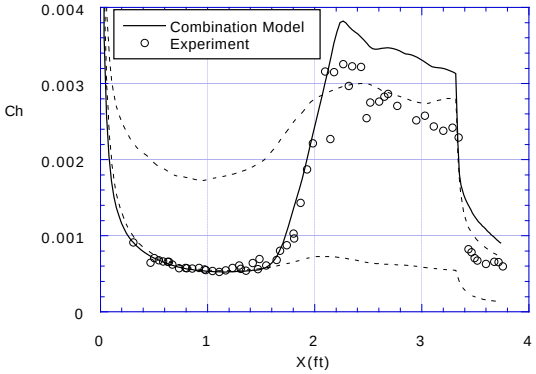

Figure 6.17: Combination model on Holden and Chadwick case

While the combination model predicts the transition length adequately for the Holden and Chadwick case, it does not for other cases. Figure 6.18 shows the results for the combination model on the Stainback case. The predicted transition length is too short by over 40%. The results for the combination model on the Kimmel DPDX=0 case (figure 6.19) show a transition length that comes up 40% too short.

The problem with the combination model predicting a transition length too short for these last two cases results from the use of Narasimha's transition length parameter, λ. Much like with the modified Schmidt and Patankar model, if the model is calibrated to work on the compression ramp case, it will not work on the Stainback or Kimmel cases. If it is calibrated to work on the Stainback and Kimmel case, it will not work on the compression ramp. It cannot be said whether the problem lies with the parameter itself, or with how it is being used with these models.

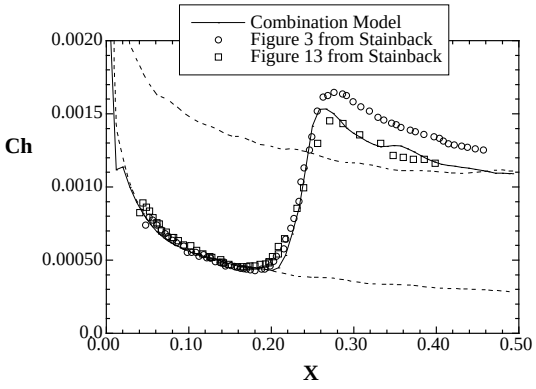

Figure 6.18: Combination model on Stainback case

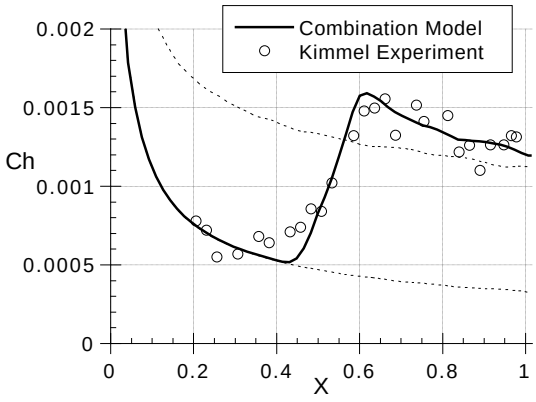

Figure 6.19: Combination model on Kimmel DPDX=0 case

6.4 Summary

Modifications have been presented for two models that increase their accuracy for the majority of the test cases investigated in this work. While the changes might not be accurate for test conditions out of the hypersonic regime investigated here, these modified models should be used for cases in this regime. When more test cases are available, it would be desired to make the modifications valid for more types of test cases.

Two modifications were made to the Schmidt and Patankar model. Introducing a turbulent spot into the boundary layer where the model is initiated starts transition immediately downstream which facilitates the use of the model. This modification is not linked to the hypersonic regime investigated here, it can theoretically be used with any flow condition.

The predicted shape of the transitional profile was changed by lowering the maximum production allowed at the beginning of the domain and letting it grow exponentially downstream. While the constants are flow specific and are only valid for the few cases presented here, the general idea of allowing the maximum production to grow exponentially downstream is valid for any flow condition.

Several modifications were made to the algebraic transition region model. The empirical transition function was modified to produce more accurate results for the hypersonic test cases tested in this work. The modified form should only be used for flows in the hypersonic regime as that is what they are developed for. Clearly, the algebraic transition region model should include a compressibility correction for the transition function as it does for the length of the transition region.

To combat the problem the algebraic transition region model has with computing flows where the momentum thickness decreases, the transition function of the algebraic model was made a function of the stream wise distance based on Narasimha transition length parameter and the results was called the combination model. While the transition region was predicted adequately for this model, the turbulent region was mispredicted for the Holden and Chadwick flow due to the use of the Baldwin and Lomax turbulence model used to compute the turbulent region. The logical step

to improve the prediction would be to use a more accurate two equation model but it has already been shown that the algebraic transition region model will not work with two equation turbulence models. So, further work was abandoned. However, when a method is found that can incorporate a more accurate turbulence model with an algebraic type transition region model, the combination model could be very successful.

Chapter 7

Conclusions

Six transition region models from the literature were implemented in the Navier-Stokes code GASP and tested against several experimental test cases. Most of the transition region models were originally designed for incompressible flow and corrections were made for compressible flow. Because GASP is a compressible Navier-Stokes code with a practical lower working limit of $M = 0.1$, test cases above this value had to be used. The only test cases found above this Mach number were in the hypersonic regime, no acceptable test cases were found during the literature search with a Mach number between 0.1 and 5.

The Baldwin and Lomax turbulence model was a simple on/off transition region model that produced short transition regions. The turbulence model itself usually adequately computed the turbulent region except for the compression ramp case. This model can be used for fast estimates of the transition region.

The Wilcox model never performed like it was intended. It was always difficult to force the model to transition at a desired location. Coupled with poor solutions and long run times, it can be stated that the Wilcox model did not perform adequately for the computed test cases. Given this information, the use of the Wilcox model for other hypersonic flows can be discouraged.

The Warren, Harris and Hassan model was unique in incorporating the effects of the first and second mode disturbances. However, the effect on the heat transfer solutions was negligible. The model in general performed adequately on all the test

cases and was easy to run considering that the transition point was information given to the model. Considering the adequate performance on the test cases in this work, the model is worthy of trial on other hypersonic test cases.

Schmidt and Patankar develop modifications for the production term in the turbulent kinetic energy equation to improve on the use of two equation models for predicting the transition region. The original modifications were made for incompressible flow which made the model difficult to run on the compressible cases as well as producing inadequate results. Modifications were presented in the current work that improved the model for most of the hypersonic cases featured within. While the new maximum production allowed in the modified formula can be scrutinized, the use of the turbulent spot with the model to enable it to be tripped at any location can be used for any case at any Mach number. The use of the Schmidt and Patankar model with the turbulent spot to model other transitional hypersonic flows is deserving of attention.

The algebraic transition region model is a pure transition region model that can be used with theoretically any turbulence model. Unfortunately, this was not true and the algebraic transition region model could not be used with two equation turbulence models. While the model produced smooth curves in the transition region, the turbulent region was overpredicted which is most likely due to the transition function being calibrated for incompressible flow. Modifications were made that improved the prediction of heat transfer in the turbulent region, but unfortunately it can only be said that these changes are valid only for the cases they were tested on. It is felt that all hypersonic cases would benefit by the use of the modified model over the unmodified model. But due to this problem and the problem with predicting transition in regions where the momentum thickness decreases, the use of the model for other hypersonic flow cases is discouraged.

The linear combination transition region model combines two complete flow fields together to form the transitional flow field. At first it appears that the model would be computationally expensive, considering the quick run times of the laminar flow field, the computational cost is not prohibitively expensive. On the downside, this model required modification of a constant, N_o, from run to run because the stated

compressibility relation was tentative. It was hoped that by selecting the value of N_o that produced the best results, a relationship between N_o and Mach number could be found. Unfortunately, the three test cases used were not enough to determine the relationship. On the positive side, the transition region was predicted adequately except that the peak at the end of the transition region was not resolved. It is believed that this model can produce adequate results on other hypersonic test cases and it is deserving of trial on them.

In summary, the Wilcox model did not perform adequately on these cases so it was reasoned that it would not perform satisfactorily on other cases so the use is discouraged. The algebraic transition region model overpredicted the heat transfer for several cases and did not transition for cases where the momentum thickness decreased. The accuracy of the algebraic transition region model on other hypersonic cases is doubtful. The Baldwin and Lomax model can be used for quick estimates. The Warren *et al.*, Schmidt and Patankar, and the linear combination model performed adequately on the test cases examined here and it is felt these models are worthy of trial on other hypersonic test cases. While these three models produced satisfactory results, the results clearly could be much more accurate. Much work still needs to be done.

Bibliography

[1] Abu-Ghannam, B. and Shaw, R., "Natural Transition of Boundary Layers – The Effects of Turbulence, Pressure Gradient, and Flow History," Journal of Mechanical Engineering Science, vol. 22, no. 5, pp. 213–228, 1980.

[2] Kimmel, R., "Experimental Transition Zone Lengths in Pressure Gradient in Hypersonic Flow," in *Symposium on Transitional and Turbulent Compressible Flows* (Kral, L. and Zang, T., eds.), vol. FED 151, pp. 117–127, ASME Fluids Engineering Conference, 1993.

[3] Warren, E., Harris, J., and Hassan, H., "A Transition Model for High Speed Flow," AIAA-94-1851-CP, 1994.

[4] Singer, B., Dinavahi, S., and Iyer, V., "Testing of Transition-Region Models: Test Cases and Data," NASA CR 4371, 1991.

[5] Singer, B., "Modeling the Transition Region," NASA CR 4371, 1993.

[6] Rodi, W. and Scheuerer, G., "Calculation of Laminar-Turbulent Boundary Layer Transition on Turbine Blades," in *Proceedings of the 65th AGARD-PEP Symposium on Heat Transfer and Cooling in Gas turbines*, (Bergen, Norway), pp. 18–1 to 18–12, 1985.

[7] Daniels, L. and Browne, W., "Calculation of Heat Transfer Rates to Gas Turbine Blades," International Journal of Heat and Mass Transfer, vol. 24, no. 5, pp. 871–879, 1981.

[8] Forest, A., "Engineering Predictions of Transitional Boundary Layers," in *AGARD Conference Proceedings*, no. 224, pp. 22–1 to 22–19, Oct. 1977.

[9] Stephens, C. and Crawford, M., "An Investigation into the Numerical Prediction of Boundary Layer Transition Using the K.Y. Chien Turbulence Model," NASA Contractor Report 185252, June 1990.

[10] Arnal, D., "Laminar-Turbulent Transition Problems in Supersonic and Hypersonic Flows," AGARD-FDP-VKI Special Course on *Aerothermodynamics of Hypersonic Vehicles*, June 1988.

[11] Abid, R., "Assessment of Two-Equation Turbulence Models for predicting Transitional Flows," in *Instability, Transition, and Turbulence* (Hussaini, Kumar, and Streett, eds.), Springer-Verlag, 1992.

[12] Narasimha, R., "The Laminar-Turbulent Transition Zone in the Boundary Layer," Progress in Aerospace Science, vol. 22, pp. 29–80, January 1985.

[13] Chen, K. and Thyson, N., "Extension of Emmons' Spot Theory to Flows on Blunt Bodies," AIAA Journal, vol. 9, pp. 821–825, May 1971.

[14] McGrory, W., Slack, D., Applebaum, M., and Walters, R., *GASP Version 2 Users Manual*. Aerosoft.

[15] White, F. M., *Viscous Fluid Flow*. McGraw-Hill, 1991.

[16] Morkovin, M., "Bypass – Transition Research Issues and Philosophy," in *Instabilities and Turbulence in Engineering Flows*, pp. 3–30, Netherlands: Kluwer Academic Publishers, 1993.

[17] Emmons, H., "The Laminar-Turbulent Transition in a Boundary Layer - Part I," Journal of Aerospace Science, vol. 18, pp. 490–498, July 1951.

[18] Schubauer, G. and Klebanoff, P., "Contributions on the Mechanics of Boundary-Layer Transition," NASA TN 3489, 1955.

[19] Schlichting, H., *Boundary-Layer Theory*. McGraw-Hill, 1979.

[20] Bertin, J. and Smith, M., *Aerodynamics for Engineers*. Prentice Hall, 1989.

[21] Mack, L., "Linear Stability Theory and the Problem of Supersonic Boundary-Layer Transition," AIAA Journal, vol. 13, pp. 278–289, Mar. 1975.

[22] Mack, L., "Stability of Axisymmetric Boundary Layers on Sharp Cones at Hypersonic Mach Numbers," AIAA Paper 87-1413, 1987.

[23] McDonald, H. and Fish, R., "Practical Calculations of Transitional Boundary Layers," International Journal of Heat and Mass Transfer, vol. 16, pp. 1729–1744, 1973.

[24] Baldwin, B. and Lomax, H., "Thin Layer Approximation and Algebraic Model for Separated turbulent Flows," AIAA Paper No. 1978-257, 1978.

[25] Arad, E., Berger, M., Israeli, M., and Wolfshtein, M., "Numerical Calculation of Transitional Boundary Layers," International Journal for Numerical Methods in Fluids, vol. 2, pp. 1–23, 1982.

[26] Patankar, S. and Spalding, D., *Heat and Mass Transfer in Boundary Layers*. Intertext, 1970.

[27] Ng, K., *Heat and Mass Transfer in Boundary Layers*. PhD thesis, University of London, Nov. 1971.

[28] Emmons, H. and Bryson, A., "The Laminar-Turbulent Transition in a Boundary Layer - Part II," in *Proceedings of the First U.S. National Congress of Applied Mechanics*, ASME, 1951.

[29] Narasimha, R., "On the Distribution of Intermittency in the Transition Region of a Boundary Layer," Journal fo the Aeronautical Sciences, pp. 711–712, Sept. 1957.

[30] Dhawan, S. and Narasimha, R., "Some properties of boundary layer flow during the transition from laminar to turbulent motion," Journal of Fluid Mechanics, vol. 3, no. 4, pp. 418–436, 1958.

[31] Dey, J. and Narasimha, R., "An integral Method for the Calculation of 2D Transitional Boundary Layers," Tech. Rep. Report 99 FM 7, Department of Aerospace Engineering, Indian Institute of Science, Bangalore, India, 1988.

[32] Rodi, W., "Experience with Two-Layer Models Combining the $k-\epsilon$ Model with a One-equation Model near the Wall," AIAA Paper No. 91-0216, 1991.

[33] Fujisawa, N., Rodi, W., and Schönung, B., "Calculation of transitional boundary layers with a two-layer model of turbulence," in *Proceedings of the 3rd International Symposium on Transport Phenomena and Dynamics of Rotating Machinery*, Apr. 1990.

[34] Schmidt, R. and Patankar, S., "Simulation Boundary Layer Transition with Low-Reynolds Number $k-\epsilon$ Turbulence Models: Part 2 - An Approach to Improving the Predictions," Journal of Turbomachinery, vol. 113, Jan. 1991.

[35] Lam, C. and Bremhorst, K., "A Modified Form of the $k-\epsilon$ Model for Predicting Wall Turbulence," ASME Journal of Fluids Engineering, vol. 103, pp. 456–460, 1981.

[36] Lund, T., "Application of the Algebraic RNG model for Transition Simulation," in *Instability, Transition, and Turbulence* (Hussaini, Kumar, and Streett, eds.), Springer-Verlag, 1992.

[37] Yakhot, V. and Orszag, S., "Renormalization Group Analysis of Turbulence. I. Basic Theory," Journal of Scientific Computing, vol. 1, no. 1, pp. 3–51, 1986.

[38] Wilcox, D., *Turbulence Modeling for CFD.* La Cañada, CA: DCW Industries, 1992.

[39] Wilcox, D., "Turbulence and Transition Modeling for High-Speed Flows," NASA CR 191473, Apr. 1993.

[40] Wilcox, D., "Reassessment of the Scale-Determining Equation for Advanced Turbulence Models," AIAA Journal, vol. 26, pp. 1299–1310, Nov. 1988.

[41] Wilcox, D., "Dilatation-Dissipation Corrections for Advanced Turbulence Models," AIAA Journal, vol. 30, pp. 2639–2646, Nov. 1992.

[42] Wilcox, D., "Progress in Hypersonic Turbulence Modeling," AIAA Paper No. 91-1785, 1991.

[43] Wilcox, D., "A Half Century Historical Review of the $k-\omega$ Model," AIAA Paper No. 91-0615, 1991.

[44] Saffman, P. and Wilcox, D., "Turbulence-Model Predictions for Turbulent Boundary Layers," AIAA Journal, vol. 12, pp. 541–546, Apr. 1974.

[45] Menter, F., "Influence of Freestream Values on $k-\omega$ Turbulence Model Predictions," AIAA Journal, vol. 30, pp. 1657–1659, Oct. 1991.

[46] Menter, F., "Zonal Two Equation $k-\omega$ Turbulence Models for Aerodynamic Flows," AIAA Paper No. 93-2906, 1993.

[47] Menter, F., "Performance of Popular Turbulence Models for Attached and Separated Adverse Pressure Gradient Flows," AIAA Journal, vol. 30, pp. 2066–2072, Aug. 1992.

[48] Johnson, D. and King, L., "A Mathematically Simple Turbulence Closure Model for Attached and Separated Turbulent Boundary Layers," AIAA Journal, vol. 23, pp. 1684–1692, Nov. 1985.

[49] Baldwin, B. and Barth, T., "A One-Equation Turbulence Transport Model for High Reynolds Number Wall-Bounded Flows," NASA TM-102847, Aug. 1990.

[50] Spalart, P. and Allmaras, S., "A One-equation turbulence Model for Aerodynamic Flows," AIAA Paper No. 92-0439, Jan. 1992.

[51] Young, T., Warren, E., Harris, J., and Hassan, H., "New Approach for Calculation of Transitional Flows," AIAA Journal, vol. 31, pp. 629–636, Apr. 1993.

[52] Micheltree, R., Salas, M., and Hassan, H., "One-Equation Turbulence Model for Transonic Airfoil Flows," AIAA Journal, vol. 28, pp. 1625–1632, Sept. 1990.

[53] Dutoya, D. and Michard, P., "A Program for Calculating Boundary Layers and Heat Transfer along Compressor and Turbine Blades," in *Numerical Methods in Heat Transfer*, New York: Wiley and Sons, 1981.

[54] Launder, B. and Spalding, D., "The Numerical Computations of Turbulent Flows," Computer Methods in Applied Mechanics and Engineering, vol. 3, pp. 269–289, 1974.

[55] Rodi, W. and Scheuerer, G., "Calculations of Heat Transfer to Convection-Cooled Turbine Blades," Journal of Engineering for Gas Turbines and Power, vol. 107, July 1985.

[56] Yand, Z. and Shih, T., "A $k - \epsilon$ Calculation of Transitional Boundary Layers," in *Instability, Transition, and Turbulence* (Hussaini, Kumar, and Streett, eds.), Springer-Verlag, 1992.

[57] Patel, V., Rodi, W., and Scheuerer, G., "Turbulence Models for Near-Wall and Low Reynolds Number Flows: A Review," AIAA Journal, vol. 23, no. 9, pp. 1308–1319, 1985.

[58] Coakley, T. and Huang, P., "Turbulence Modeling for High Speed Flows," AIAA Paper No. 92-0436, 1992.

[59] Speziale, C., Abid, R., and Anderson, E., "A Critical Evaluation of Two-Equation Models for Near Wall Turbulence," AIAA Paper No. 90-1481, 1990.

[60] Schmidt, R., *Two-Equation Low-Reynolds-Number Turbulence Modeling of Transitional Boundary Layer Flow Characteristic of Gas Turbine Blades*. PhD thesis, University of Minnesota, 1987.

[61] Johnson, K., "Heat Transfer Calculations on Turbine Airfoils," Master's thesis, The University of Texas at Austin, 1987.

[62] Chien, K., "Predictions of Channel and Boundary-Layer Flows with a Low-Reynolds-Number Turbulence Model," AIAA Journal, vol. 20, pp. 33–38, Jan. 1982.

[63] Chang, C., Singer, B., Dinavahi, S., El-Hady, N., Pruett, C., Harris, J., Streett, C., Zang, T., and Wilcox, D., "Transition Region Modeling for Compressible Flow," NASP Contractor Report 1142, Feb. 1993.

[64] Singer, B., Dinavahi, S., and Zang, T., "Evaluation of a Compressible Transition Model," NASP Contractor Report 1109, Jan. 1991.

[65] Singer, B. and Dinavahi, P., "Testing of Transition-Region Models," Journal of Fluids Engineering, vol. 114, pp. 73–79, Mar. 1992.

[66] Dinavahi, S. P., "Comparison of Two Transition Models," in *Instability, Transition, and Turbulence* (Hussaini, Kumar, and Streett, eds.), Springer-Verlag, 1992.

[67] Stainback, P., Fisher, M., and Wagner, R., "Effects of Wind-Tunnel Disturbances on Hypersonic Boundary Transition," AIAA Paper No. 72-181, 1972.

[68] Cebeci, T. and Smith, A., *Analysis of Turbulent Boundary Layers*. Academic Press, 1974.

[69] Wilcox, D., *User's guide for the EDDYBL computer program*. 4367 Troost Ave, Studio City, CA 91604: DCW Industries, 1976.

[70] Fisher, D. and Dougherty, N., "In-Flight Transition Measurement on a 10° Cone at Mach Numbers From 0.5 to 2.0," NASA Technical Paper 1971, 1982.

[71] Hylton, L., Mihelc, M., Turner, E., Nealy, D., and York, R., "Analytical and Experimental Evaluation of the Heat Transfer Distribution over the surfaces of Turbine Vanes," NASA CR 168015, May 1983.

[72] Wang, T., Simon, T., and Buddhavarapu, J., "Heat Transfer and Fluid Mechanics Measurements in Transitional Boundary Layer Flows," Journal of Engineering for Gas Turbines and Power, vol. 107, pp. 1007–1015, Oct. 1985.

[73] Kimmel, R., "The Effect of Pressure Gradients on Transition Zone Length in Hypersonic Boundary Layers," Tech. Rep. WL-TR-94-3012, Wright Laboratory, Wright Patterson AFB, Ohio, Dec 1993.

[74] Holden, M. and Chadwick, K., "Studies of Laminar, Transitional, and Turbulent Hypersonic Flows Over Curved Compression Surfaces," Tech. Rep. 2610-5, Calspan-UB Research Center, 1994.

[75] Lin, C., *Turbulent Flows and Heat Transfer*. Princeton University Press, 1959.

[76] Madavan, N. and Rai, M., "Direct Numerical Simulation of Boundary Layer Transition on a Heated Flat Plate with Elevated Freestream Turbulence," AIAA Paper No. 95-0771, 1995.

[77] Rai, M. and Moin, P., "Direct Simulations of Turbulent Flow using Finite-Difference Schemes," Journal of Computational Physics, vol. 96, pp. 15–53, 1991.

[78] Blair, M., "Influence of Free-Stream Turbulence on Turbulence on Turbulent Boundary Layer Heat Transfer and Mean Profile Development, Part 1 Experimental Data," ASME Journal of Heat Transfer, vol. 105, pp. 33–40, 1983.

[79] Suder, K., O'Brien, J., and Reshotko, E., "Experimental Study of Bypass Transition in a Boundary Layer," NASA TM-100913, 1988.

[80] Sohn, K. and Reshotko, E., "Experimental Study of Boundary Layer Transition with Elevated Freestream Turbulence on a Heated Plate," NASA CR-187068, 1991.

[81] Liou, W. and Shih, T., "On the Basic Equations for the Second-Order Modeling of Compressible Turbulence," NASA Technical Memorandum 105277, Oct. 1991.

[82] Favre, A., "Equations des Gaz Turbulents Compressibles," Journal de Mecanique, vol. 4, no. 3, pp. 361–390, 1965.

[83] Tennekes, H. and Lumley, J., *A First Course in Turbulence*. Cambridge, Massachusetts, and London, England: The MIT Press, 1972. ISBN 0 262 20019 8.

[84] Launder, B., Reece, G., and Rodi, W., "Progress in the development of a Reynolds-stress turbulence closure," Journal of Fluid Mechanics, vol. 68, no. 3, pp. 537–566, 1975.

[85] Chen, H. and Patel, V., "Practical Near-Wall turbulence Models for Complex Flows Including Separation," AIAA Paper No. 87-1300, June 1987.

[86] Walker, G., "Transitional Flow on Axial Turbomachine Blading," AIAA Journal, vol. 27, pp. 595–602, May 1989.

[87] Schetz, J., *Foundations of Boundary Layer Theory for Momentum, Heat, and Mass Transfer*. Prentice-Hall, Inc., 1984. ISBN 0-13-329334-3.

[88] Eckert, E., "Engineering Relations for Heat Transfer and Friction in High-Velocity Laminar and Turbulent Boundary-Layer Flow Over Surfaces with Constant Pressure and Temperature," Transactions of the ASME, vol. 78, p. 1273, Aug. 1956.

[89] Arnal, D., "Three-Dimensional Boundary Layers: Laminar-Turbulent Transition," AGARD-FDP-VKI Special Course on *Calcul Des Limites Tridimensionelles Avec Ou Sans Decollement*, Apr. 1986.

[90] Abid, R., "A Study of Turbulence Models for Prediction of Transitional Boundary Layers," in *Instability, Transition, and Turbulence* (Hussaini, Kumar, and Streett, eds.), Springer-Verlag, 1992.

[91] Blair, M. and Werle, M., "Combined Influence of Free-Stream Turbulence on the Zero Pressure Gradient Fully Turbulent Boundary Layer," tech. rep., UTRC Report R81-914388-17, 1981.

Appendix A

Source Code

The six transition region models were all implemented in the Navier-Stokes code GASP. What follows is a listing of the subroutines added to GASP for these transition region models. There were of course, slight changes and modifications to the existing routines of GASP. These will be discussed for the routines that were important.

All the models were implemented for iterations on the k plane.

A.1 Algebraic Transition Region Model

Subroutine algtran is the main routine of the algebraic transition region model, it is called from subroutine visck.

```
#include "gasp.h"
************************************************************
*                                                          *
*      Transition Region Model                             *
*                                                          *
************************************************************
c
      subroutine algtran(q,thp,idim,jdim,itrip,nspec,trp,
     .                   rmut,ivscoef,rvscoef,ddj0,neqn,nnev,t)
c
      INTEGER idim,jdim,neqn,nspec,nnev
      REAL q(-1:idim+1,-1:jdim+1,neqn)
      REAL thp(0:idim,0:jdim,NTHP)
      REAL trp(0:idim,0:jdim,NTRP)
      REAL rmut(idim-1,jdim-1)
      REAL ddj0(jdim,idim-1)
c
c     temporary space
c
      REAL  t(1)
c
c     viscous coefficients
c
      INTEGER ivscoef(NIVSCOEF)
      REAL    rvscoef(NRVSCOEF)
c
```

```
c     pointers!
c
      INTEGER itheta,irme,irdelta,igammat,itmp
c
      INTEGER itrip,istrthta
c
c     pointers for temp space
c
      itheta=1
      irme = itheta + idim
      irdelta = irme + idim
      igammat = irdelta + idim
      itmp = igammat + idim*jdim
c
c     We must look at itrip.
c     If it is equal to 0 then we
c     are space marching and this is the first
c     plane of the transition region.
c     That means that we must store theta
c     of this plane.
c
      istrthta = 0
      if (itrip.eq.0) then
         itrip = 1
         istrthta = 1
      endif
c
c     if itrip = -1 then we are
c     space marching and have not
c     reached the trip point yet
c
      if (itrip.lt.0) then
         t(igammat) = 0
         goto 100
      endif
c
c     compute delta and Me for the part
c     of the flow in the transition region
c
      call bledge(q,idim,jdim,neqn,t(irme),t(irdelta),itrip,thp,
     .            nspec,t(itmp))
c
c     compute theta!
c
      call momthick(q,idim,jdim,itrip,t(itheta),t(irdelta),neqn,
     .              nspec,ddj0,istrthta,rvscoef,t(itmp))
c
c     compute the transition function
c
      call trnsfunc(idim,jdim,nspec,t(igammat),t(irme),
     .                                itrip,t(itheta),rvscoef)
c
c     the one dimensional streawise transition function
c     has been included.  Now include normal to the wall
c     affects, i.e. The top and bottom have walls and
c     only one undergoes transition
c
  100 continue
c
      call trnsj(idim,jdim,t(igammat),t(irdelta),itrip)
c
c     add the turbulent eddy viscosity
c     to the laminar viscosity using the
c     transition function
c
      call addtran(idim,jdim,nspec,nnev,neqn,trp,thp,rmut,
```

```
     .      ivscoef,rvscoef,t(igammat),t(itmp))
c
      return
c
      end
c
*********************************************************
c
      subroutine trnsj(idim,jdim,gammat,rdelta,itrip)
c
      INTEGER idim,jdim,itrip,i,j
c
      REAL gammat(idim,jdim), rdelta(idim)
c
c     In the future, parameters will be read
c     out of the input deck.  For now this is
c     just being hard wired for the turbine case
c
c     If we are space marching, don't worry about
c     Laminar and transition regions, just extrapolate
c     values
c
      if (itrip.lt.2) then
c
      do 5 j = 2, jdim
c
      gammat(1,j) = gammat(1,1)
c
    5 continue
c
      else
c
c     O.K. We are in global!
c
c     this part is for the laminar region(streamwise)
c
      do 10 i = 1, itrip-1
      do 10 j = 1, jdim
c
      gammat(i,j) = 0.0
c
   10 continue
c
c     O.k.  this is for the transition and turbulent
c     part.   the values were originally read into
c     j = 1.  set the values up to rdelta equal
c     to this value
c
      do 20 i = itrip, idim
c
      gammat(i,j) = gammat(i,1)
c
   20 continue
c
c     O.k., now zero out the top laminar wall
c
c     do 30 i = itrip, idim
c
c     do 30 j = int(rdelta(i))+6 , jdim
c
c     gammat(i,j) = 0.0
c
c  30 continue
c
c     End of loop that differentiates between global
c     and space marching
```

```
c
      endif
c
      return
c
      end
c
*************************************************************
c
      subroutine bledge(q,idim,jdim,neqn,rme,rdelta,itrip,
     .                  thp,nspec,rmach)
c
      REAL q(-1:idim+1,-1:jdim+1,neqn)
      REAL thp(0:idim,0:jdim,NTHP)
      REAL rme(idim)
      REAL rdelta(idim)
c
      INTEGER idim,jdim,neqn,nspec,iu,itrip
      INTEGER i,j,jstart
c
      REAL rmach(0:idim,0:jdim)
c
c     setup pointers and the like
c
      iu = nspec+1
      jstart = 3
c
c     compute the Mach Number for the entire domain
c
      call mach2(idim,jdim,rmach,q(-1,-1,iu),thp(0,0,iSnd))
c
c     set delta equal to zero for the laminar
c     region
c
      do 10 i=1,itrip-1
        rdelta(i)=0.0
        rme(i)=0.0
 10   continue
c
c  Now start marching through the transition region.
c
      do 40 i = itrip,idim-1
c
c  Now work up from wall until values
c  of Mach Number are close to each other
c
         jstart = int(rdelta(i-1)/2.0)
         if (jstart.le.3.or.jstart.gt.jdim) jstart = 3
         do 30 j = jstart,jdim-1
c
            if(rmach(i,j-1)/rmach(i,j).gt.0.99) then
              rdelta(i) = real(j)
              rme(i) = rmach(i,j)
              goto 35
            endif
c
  30     continue
c
c  The edge of the Boundary Layer was never found.
c  The flow must really be messed up.
c  just set edge conditions to jdim-1.
c  Everything will work out later
c
         rdelta(i) = real(jdim)
         rme(i) = rmach(i,jdim-1)
```

```
c
  35    continue
c
  40    continue
c
        return
        end
c
*************************************************************
c
      subroutine trnsfunc(idim,jdim,nspec,gammat,rme,
     .                           itrip,theta,rvscoef)
c
      INTEGER idim,jdim,i,nspec
      INTEGER itrip
c
      REAL ch1,gammat(idim,jdim)
      REAL rvscoef(NRVSCOEF)
      REAL rme(idim)
      REAL theta(idim)
      REAL thetatrip
c
c     Gammat has been converted to a two dimensional
c     array.  This routine calculates only the one dimensional
c     streamwise values. So everything is stuck into j =1
c     and then a later routine will fill in the j values
c
c     zero out transition function for laminar
c     region
c
      do 10 i = 1,itrip-1
         gammat(i,1) = 0.0
  10  continue
c
c     We must determine whether we are doing space
c     marching or global iteration.  If it is global
c     thetatrip = theta(itrip)
c     if it is space marching
c     thetatrip = RVSCOEF(Ithtrp)
c
      if (idim.gt.2) then
         thetatrip = theta(itrip)
      else
         thetatrip = rvscoef(Ithtrp)
      endif
c
c     start marching down and computing the transition
c     function
c
      if (thetatrip.eq.0.0) thetatrip = RSMALL
c
      do 20 i = itrip,idim-1
c
         ch1 = (theta(i)/thetatrip-1.0+0.005*rme(i)*rme(i))/
     .         (1.0+0.02*rme(i)*rme(i))
c
c     different values of chi1 results in different formulas
c     for gammat
c
      if (ch1.le.0.25) then
c
          gammat(i,1) = 1.0 - EXP(-4.5*(ch1*
     .    (1.0+0.02*rme(i)*rme(i))-0.005*rme(i)*rme(i))**2)
c
      else if(ch1.le.0.75) then
```

```
c
           gammat(i,1) = 18.628*ch1**4 -
     .     55.388*ch1**3 + 52.369*ch1**2 - 16.501*ch1
     .     + 1.893
c
      else if(ch1.le.3) then
c
           gammat(i,1)=1.25-0.25*SIN(3.14159*
     .       (0.444*ch1-0.833))
c
      else if(ch1.gt.3) then
c
         gammat(i,1)=1.0
c
      end if
c
  20  continue
c
      return
      end
c
*****************************************************************
c
      subroutine momthick(q,idim,jdim,itrip,theta,rdelta,neqn,
     .                    nspec,ddj0,istrthta,rvscoef,rinte)
c
      INTEGER idim,jdim,neqn,nspec
c
      REAL q(-1:idim+1,-1:jdim+1,neqn)
c
      REAL ubar,ubare,rho,rhoe
      REAL theta(idim)
      REAL rvscoef(NRVSCOEF)
      REAL rinte(0:jdim)
      REAL rdelta(idim)
      REAL ddj0(jdim,idim-1)
c
      INTEGER idelta,itrip
      INTEGER iu,iv,iw,irho
      INTEGER i,j,istrthta
c
c     set up pointers
c
      iu = nspec+1
      iv = iu + 1
      iw = iv + 1
      irho = 1
c
c     zero out theta for the entire domain
c
      do 10 i = 1,idim
         theta(i)=0.0
  10  continue
c
c     start marching in the transition region
c
      do 20 i = itrip,idim-1
c
c     Compute the integrand for theta at this location
c
      idelta = int(rdelta(i))
           ubare = (q(i,idelta,iu)*q(i,idelta,iu)
     .           +q(i,idelta,iv)*q(i,idelta,iv)
     .           +q(i,idelta,iw)*q(i,idelta,iw))**(.5)
           rhoe = q(i,idelta,irho)
```

```
c
         do 30 j = 0,idelta
           ubar = (q(i,j,iu)*q(i,j,iu)+q(i,j,iv)*q(i,j,iv)
     .           +q(i,j,iw)*q(i,j,iw))**(.5)
           rho = q(i,j,irho)
           rinte(j)=(rho*ubar)*(1.0-(ubar/ubare))/(rhoe*ubare)
 30      continue
c
c     Now start adding up the integral
c
          theta(i)=theta(i) +
     .         .5*(rinte(0)+rinte(1))*(ddj0(1,i))
          do 40 j = 2,idelta
             theta(i)=theta(i)  +
     .         .5*(rinte(j-1)+rinte(j))*(ddj0(j,i)-ddj0(j-1,i))
  40      continue
c
  20   continue
c
c      If we are space marching and this is the
c      first plane in the transition region
c      we must store the theta of this plane
c
       if (istrthta.ne.0) rvscoef(Ithtrp) = theta(1)
c
       return
       end
c
*****************************************************************
c
      subroutine addtran(idim,jdim,nspec,nnev,neqn,trp,thp,rmut,
     .                   ivscoef,rvscoef,gammat,rt)
c
      INTEGER idim,jdim,nspec,nnev,neqn
      REAL    trp(0:idim,0:jdim,NTRP),
     .        thp((idim+1)*(jdim+1),NTHP),
     .        rmut(idim-1,jdim-1)
c
c     viscous coefficients
c
      INTEGER ivscoef(NIVSCOEF)
      REAL    rvscoef(NRVSCOEF)
c
c     temp space
c
      REAL    rt(0:idim,0:jdim,1)
c
c     local variables
c
      INTEGER i,j,icpm,nlen
c
c     transition
c
      REAL gammat(idim,jdim)
c
c     we need cp mixture for addition of kt
c
      icpm = 1
c
      nlen = (idim+1)*(jdim+1)
      call cpmix(nlen,thp(1,iG),thp(1,iR),rt(0,0,icpm))
c
c     add mut, kt, and dft to the transport prop array
c
      if(ivscoef(Ikeps) .ne. FALSE) then
```

```
c
c       This is a 2-equation model, first we need muk and mueps
c
        do 100 j = 1,jdim-1
          do 100 i = 1,idim-1
            trp(i,j,iMuk) = trp(i,j,iMul)+gammat(i,j)* rmut(i,j)/
     .                                          rvscoef(Iprk)
            trp(i,j,iMueps)=trp(i,j,iMul)+gammat(i,j)* rmut(i,j)/
     .                                            rvscoef(Ipreps)
  100   continue
c
      end if
c
c     these are done for all turbulent cases
c
      do 210 j = 1,jdim-1
        do 200 i = 1,idim-1
          trp(i,j,iMul) = trp(i,j,iMul) + gammat(i,j)*rmut(i,j)
          trp(i,j,iKl) = trp(i,j,iKl)
     .               + gammat(i,j)*rmut(i,j)*rt(i,j,icpm)/rvscoef(Iprt)
          trp(i,j,iDfl) =trp(i,j,iDfl)+gammat(i,j)*rmut(i,j)
     .                  /rvscoef(Isct)
  200 continue
  210 continue
c
      return
      end
c
*********************************************************************
c
c +-------------------------------------------------------------+
c |                         MACH2                               |
c +-------------------------------------------------------------+
c
      subroutine mach2(idim,jdim,machno,vel,a)
c
      INTEGER idim,jdim,i,j
      REAL    machno(0:idim,0:jdim),vel(-1:idim+1,-1:jdim+1,3)
      REAL    a(0:idim,0:jdim)
c
c     calculate mach number from velocities & speed of sound
c
      do 100 i=0,idim
      do 100 j=0,jdim
        machno(i,j) = sqrt(vel(i,j,1)*vel(i,j,1)+vel(i,j,2)*vel(i,j,2)+
     .                     vel(i,j,3)*vel(i,j,3))/a(i,j)
  100 continue
c
      return
      end
c
```

A.2 Schmidt and Patankar

The following routines were used for the Schmidt and Patankar model. Turbprod is the main routine and it is called from visck.

```
c
c    subroutine turbprod
c
c    This subroutine implements the Schmidt and Patankar
c    modification to the production of turbulence kinetic
```

```
c     energy.
c
      subroutine turbprod(k,idim,jdim,kdim,nspec,nnev,neqn,q,
     .                    thp,trp,itrippass,qinf,rmut,xyz,cke,res,
     .                    kesrc,rdelta,ue,vol,ddj0,prodold,t)
c
      INTEGER k,idim,jdim,kdim,nspec,neqn,itrippass,nnev,itrip
      INTEGER idelta,itripab
c
      REAL q(-1:idim+1,-1:jdim+1,neqn,k-2:k+2)
      REAL thp(0:idim,0:jdim,NTHP,k-1:k+1)
      REAL trp(0:idim,0:jdim,NTRP),qinf(neqn+2)
      REAL rmut(idim-1,jdim-1),xyz(idim,jdim,3,k-1:k)
      REAL cke(idim-1,jdim-1,5),res(idim-1,jdim-1,neqn)
      REAL kesrc(idim-1,jdim-1,2),vol(idim-1,jdim-1,k-1:k+1)
c     REAL prodold(jdim,2),ddj0(jdim,idim-1),retheta
      REAL prodold(jdim,4),ddj0(jdim,idim-1),retheta
c
c     Temp array
c
      REAL  t(1)
c
      REAL ue(idim),rdelta(idim),a,b
c
c     Pointers!
c
      INTEGER iu,iv,iw,ik,ieps,itmp
c
c     Define Pointers for Q and temp array
c
      iu=nspec+1
      iv=nspec+2
      iw=nspec+3
      ik=nspec+nnev+5
      ieps=nspec+nnev+6
      itmp = 1
c
c     Take the positive part of itripass
c
      itrip =  abs(itrippass)
      itripab = itrip
c
c     O.K. We must determine whether we are doing space
c     marching or global iteration
c
      if (idim.lt.5) then
c
c        We are doing space marching!
c        We must make a bunch of changes now
c        because this was originally coded up
c        assuming global iteration
c
c        itripab is used to make sure that the
c        edge velocity is passed correctly into
c        subroutine getab
c
         itripab = 1
c
c        O.K., we must determine if we are
c        setting the beginning location for
c        the model or if we are going to
c        use retheta
c
         if (itrip.gt.(idim+jdim+kdim)) then
c
```

```
c        O.K. we are going to use retheta = 125
c        as our starting point! We first need to get delta.
c        (note the 1 being passed is for itrip)
c
         call bledge3(q(-1,-1,1,k),idim,jdim,neqn,ue,rdelta,
     .             1,thp(0,0,1,k),nspec,t(itmp))
c
c        Subroutine getret computes the Reynolds
c        number based on momentum thickness. It is
c        basically the subroutine momthick
c
         call getret(q(-1,-1,1,k),idim,jdim,retheta,rdelta,neqn,
     .                thp(0,0,1,k),trp,ue,nspec,ddj0,rmut,t(itmp))
c
c        Set retheta = 0 for the first plane
c
         if (k.le.3)  retheta = 0.0
c
c        Check to see if retheta = 125
c
         if (retheta.ge.125.0) then
c
c        It is time to start the model!
c        Set the global itrip and the local itrip
c        to the value
c        of the current plane
c
            itrippass = -k
            itrip = k
c
            write(*,*) 'Schmidt Started at ', k
            write(*,*) 'Re theta = ', retheta
c
c        The subroutine will now then function normally
c
         else
c
c        If is not time to start the schmidt model yet
c        set itrip greater than k so that the routine
c        keeps in the laminar region
c
             itrip = k+1
c
         endif
c
c        This endif is for the retheta=125 block
c
         endif
c
c        O.K., it is time to see where the location
c        of itrip puts us
c
         if (k.lt.itrip) then
c
c           K is less than itrip, so in this region
c           the production is set to zero
c
         itrip = 0
c
         else if (k.eq.itrip) then
c
c        This is the first station in the transition region
c        set itrip = -1 and that will alert subroutine schpat
c
         itrip = -1
c
```

```
         else
c
c        We are in the transition region.
c        Set itrip = 1.  The subroutines will
c        know that that means we are space marching
c
         itrip = 1
c
         endif
c
      endif
c
c     We must determine the edge of the boundary layer
c
c     Use bledge3, which is a copy of bledge2 from lintran
c     except the dimensions on thp are different
c
      call bledge3(q(-1,-1,1,k),idim,jdim,neqn,ue,rdelta,
     .             itrip,thp(0,0,1,k),nspec,t(itmp))
c
c     Cool, now we have the edge of the boundary layer
c     and the velocity at the edge of the boundary layer.
c     We don't need the whole rdelta now, we just need
c     it at one location
c
      idelta = int(rdelta(itripab))
c
c     We should now compute A and B
c
      call getab(idim,jdim,neqn,nspec,nnev,qinf,ue(itripab),
     .   thp(0,0,1,k),trp,idelta,itrip,rmut,a,b)
c
c     It is time now to call the main routine that
c     computes the production and implements
c     the Schmidt and Patankar routine
c
      call schpat(k,idim,jdim,kdim,nspec,nnev,neqn,q,res,rmut,
     .    itrip,a,b,kesrc,cke,xyz,
     .    thp(0,0,iRho,k),idelta,vol(1,1,k),prodold)
c
c     We are Done!
c
      return
      end
c
*****************************************************************
c
c     Subroutine getab
c
c     This subroutine computes constants A and B
c     from Schmidt and Patankar.
c
      subroutine getab(idim,jdim,neqn,nspec,nnev,qinf,ue,thp,trp,
     .                 idelta,itrippass,rmut,a,b)
c
      INTEGER idim,jdim,neqn,nspec,nnev
      INTEGER i,idelta,itrip,itrippass
c
      REAL qinf(neqn+2),vmag,ue
      REAL tu,a,b,rm(0:7,2),rmut(idim-1,jdim-1)
      REAL thp(0:idim,0:jdim,NTHP)
      REAL trp(0:idim,0:jdim,NTRP)
c
c     Pointers
c
```

```
      INTEGER iu,iv,iw,ik
c
c     Set up Pointers
c
      iu = nspec+1
      iv = nspec+2
      iw = nspec+3
      ik = nspec+nnev+5
c
c     Check to see if itrippass = 0.  if
c     it is, then we don't need a and b, bounce
c     out of this subroutine.
c
      if (itrippass.ne.0) then
c
      itrip = abs(itrippass)
c
c     Find tu based on inf conditions
c
      vmag=sqrt(qinf(iu)*qinf(iu)+qinf(iv)*qinf(iv)+
     .            qinf(iw)*qinf(iw))

      tu = sqrt(qinf(ik))/vmag*100.0
c
c     If tu is out of bounds, set it = to nearest bound
c
      if (tu.lt.0.5) tu = 0.5
      if (tu.gt.9.0) tu = 9.0
c
c     Set m=curve fit constants
c
c     For "a"
c
      rm(0,1) = 8.3962216311
      rm(1,1) = -9.0379773565
      rm(2,1) = 6.655639379
      rm(3,1) = -2.3673563939
      rm(4,1) = 0.36985006533
      rm(5,1) = -.021869901214
      rm(6,1) = -.00018445193299
      rm(7,1) = 4.5552714312e-5
c
c     for "b"
c
      rm(0,2) = 0.1420241491
      rm(1,2) = -.52437688556
      rm(2,2) = .82989588974
      rm(3,2) = -0.61482537497
      rm(4,2) = .3255611601
      rm(5,2) = -0.069266716607
      rm(6,2) = .006397622876
      rm(7,2) = -0.00021663067148
c
c     Compute A and B using curve fits.
c
      a = 0.0
      b = 0.0
c
      do 10 i = 0,7
       a = a + rm(i,1)*tu**i
       b = b + rm(i,2)*tu**i
 10   continue
c
c     These values of a have been non-dimensionalized.
c     They must be re-dimensionalized because this is
c     not the GASP scheme.  Since the variables used
```

```
c     to dimensionalize it are non-dimensionalized
c     by GASP, the final product is non dimensional
c     NOTE: we are subtracting out the eddy viscosity
c     from the total viscosity.
c
      a = a*thp(itrip,idelta,iRho)*ue*ue/(trp(itrip,idelta,iMul)
     .                - rmut(itrip,idelta))
      b = b*thp(itrip,idelta,iRho)**3*ue**6/
     .          (trp(itrip,idelta,iMul)-rmut(itrip,idelta))**2
c
c     Lastly, the values in the graph that
c     was done for the curve fits were offset
c     by many orders.  Convert these to what they
c     should be.
c
      a = a*1.0e-6
      b = b*1.0e-12
c
      else
c
c     itrip = 0, we are space marching and we are setting
c     the production equal to zero
c
      a=0.0
      b=0.0
c
      endif
c
c     we are done!
c
      return
      end
c
*****************************************************************
c
c    Subroutine schpat
c
c    This routine implements the Schmidt and Patankar
c    turbulence kinetic energy production limit
c
      subroutine schpat(k,idim,jdim,kdim,nspec,nnev,neqn,q,res,rmut,
     .     itrip,a,b,kesrc,cke,xyz,rho,idelta,vol,prodold)
c
      INTEGER k,idim,jdim,kdim,i,j
      INTEGER nspec,nnev,neqn
      INTEGER ik,ieps,iu,iv,iw
      INTEGER itrip, idelta
c
      REAL q(-1:idim+1,-1:jdim+1,neqn,k-2:k+2)
      REAL res(idim-1,jdim-1,neqn),a,b
      REAL kesrc(idim-1,jdim-1,2)
      REAL cke(idim-1,jdim-1,5),xyz(idim,jdim,3,k-1:k)
      REAL rmut(idim-1,jdim-1),rho(0:idim,0:jdim)
      REAL c1,vmag,prodold(jdim,4),prod,prodmax,dist
      REAL ue,vol(idim-1,jdim-1)
c
      REAL x,xt,rlamda
c
      INTEGER itripwork, itrippass
      itripwork = abs(itrippass)
c
c    Set up pointers and general constants
c
      c1 = -2.0/3.0
```

```
      iu = nspec + 1
      iv = nspec + 2
      iw = nspec + 3
      ik = nspec+nnev+5
      ieps = nspec+nnev+6
c
c     Pull x,xt and rlamda out of the new prodold array
c
      x = prodold(7,3)
      xt = prodold(2,3)
      rlamda = prodold(4,3)
c
c     If itrip = -1 was passed, this is the first station
c     of the transition region and prodold = 0
c
      if (itrip.lt.0) then
c
         do 5 j = 1,jdim
            prodold(j,1) = 0.0
            prodold(j,2) = 0.0
   5     continue
c
         itrip = 1
c
      endif
c
      do 10 i = 1,idim-1
c
        ue = sqrt(q(i,idelta,iu,k)**2+q(i,idelta,iv,k)**2
     .               + q(i,idelta,iw,k)**2)
c
       if ((i.lt.itrip).or.(itrip.eq.0)) then
c
c      We are still in the "laminar" region
c      set the TKE production to zero.  That
c      is done by adding it back into what
c      it was subtracted out of in addke*
c
         do 20 j = 1,jdim-1
           res(i,j,ik) = res(i,j,ik) + cke(i,j,1)*(
     .       rmut(i,j)*kesrc(i,j,1)+c1*rho(i,j)*
     .       q(i,j,ik,k)*kesrc(i,j,2))
 20      continue
c
      else
c
c     We are now in the "Turbulent Region".  It
c     is time to start using the Schmidt and Patankar
c     routine.
c
         do 30 j = 1,jdim-1
          vmag = sqrt(q(i,j,iu,k)*q(i,j,iu,k)+q(i,j,iv,k)*q(i,j,iv,k)
     .               + q(i,j,iw,k)*q(i,j,iw,k))
c
c     We now compute the production at the upstream
c     cell.  If the current i is itrip, then
c     the upstream cell is in the "laminar region"
c     and prodold is 0.0
c     This is only true if we are in global iteration.
c
         if ((idim.gt.2).and.(i.eq.itrip)) prodold(j,1) = 0.0
c
         prod = cke(i,j,1)*(rmut(i,j)*kesrc(i,j,1)
     .           + c1*rho(i,j)*q(i,j,ik,k)*kesrc(i,j,2))
```

```
c
c     Compute the distance between cells
c     this is going to be different depending
c     on whether we are space marching or
c     doing global iteration
c
      if (idim.gt.2) then
c
c     Global
c
         dist = sqrt((xyz(i,j,1,k)-xyz(i-1,j,1,k))**2 +
     .               (xyz(i,j,2,k)-xyz(i-1,j,2,k))**2 +
     .               (xyz(i,j,3,k)-xyz(i-1,j,3,k))**2)
c
      else
c
c     Space Marching
c
         dist = sqrt((xyz(i,j,1,k)-xyz(i,j,1,k-1))**2 +
     .               (xyz(i,j,2,k)-xyz(i,j,2,k-1))**2 +
     .               (xyz(i,j,3,k)-xyz(i,j,3,k-1))**2)
c
      endif
c
c     compute the maximum increase in production
c     using S&A
c
         prodmax = vol(i,j)*(a*prodold(j,1)+b)*dist/vmag
c
c
c      It is time to determine what value of prod should be used.
c
            if (prod.gt.prodold(j,1)+prodmax) then
c
c       Production is too high. It must be set
c       to the limited value which involves
c       adding what was subtracted out of the residual
c       array and subtracting out the new production
c
        write(*,*) 'production is too high at',j
c
               res(i,j,ik) = res(i,j,ik) + prod -
     .                     (prodold(j,1)+prodmax)
c
                prod = prodold(j,1)+prodmax
c
            endif
c
c        O.K. we have changed the value of the production
c        Now we have to store the current value of production
c        in  prodold.  Now that will be different depending
c        on if we are space marching or in global iteration
c
         if (idim.lt.3) then
c
c        We are space marching.  Do NOT put
c        the current value of prod into prodold.
c        Instead put it in the (,2) spot.  This will
c        be rotated into the (,1) spot when this plane
c        is completed
c
         prodold(j,2) = prod
c
         else
c
```

```
c        We are in global iteration
c
c        Set the old production of this cell
c        to be used when computing the production
c        of the next cell.  If the production is negative
c        set it equal to zero.
c
            if (prod.gt.0.0) then
               prodold(j,1) = prod
            else
               prodold(j,1) = 0.0
            endif
c
         endif
c
   30    continue
c
         endif
c
   10    continue
c
         return
         end
c
*************************************************************
c
      subroutine bledge3(q,idim,jdim,neqn,ue,rdelta,itrippass,
     .                   thp,nspec,utot)
c
      REAL q(-1:idim+1,-1:jdim+1,neqn)
      REAL thp(0:idim,0:jdim,NTHP)
      REAL ue(idim)
      REAL rdelta(idim)
c
      INTEGER idim,jdim,neqn,nspec,iu,itrip,itrippass
      INTEGER i,j,jstart
c
      REAL utot(0:idim,0:jdim)
c
c     setup pointers and the like
c
      iu = nspec+1
      jstart = 3
c
c     itrip, itrippass are needed because of the difference
c     between space marching and global iteration
c
      itrip = itrippass
      if (itrip.lt.1) itrip = 1
c
c     compute the total velocity for the entire domain
c
      call findutot2(idim,jdim,utot,q(-1,-1,iu))
c
c     set delta equal to zero for the laminar
c     region
c
      do 10 i=1,itrip-1
        rdelta(i)=0.0
        ue(i)=0.0
 10   continue
c
c  Now start marching through the transition region.
c
      do 40 i = itrip,idim
```

```
c
c  Now work up from wall until values
c  of Mach Number are close to each other
c
         jstart = int(rdelta(i-1)/2.0)
         if (jstart.le.3.or.jstart.gt.jdim) jstart = 3
         do 30 j = jstart,jdim-1
c
            if(utot(i,j-1)/utot(i,j).gt.0.99) then
              rdelta(i) = real(j) + 1.0
              ue(i) = utot(i,j+1)
              goto 35
            endif
c
  30     continue
c
c  The edge of the Boundary Layer was never found.
c  The flow must really be messed up.
c  just set edge conditions to jdim-1.
c  Everything will work out later
c
         rdelta(i) = real(jdim)
         ue(i) = utot(i,jdim-1)
c
  35     continue
c
  40     continue
c
         return
         end
c
**********************************************************************
c
      subroutine getret(q,idim,jdim,retheta,rdelta,neqn,
     .                  thp,trp,ue,nspec,ddj0,rmut,rinte)
c
      INTEGER idim,jdim,neqn,nspec
c
      REAL q(-1:idim+1,-1:jdim+1,neqn)
c
      REAL ubar,ubare,rho,rhoe
      REAL theta,retheta,ue(idim)
      REAL rinte(0:jdim)
      REAL rdelta(idim),rmut(idim-1,jdim-1)
      REAL ddj0(jdim,idim-1)
      REAL thp(0:idim,0:jdim,NTHP)
      REAL trp(0:idim,0:jdim,NTRP)
c
      INTEGER idelta,i,j
      INTEGER iu,iv,iw,irho
c
c     set up pointers
c
      iu = nspec+1
      iv = iu + 1
      iw = iv + 1
      irho = 1
c
c     zero out theta
c
      theta=0.0
c
c     We are just looking at theta for this one
c     station
c
```

```
      i = 1
c
c     Compute the integrand for theta at this location
c
      idelta = int(rdelta(i))
           ubare = (q(i,idelta,iu)*q(i,idelta,iu)
     .           +q(i,idelta,iv)*q(i,idelta,iv)
     .           +q(i,idelta,iw)*q(i,idelta,iw))**(.5)
           rhoe = q(i,idelta,irho)
c
         do 30 j = 0,idelta
           ubar = (q(i,j,iu)*q(i,j,iu)+q(i,j,iv)*q(i,j,iv)
     .           +q(i,j,iw)*q(i,j,iw))**(.5)
           rho = q(i,j,irho)
           rinte(j)=(rho*ubar)*(1.0-(ubar/ubare))/(rhoe*ubare)
 30      continue
c
c     Now start adding up the integral
c
          theta= theta +
     .         .5*(rinte(0)+rinte(1))*(ddj0(1,i))
          do 40 j = 2,idelta
             theta= theta  +
     .       .5*(rinte(j-1)+rinte(j))*(ddj0(j,i)-ddj0(j-1,i))
  40      continue
c
c      O.K. Now we have theta ==>  Compute Retheta
c      Note, we want to base Re on the molecular
c      viscosity, not the molecular plus the
c      eddy, so subtract out the eddy viscosity
c
      retheta = thp(i,idelta,iRho)*ue(i)*theta
     .           /(trp(i,idelta,iMul)-rmut(i,idelta))
c
c     Mission Accomplished!
c
      return
      end
c
*****************************************************************
c
c +-------------------------------------------------------------+
c |                          findutot2                          |
c +-------------------------------------------------------------+
c
      subroutine findutot2(idim,jdim,utot,vel)
c
      INTEGER idim,jdim,i,j
      REAL    utot(0:idim,0:jdim),vel(-1:idim+1,-1:jdim+1,3)
c
c     calculate velocity
c
      do 100 i=0,idim
      do 100 j=0,jdim
        utot(i,j) = sqrt(vel(i,j,1)*vel(i,j,1)+vel(i,j,2)*vel(i,j,2)+
     .                   vel(i,j,3)*vel(i,j,3))
  100 continue
c
      return
      end
```

A.3 Warren, Harris and Hassan

The following routines were used to compute the Warren, Harris and Hassan model, which is referred to as the HYBRID model in the code.

The first two routines getle and getlu are called from the routines that computes the eddy viscosity and epsilon. hybrig is the main routine for the Warren, Harris and Hassan model that is called from visck.

```
      subroutine getlu(idim,jdim,lu,tke,rho,ddj0,tw,taw,rmul,vort)
c
      INTEGER idim,jdim,i,j
c
      REAL kappa,c1,c2,y
      REAL tke(jdim-1),rho(jdim-1),ddj0(jdim,idim-1)
      REAL lu(jdim-1),tw,taw,rmul(jdim-1)
c
c     Pseudo-Baldwin Lomax variables
c
      INTEGER nymax
      REAL vort(0:idim,0:jdim),fmax,f
      REAL rcvmgt,aplus,yplusoy,damp
c
c     Set the values of some parameters
c
      kappa = 0.41
      c1 = 6.08580619*kappa
      c2 = 70.0*(tw/taw)**.5
      i=1
c
      aplus = 26.0
      yplusoy = sqrt(abs(rho(1)*vort(1,0)/rmul(1)))/aplus
c
c     O.K., we must get the pseudo Baldwin-Lomax
c     Fmax and Ymax, must of this was taken from
c     Subroutine mutbl
c
      fmax = 1.e-10
      nymax = 1
c
      do 5 j = 1,jdim-1
c
         damp = 1.0 - exp(-yplusoy*ddj0(j,i))
         f = vort(i,j)*ddj0(j,i)*damp
c
         if (fmax.lt.f) then
            fmax=f
            nymax=j
         endif
c
c     Take the First Maximum(degani-schiff)
c
         if (f    .lt.      0.9*fmax) go to 7
c
    5 continue
c
    7 continue
c
c     O.K., we have computed ymax. Now compute Lu
c
      do 10 j = 1,jdim-1
c
         y = ddj0(j,i)
c
```

```
         lu(j) = c1*y*(RONE - EXP(-(tke(j)**.5)*rho(j)*y/
     .          (c2*rmul(j))))
c
c     O.K. now take the lesser of ymax and Lu
c
         lu(j) = RCVMGT(lu(j),ddj0(nymax,i),lu(j) .lt. ddj0(nymax,i))
c
   10 continue
c
      return
      end
c
*****************************************************************
c
      subroutine getle(idim,jdim,le,tke,rho,disn,rmul,vort,u)
c
      INTEGER idim,jdim,i,j,idelta
c
      REAL kappa,c1,y
      REAL tke(idim-1,jdim-1),rho(jdim-1),disn(jdim-1)
      REAL le(jdim-1),rmul(jdim-1)
      REAL u(jdim-1),re
c
c     Pseudo-Baldwin Lomax variables
c
      INTEGER nymax
      REAL vort(0:idim,0:jdim),fmax,f
      REAL rcvmgt,aplus,yplusoy,damp
c
c     Set the values of some parameters
c
      kappa = 0.41
      c1 = kappa*(0.09)**(-3./4.)
      i=1
c
      aplus = 26.0
      yplusoy = sqrt(abs(rho(1)*vort(1,0)/rmul(1)))/aplus
c
c     O.K., we must get the pseudo Baldwin-Lomax
c     Fmax and Ymax, must of this was taken from
c     Subroutine mutbl
c
      fmax = 1.e-10
      nymax = 1
c
      do 5 j = 1,jdim-1
c
         damp = 1.0 - exp(-yplusoy*disn(j))
         f = vort(i,j)*disn(j)*damp
c
         if (fmax.lt.f) then
            fmax=f
            nymax=j
         endif
c
c     Take the First Maximum(degani-schiff)
c
         if (f    .lt.      0.9*fmax) go to 7
c
    5 continue
c
    7 continue
c
c     O.K., we have computed ymax. Now compute Le
c
```

```
      if (nymax.le.15) nymax = 15
c
c      We must find the edge of the boundary layer
c      to find re
c
      do 20 j = 5, 50
c
      if (u(j-1).gt.(0.99*u(j))) then
          idelta=j
          goto 21
      endif
c
      idelta = j
c
   20 continue
   21 continue
c
      re = rho(idelta)*u(idelta)/rmul(idelta)
c
      do 10 j = 1,jdim-1
c
         y = disn(j)
c
         le(j) = c1*y*(RONE - EXP(-(tke(i,j)**.5)*re*y/
     .           (2.0*c1)))
c
c     O.K. now take the lesser of ymax and Le
c
         le(j) = RCVMGT(le(j),disn(nymax),le(j) .lt. disn(nymax))
c
   10 continue
c
      return
      end
c
*****************************************************************
c
      subroutine hybridg(k,idim,jdim,kdim,nspec,nnev,neqn,q,
     .      ivscoef,history,ddj0,xyz,thp,rbccoef,refqty,
     .      rvscoef,trp,t)
c
      INTEGER k,idim,jdim,kdim,nspec,nnev,neqn
      INTEGER itrip,idelta
c
      REAL q(-1:idim+1,-1:jdim+1,neqn,k-2:k+2)
      REAL history(2*jdim)
      REAL ue,ueold,theta,rlt2
c
      REAL ddj0(jdim,idim-1),xyz(idim,jdim,3,k-1:k)
c
      REAL thp(0:idim,0:jdim,NTHP)
      REAL trp(0:idim,0:jdim,NTRP)
      REAL rbccoef(NRBCCOEF),refqty(NREFQTY)
      REAL rvscoef(NRVSCOEF)
c
      INTEGER ivscoef(NIVSCOEF)
c
      REAL xsi,rn2,rno
c
c     First and second mode disturbances
c
      REAL  up,me,tke,re
      REAL  tstar,te,tw,rhostar,mustar,deltast,restar,wfirst
c
c     temp space
```

```
c
      REAL t(1)
c
      INTEGER igamma,ixt,ixtm1,ilamda,itmp,ifirst,isecond,ix
c
c     Set pointers for history
c
      igamma=1
      ixt=2
      ixtm1=3
      ilamda = 4
      ifirst = 5
      isecond = 6
      ix = 7
c
c     Set pointers for tmp space
c
      itmp=1
c
c     pull itrip from ivscoef array
c
      itrip = abs(ivscoef(Itrip))
c
      if (itrip.eq.0) then
c
      history(igamma) = 1.0
c
      else if(k.lt.itrip-1) then
c
         history(igamma) = 0.0
c
      else if (k.eq.itrip-1) then
c
         history(igamma) = 0.0
c
c     We need the "x" location so that we can find
c     duedx for the next plane
c
         history(ixtm1)=xyz(1,1,1,k)
c
      else if (k.eq.itrip) then
c
         history(ixt)=xyz(1,1,1,k)
         history(ix)=xyz(1,1,1,k)
c
c        Get ue for previous plane
c
         call hybridbledge(q(-1,-1,1,k-1),idim,jdim,ueold,
     .                  idelta,itrip,nspec,neqn)
c
c        Get ue and stuff for this plane
c
         call hybridbledge(q(-1,-1,1,k),idim,jdim,ue,
     .                  idelta,itrip,nspec,neqn)
c
         call hybridmomthick(q(-1,-1,1,k),idim,jdim,neqn,nspec,
     .                     idelta,t(itmp),theta,ddj0)
c
         call hgetlt2(rlt2,ueold,ue,theta,history,thp,trp,idelta,
     .                 idim,jdim,nspec)
c
         rno = .0002
c
         if (rlt2.gt.0.0) then
c
```

```
            rn2 = rno + 0.24*rlt2*rlt2
c
         else
c
            rn2 = rno - 323.0*rlt2*rlt2*rlt2
c
         endif
c
         call hgetlamda(history(ilamda),thp,trp,idim,jdim,ue,idelta,
     .                  rn2,theta,nspec)
c
c        Since this is the first plane, set gamma = 0
c
         history(igamma) = 0.0
c
       else if (k.gt.itrip) then
c
         history(ix) = xyz(1,1,1,k)
         xsi = (xyz(1,1,1,k) - history(ixt))/history(ilamda)
c
         history(igamma) = 1.0 - EXP(-0.411*xsi*xsi)
c
       endif
c
c      Let's compute the length scale from the second mode disturbances
c
       if ((itrip.ne.0).and.(k.ge.itrip)) then
c
c      Compute parameters needed for both first and second mode
c      Disturbances
c
         call hybridbledge(q(-1,-1,1,k),idim,jdim,ue,
     .                  idelta,itrip,nspec,neqn)
c
         me = ue/thp(1,idelta,iSnd)
         tke = q(1,idelta,neqn-1,k)
c
c        First Mode
c
         te =  thp(1,idelta,iTemp)
         tw = rbccoef(Itwall)
         tstar = te*(1.0+0.032*me*me+0.58*(tw/te-1.0))
         rhostar = thp(1,idelta,iRho)*te/tstar
c
c        We need the displacement thickness
c
         call hybriddisthick(q(-1,-1,1,k),idim,jdim,neqn,nspec,
     .                     idelta,t(itmp),deltast,ddj0)
c
c        We need to approximate the viscosity.
c
         call hybridmu(ivscoef(Imodlmu),tstar,
     .                 rvscoef(Imu),refqty,mustar)
c
         restar = rhostar*ue/mustar
c
         wfirst = ue*ue*rhostar/mustar*3.2*(restar*deltast)**(-1.5)
c
         history(ifirst) = .05*tke**.5/wfirst
c
c        Second Mode
c
         up = ue*0.94
         re = thp(1,idelta,iRho)*ue/trp(1,idelta,iMul)
c
```

```
         history(isecond)= (.23/up)*me*me*
     .           (tke*xyz(1,1,1,k)/re)**.5
c
      else
c
      history(ifirst) = 0.0
      history(isecond) = 0.0
c
      endif
c
      return
      end
c
*****************************************************************
c
      subroutine hybridbledge(q,idim,jdim,ue,idelta,itrip,
     .                        nspec,neqn)
c
      INTEGER idim,jdim,neqn,nspec,iu,iv,iw,itrip
      INTEGER i,j,jstart,idelta
c
      REAL q(-1:idim+1,-1:jdim+1,neqn)
      REAL ue,uold,u
c
c     Setup pointers and the like
c
      iu = nspec+1
      iv = iu+1
      iw = iv+1
c
      i = 1
c
      jstart = 5
c
      uold = sqrt(q(i,jstart-1,iu)*q(i,jstart-1,iu)
     .        +   q(i,jstart-1,iv)*q(i,jstart-1,iv)
     .        +   q(i,jstart-1,iw)*q(i,jstart-1,iw))
c
      do 10 j = jstart,jdim-1
c
         u =    sqrt(q(i,j,iu)*q(i,j,iu)
     .           +   q(i,j,iv)*q(i,j,iv)
     .           +   q(i,j,iw)*q(i,j,iw))
c
         if(uold.gt.0.99*u) goto 20
c
         uold = u
c
   10 continue
   20 continue
c
      ue = u
      idelta = j
c
      return
      end
c
*****************************************************************
c
      subroutine hybridmomthick(q,idim,jdim,neqn,nspec,idelta,
     .                          rinte,theta,ddj0)
c
      INTEGER idim,jdim,neqn,nspec
      INTEGER iu,iv,iw,irho,i,j,idelta
c
```

```
      REAL q(-1:idim+1,-1:jdim+1,neqn)
      REAL rinte(0:jdim)
      REAL ubare,rhoe,ubar,rho,theta
      REAL ddj0(jdim,idim-1)
c
c     Set pointers and the like
c
      iu = nspec+1
      iv = iu + 1
      iw = iv + 1
      irho = 1
c
      i = 1
c
      theta = 0.0
c
           ubare = (q(i,idelta,iu)*q(i,idelta,iu)
     .           +q(i,idelta,iv)*q(i,idelta,iv)
     .           +q(i,idelta,iw)*q(i,idelta,iw))**(.5)
           rhoe = q(i,idelta,irho)
c
         do 10 j = 0,idelta
           ubar = (q(i,j,iu)*q(i,j,iu)+q(i,j,iv)*q(i,j,iv)
     .           +q(i,j,iw)*q(i,j,iw))**(.5)
           rho = q(i,j,irho)
           rinte(j)=(rho*ubar)*(1.0-(ubar/ubare))/(rhoe*ubare)
 10      continue
c
c      Now start adding up the integral
c
          theta=theta +
     .         .5*(rinte(0)+rinte(1))*(ddj0(1,i))
          do 20 j = 2,idelta
             theta=theta  +
     .       .5*(rinte(j-1)+rinte(j))*(ddj0(j,i)-ddj0(j-1,i))
  20      continue
c
      return
      end
c
*****************************************************************
c
      subroutine hgetlt2(rlt2,ueold,ue,theta,history,thp,trp,idelta,
     .                   idim,jdim,nspec)
c
          INTEGER idim,jdim,nspec,idelta
c
          REAL ue,ueold,theta,rnu,duedx,rlt2,dist
          REAL thp(0:idim,0:jdim,NTHP)
          REAL trp(0:idim,0:jdim,NTRP)
          REAL history(2*jdim)
c
          INTEGER ixt,ixtm1,i
c
c         pointers for history array
c
          ixt = 2
          ixtm1 = ixt+1
c
          i = 1
c
          rnu = trp(i,idelta,iMul)/thp(i,idelta,iRho)
c
          dist = history(ixt)-history(ixtm1)
```

```
c
          duedx = (ue-ueold)/dist
c
          rlt2 = duedx*theta*theta/rnu
c
          return
          end
c
*****************************************************************
c
      subroutine hgetlamda(rlamda,thp,trp,idim,jdim,ue,idelta,
     .                     rn2,theta,nspec)
c
      INTEGER idim,jdim,nspec,idelta,i
c
      REAL retheta,ue,rn2,theta,rlamda
      REAL thp(0:idim,0:jdim,NTHP)
      REAL trp(0:idim,0:jdim,NTRP)
c
      i = 1
c
      retheta = thp(i,idelta,iRho)*ue*theta/
     .          trp(i,idelta,iMul)
c
      rlamda = sqrt(0.411*retheta**3/rn2)*trp(i,idelta,iMul)
     .         /ue/thp(i,idelta,iRho)
c
      return
      end
c
*****************************************************************
c
      subroutine hybriddisthick(q,idim,jdim,neqn,nspec,idelta,
     .                          rinte,deltast,ddj0)
c
      INTEGER idim,jdim,neqn,nspec
      INTEGER iu,iv,iw,irho,i,j,idelta
c
      REAL q(-1:idim+1,-1:jdim+1,neqn)
      REAL rinte(0:jdim)
      REAL ubare,rhoe,ubar,rho,deltast
      REAL ddj0(jdim,idim-1)
c
c     Set pointers and the like
c
      iu = nspec+1
      iv = iu + 1
      iw = iv + 1
      irho = 1
c
      i = 1
c
      deltast = 0.0
c
           ubare = (q(i,idelta,iu)*q(i,idelta,iu)
     .            +q(i,idelta,iv)*q(i,idelta,iv)
     .            +q(i,idelta,iw)*q(i,idelta,iw))**(.5)
           rhoe = q(i,idelta,irho)
c
         do 10 j = 0,idelta
           ubar = (q(i,j,iu)*q(i,j,iu)+q(i,j,iv)*q(i,j,iv)
     .            +q(i,j,iw)*q(i,j,iw))**(.5)
           rho = q(i,j,irho)
           rinte(j)=(1.0-(rho*ubar/ubare/rhoe))
```

```
 10      continue
c
c      Now start adding up the integral
c
           deltast=deltast +
     .         .5*(rinte(0)+rinte(1))*(ddj0(1,i))
           do 20 j = 2,idelta
              deltast=deltast  +
     .        .5*(rinte(j-1)+rinte(j))*(ddj0(j,i)-ddj0(j-1,i))
  20       continue
c
c     Make sure that deltast is not negative
c
      if (deltast.lt.0.0) then
          deltast = 1.0e-8
      endif
c
      return
      end
c
*****************************************************************
c
      subroutine hybridmu(imodlmu,temp,rmucoef,refqty,rmu)
c
      INTEGER imodlmu
c
      REAL temp,rmucoef(3),refqty(NREFQTY)
      REAL rmu,tempd,rmud,t1
c
c     Dimensionalize the temperature
c
      tempd =  temp * refqty(iTmpref)
c
c     Decide which viscosity model is being used
c
c     Blottner's model
c
      if (imodlmu.eq.1) then
c
      t1 = log(tempd)
      rmud = 0.1*EXP((rmucoef(1)*t1+rmucoef(2))*t1+rmucoef(3))
c
      endif
c
c     Southerland Model
c
      if (imodlmu.eq.2) then
c
      t1 = tempd/rmucoef(2)
      rmud = rmucoef(1)*t1*sqrt(t1)*(rmucoef(2)+
     .       rmucoef(3))/(tempd+rmucoef(3))
c
      endif
c
c     non-dimensionalize mixture laminar viscosity
c
      rmu = rmud/refqty(iMuref)
c
      return
      end
c
```

A.4 Linear Combination Transition Region Model

The linear combination model has been implemented as a separate program that takes the restart files from a fully laminar and fully turbulent flow and creates a transitional solution. The parts of the program that read in the solution file and print it out were taken directly from gasp. What follows is the routines that computes the transitional flow field

```
c
c     This subroutine sorts out all the arrays and stuff
c     and calls the subroutine that runs the linear
c     transition region model.
c
#include "gasp.h"
c
      subroutine settran(idim,jdim,kdim,qlam,qturb,qnew,
     .                   nspec,nnev,neqn,itherm,
     .                   ithcoef,rthcoef,iliu,rliu,
     .                   refqty,qinf,ivscoef,rvscoef,
     .                   gridfil,ddj0,qlam1,qturb1,qnew1,t)

      INTEGER idim,jdim,kdim,neqn,nspec,nnev
c
      REAL qlam(-1:idim+1,-1:jdim+1,neqn,-1:kdim+1)
      REAL qturb(-1:idim+1,-1:jdim+1,neqn,-1:kdim+1)
      REAL qnew(-1:idim+1,-1:jdim+1,neqn,-1:kdim+1)
c
c    This q arrays are used if the grid is in the i plane
c
      REAL qlam1(-1:kdim+1,-1:jdim+1,neqn,-1:idim+1)
      REAL qturb1(-1:kdim+1,-1:jdim+1,neqn,-1:idim+1)
      REAL qnew1(-1:kdim+1,-1:jdim+1,neqn,-1:idim+1)
c
      REAL ddj0(jdim,idim-1)
c
c     coefficients for the thermodynamics
c
      INTEGER itherm
      INTEGER ithcoef(nspec,NITHCOEF),iliu(NILIU)
      REAL    rthcoef(nspec,NRTHCOEF),rliu(NRLIU)
      REAL    refqty(NREFQTY),qinf(neqn+2)
c
c     viscous thermal coefficients
c
      INTEGER ivscoef(NIVSCOEF)
      REAL    rvscoef(NRVSCOEF)
c
      INTEGER nlen
c
      INTEGER ithp,itrp,itmp,ixyz
c
c      These are used to shuffle the grids
c
      INTEGER i,j,k,n,ixyz1,iddj01
c
      character*60 gridfil
c
c     Temp Space
c
      REAL t(1)
c
c     set up pointers for temp space and
c     the like
```

```
c
c     the size on itrp and ithp is larger than
c     needed because we don't know yet what
c     plane the solution is in
c
      ithp = 1
      itrp = ithp+(idim+3)*(jdim+3)*(kdim+3)*NTHP
      ixyz = itrp+(idim+3)*(jdim+3)*(kdim+3)*NTRP
      ixyz1 = ixyz+3*idim*jdim*kdim
      iddj01 = ixyz1+3*idim*jdim*kdim
      itmp = iddj01+jdim*(kdim-1)
c
c     We must find nlen
c
      nlen = (idim+3)*(jdim+3)
c
c     We need to read in the grid
c
      call rgridck(gridfil,idim,jdim,kdim,1,kdim,t(ixyz))
c
c     Check to see whether we are in the i or k plane
c
      if (idim.gt.2) then
c
c     kplane!
c
c     We need to get thp and trp
c
        call getthp(qlam(-1,-1,1,1),t(ithp),nspec,nnev,neqn,nlen,itherm,
     .              ithcoef,rthcoef,iliu,rliu,ivscoef(Ikeps),refqty,
     .              qinf,t(itmp))
c
        call gettrp(nlen,nspec,nnev,neqn,qlam(-1,-1,1,1),t(ithp),
     .          t(itrp),ivscoef,rvscoef,rthcoef,refqty,t(itmp))
c
c    O.K.  It is time to call the subroutine
c    that implements the transition region model.
c
      call lincom(idim,jdim,kdim,neqn,nspec,qlam(-1,-1,1,1)
     .            ,qturb(-1,-1,1,1),qnew(-1,-1,1,1),
     .            t(ithp),t(itrp),ddj0,t(ixyz),rvscoef,t(itmp))
c
      else
c
c     We are in the i plane!
c     Try to put everything in temporary k plane
c     form
c
      do 10 i = -1,idim+1
      do 10 j = -1,jdim+1
      do 10 k = -1,kdim+1
      do 10 n = 1,neqn
         qlam1(k,j,n,i)=qlam(i,j,n,k)
         qturb1(k,j,n,i)=qturb(i,j,n,k)
         qnew1(k,j,n,i)=qnew(i,j,n,k)
  10  continue
c
c     The grid needs to be moved to!
c
      call movegrid(idim,jdim,kdim,t(ixyz),t(ixyz1))
c
c     Don't forget nlen needs to be changed!
c
      nlen = (kdim+3)*(jdim+3)
```

```
c
c     ddj0 is no longer correct!
c     We must *estimate* a new one
c
      call getddj01(kdim,jdim,idim,t(ixyz1),t(iddj01),t(itmp))
c
c     O.K. the q vector and grid and in the correct
c     form, lets call the necessary routines
c
       call getthp(qlam1(-1,-1,1,1),t(ithp),nspec,nnev,neqn,nlen,itherm,
     .              ithcoef,rthcoef,iliu,rliu,ivscoef(Ikeps),refqty,
     .              qinf,t(itmp))
c
        call gettrp(nlen,nspec,nnev,neqn,qlam1(-1,-1,1,1),t(ithp),
     .          t(itrp),ivscoef,rvscoef,rthcoef,refqty,t(itmp))
c
      call lincom(kdim,jdim,idim,neqn,nspec,qlam1(-1,-1,1,1)
     .            ,qturb1(-1,-1,1,1),qnew1(-1,-1,1,1),
     .            t(ithp),t(itrp),t(iddj01),t(ixyz1),rvscoef,t(itmp))
c
c     Everything has been computed on the working
c     arrays, need to shift back to the real arrays
c
      do 20 i = -1,idim+1
      do 20 j = -1,jdim+1
      do 20 k = -1,kdim+1
      do 20 n = 1,neqn
         qlam(i,j,n,k)=qlam1(k,j,n,1)
         qturb(i,j,n,k)=qturb1(k,j,n,1)
         qnew(i,j,n,k)=qnew1(k,j,n,1)
  20  continue
c
c     we are done!
c
      endif
c
      return
      end
c
****************************************************************
c
c     This takes a Laminar and turbulent flow field
c     and combines them using a Linear combination
c     using the intermittency.
c
      subroutine lincom(idim,jdim,kdim,neqn,nspec,qlam,qturb,qnew,
     .                  thp,trp,ddj0,xyz,rvscoef,t)
c
      INTEGER idim,jdim,kdim,neqn,nspec
c
      REAL qlam(-1:idim+1,-1:jdim+1,neqn)
      REAL qturb(-1:idim+1,-1:jdim+1,neqn)
      REAL qnew(-1:idim+1,-1:jdim+1,neqn)
      REAL rvscoef(NRVSCOEF)
      REAL thp(-1:idim+1,-1:jdim+1,NTHP)
      REAL trp(-1:idim+1,-1:jdim+1,NTRP)
      REAL ddj0(jdim,idim-1)
      REAL xyz(idim,jdim,3,kdim)
c
      REAL rno,rn2,rlt2,rlamda
c
      INTEGER ixt0,ixt2
c
      INTEGER itmp,irdelta,igamma,itheta,iue
```

```
c
c     Temp Space
c
      REAL t(1)
c
c     Set up pointers for Temp space
c
      itheta = 1
      iue = itheta + idim
      irdelta = iue + idim
      igamma = irdelta + idim
      itmp = igamma + idim*(jdim+3)
c
c     Hardwire some constants for now
c
      ixt0 = 25
      ixt2 = 25
c
c     We will need ue and delta to compute theta
c
      call bledge2(qlam,idim,jdim,neqn,t(iue),t(irdelta),ixt0,
     .             thp,nspec,t(itmp))
c
c     Cool, now we must find theta
c
      call momthick(qlam,idim,jdim,ixt0,t(itheta),t(irdelta),
     .              neqn,nspec,ddj0,0,rvscoef,t(itmp))
c
c     we need lt2
c
      call getlt2(rlt2,t(iue),t(itheta),ixt2,xyz,thp,trp,t(irdelta),
     .            idim,jdim,nspec)
c
c     We must find No
c
      call getno(rno)
c
c     Now we need n2
c
      call getn2(rn2,rno,rlt2)
c
c     now we need to get lamda
c
      call getlamda(rlamda,thp,trp,idim,jdim,t(iue),t(irdelta),
     .              ixt2,rn2,t(itheta),nspec)
c
c     We are almost done, we now need to find the
c     intermittency
c
      call intermit(idim,jdim,ixt0,t(igamma),xyz,rlamda)
c
c     O.K. we have the intermittency for the one
c     dimensional streamwise case.  We need to include
c     2d affects, i.e. one wall has transition, the top
c     wall does not.  The subroutine we are calling
c     is basically a copy of the one used with
c     the algebraic model.  The difference
c     is the size of the gamma array
c
      call trnsj2(idim,jdim,t(igamma),t(irdelta),ixt0)
c
c     We have the intermittency.  Now let us try
c     combining the q vectors.
c
      call combine(qlam,qturb,qnew,idim,jdim,neqn,t(igamma))
```

```
      return
      end
c
*********************************************************
c
c     This subroutine is the same as trnsj except
c     the dimension on gammat is different
c
      subroutine trnsj2(idim,jdim,gammat,rdelta,itrip)
c
      INTEGER idim,jdim,itrip,i,j
c
      REAL gammat(idim,-1:jdim+1), rdelta(idim)
c
c     In the future, parameters will be read
c     out of the input deck.  For now this is
c     just being hard wired for the turbine case
c
c     this part is for the laminar region(streamwise)
c
      do 10 i = 1, itrip-1
      do 10 j = -1,jdim+1
c
      gammat(i,j) = 0.0
c
   10 continue
c
c     O.k.  this is for the transition and turbulent
c     part.   the values were originally read into
c     j = 1.  set the values up to rdelta equal
c     to this value
c
      do 20 i = itrip, idim
c
      do 20 j = -1 , int(rdelta(i)) + 9
c
      gammat(i,j) = gammat(i,-1)
c
   20 continue
c
c     O.k., now zero out the top laminar wall
c
      do 30 i = itrip, idim
c
      do 30 j = int(rdelta(i))+10 , jdim +1
c
      gammat(i,j) = 0.0
c
   30 continue
c
      return
c
      end
c
*********************************************************************
c
      subroutine getno(rno)
c
      REAL rno
c
      rno = 0.0002
c
      return
      end
c
```

```
**********************************************************************
c
      subroutine bledge2(q,idim,jdim,neqn,ue,rdelta,itrip,
     .                   thp,nspec,utot)
c
      REAL q(-1:idim+1,-1:jdim+1,neqn)
      REAL thp(-1:idim+1,-1:jdim+1,NTHP)
      REAL ue(idim)
      REAL rdelta(idim)
c
      INTEGER idim,jdim,neqn,nspec,iu,itrip
      INTEGER i,j,jstart
c
      REAL utot(0:idim,0:jdim)
c
c     setup pointers and the like
c
      iu = nspec+1
      jstart = 3
c
c     compute the Mach Number for the entire domain
c
      call findutot(idim,jdim,utot,q(-1,-1,iu))
c
c     set delta equal to zero for the laminar
c     region
c
      do 10 i=1,itrip-2
        rdelta(i)=0.0
        ue(i)=0.0
 10   continue
c
c  Now start marching through the transition region.
c
      do 40 i = itrip-1,idim
c
c  Now work up from wall until values
c  of Mach Number are close to each other
c
         jstart = int(rdelta(i-1)/2.0)
         if (jstart.le.3.or.jstart.gt.jdim) jstart = 3
         do 30 j = jstart,jdim-1
c
            if(utot(i,j-1)/utot(i,j).gt.0.99) then
              rdelta(i) = real(j) + 1.0
              ue(i) = utot(i,j+1)
              goto 35
            endif
c
  30     continue
c
c  The edge of the Boundary Layer was never found.
c  The flow must really be messed up.
c  just set edge conditions to jdim-1.
c  Everything will work out later
c
        rdelta(i) = real(jdim)
        ue(i) = utot(i,jdim-1)
c
  35    continue
c
  40    continue
c
        return
        end
```

```
c
*****************************************************************
c
c +-------------------------------------------------------------+
c |                          findutot                           |
c +-------------------------------------------------------------+
c
      subroutine findutot(idim,jdim,utot,vel)
c
      INTEGER idim,jdim,i,j
      REAL    utot(0:idim,0:jdim),vel(-1:idim+1,-1:jdim+1,3)
c
c     calculate velocity from velocities & speed of sound
c
      do 100 i=0,idim
      do 100 j=0,jdim
        utot(i,j) = sqrt(vel(i,j,1)*vel(i,j,1)+vel(i,j,2)*vel(i,j,2)+
     .                   vel(i,j,3)*vel(i,j,3))
  100 continue
c
      return
      end
c
*****************************************************************
c
      subroutine getlt2(rlt2,ue,theta,ixt2,xyz,thp,trp,rdelta,
     .                  idim,jdim,nspec)
c
      INTEGER idim,jdim,nspec
      INTEGER idelta,ixt2
c
      REAL xyz(idim,jdim,3)
      REAL rdelta(idim),ue(idim),theta(idim)
      REAL rnu,duedx,rlt2
      REAL dist
c
      REAL thp(-1:idim+1,-1:jdim+1,NTHP)
      REAL trp(-1:idim+1,-1:jdim+1,NTRP)
c
      idelta = int(rdelta(ixt2))
c
      rnu = trp(ixt2,idelta,iMul)/thp(ixt2,idelta,iRho)
c
c     We need the distance between the points
c
      call getdist(idim,jdim,ixt2,ixt2-1,1,1,xyz,dist)
c
      duedx = (ue(ixt2)-ue(ixt2-1))/dist
c
      rlt2 = duedx*theta(ixt2)*theta(ixt2)/rnu
c
      return
      end
c
*****************************************************************
c
      subroutine getn2(rn2,rno,rlt2)
c
      REAL rn2,rno,rlt2
c
      if (rlt2.gt.0.0) then
c
        rn2 = rno + 0.24*rlt2*rlt2
c
      else
```

```
c
        rn2 = rno - 323.0*rlt2*rlt2*rlt2
c
      endif
c
      return
      end
c
*************************************************************
c
      subroutine getlamda(rlamda,thp,trp,idim,jdim,ue,rdelta,
     .                    ixt2,rn2,theta,nspec)
c
      INTEGER idim,jdim,nspec
c
      REAL retheta,ue(idim),rn2,theta(idim),rdelta(idim)
      REAL rlamda
      REAL thp(-1:idim+1,-1:jdim+1,NTHP)
      REAL trp(-1:idim+1,-1:jdim+1,NTRP)
c
      INTEGER idelta,ixt2
c
      idelta = int(rdelta(ixt2))
c
      retheta = thp(ixt2,idelta,iRho)*ue(ixt2)*theta(ixt2)
     .           /trp(ixt2,idelta,iMul)
c
      rlamda = sqrt(0.411*retheta**3/rn2)*trp(ixt2,idelta,iMul)
     .         /ue(ixt2)/thp(ixt2,idelta,iRho)
c
      return
      end
c
*************************************************************
c
      subroutine intermit(idim,jdim,ixt0,gamma,xyz,rlamda)
c
      INTEGER idim,jdim
      INTEGER i,ixt0
c
      REAL gamma(idim,-1:jdim+1)
      REAL xyz(idim,jdim,3)
      REAL rlamda,dist
c
c     This routine is being modified to take into
c     account flows where the j0 and jdim surface
c     have viscous affects. Therefore a "j" dependency
c     is being added to gamma.  For now we will stick the
c     one dimensional streamwise affects into the j = -1
c     slot
c
      do 10 i = 1,idim-1
c
        gamma(i,-1) = 0.0
c
   10 continue
c
      do 20 i = ixt0+1, idim-1
c
c     Get distance
c
      call getdist(idim,jdim,i,ixt0,1,1,xyz,dist)
c
        gamma(i,-1)=1.0-EXP(-0.411*(dist/rlamda)**2)
c
```

```
   20 continue
c
      return
      end
c
*************************************************************
c
      subroutine combine(qlam,qturb,qnew,idim,jdim,neqn,gamma)
c
      INTEGER i,j,n,idim,jdim,neqn
c
      REAL qlam(-1:idim+1,-1:jdim+1,neqn)
      REAL qturb(-1:idim+1,-1:jdim+1,neqn)
      REAL qnew(-1:idim+1,-1:jdim+1,neqn)
      REAL gamma(idim,-1:jdim+1)
c
c     Do the entire plane including Ghost cells.
c     This is implemented until the BC routine
c     is added to take care of these ghost
c     cells on the plane
c
      do 10 i = 1,idim-1
      do 10 j = -1,jdim+1
      do 10 n = 1,neqn
c
        qnew(i,j,n) = (1.0-gamma(i,j))*qlam(i,j,n)+gamma(i,j)*
     .                qturb(i,j,n)
c
  10  continue
c
c     Set the ghost cells before the domain to the
c     Laminar value and set the ghost cells after the
c     domain to the fully turbulent values
c
      do 20 i = -1,0
      do 20 j = -1,jdim+1
      do 20 n = 1,neqn
c
        qnew(i,j,n) = qlam(i,j,n)
c
   20 continue
c
      do 30 i = idim,idim+1
      do 30 j = -1,jdim+1
      do 30 n = 1,neqn
c
        qnew(i,j,n) = qturb(i,j,n)
c
   30 continue
c
      return
      end
c
*************************************************************
c
      subroutine getdist(idim,jdim,i1,i2,j1,j2,xyz,dist)
c
      INTEGER idim,jdim,i1,i2,j1,j2
c
      REAL xyz(idim,jdim,3)
      REAL dist
c
      dist = ((xyz(i1,j1,1)-xyz(i2,j2,1))**2
     .     + (xyz(i1,j1,2)-xyz(i2,j2,2))**2
     .     + (xyz(i1,j1,3)-xyz(i2,j2,3))**2 )**.5
```

```
c
      return
      end
c
*************************************************************
c
      subroutine movegrid(idim,jdim,kdim,xyz,xyz1)
c
      INTEGER idim,jdim,kdim,i,j,k,n
      REAL xyz(idim,jdim,3,kdim)
      REAL xyz1(kdim,jdim,3,idim)
c
      do 10 i = 1,idim
      do 10 j = 1,jdim
      do 10 k = 1,kdim
      do 10 n = 1,3
c
         xyz1(k,j,n,i)=xyz(i,j,n,k)
c
   10 continue
c
      return
      end
c
*************************************************************
c
      subroutine getddj01(idim,jdim,kdim,xyz,ddj01,xyzc)
c
      INTEGER idim,jdim,kdim,i,j,n
c
      REAL xyz(idim,jdim,3,kdim)
      REAL xyzc(idim,0:jdim,3,kdim)
      REAL ddj01(jdim,idim-1)
c
c     We must get the cell centered value for the grid
c
      do 5  i = 1,idim-1
      do 5  j = 1,jdim-1
      do 5  n = 1,3
         xyzc(i,j,n,1) = .25*(xyz(i,j,n,1)+xyz(i+1,j,n,1)+
     .                        xyz(i,j+1,n,1)+xyz(i+1,j+1,n,1))
    5 continue
c
      do 7 i = 1,idim-1
      do 7 n = 1,3
          xyzc(i,0,n,1) = .5*(xyz(i,1,n,1)+xyz(i+1,1,n,1))
    7 continue
c
      do 10 i = 1,idim-1
      do 10 j = 1,jdim-1
        ddj01(j,i) = ((xyzc(i,j,1,1)-xyzc(i,0,1,1))**2
     .              +  (xyzc(i,j,2,1)-xyzc(i,0,2,1))**2
     .              +  (xyzc(i,j,3,1)-xyzc(i,0,3,1))**2)**(.5)
   10 continue
c
      return
      end
```

A.5 Wilcox

The two equation turbulence modeling was coded up in GASP very general so that more $k-\epsilon$ models could be implemented very easily. To implement the Wilcox $k-\omega$

turbulence model several changes had to be made because the second turbulence variable was ω not ϵ. In general, the implementation was easy and will not be shown here.

For the transition region model part, the boundary condition routine was changed to allow for the roughness boundary condition, this will not be shown.

A.6 Baldwin and Lomax

The Baldwin and Lomax came implemented in GASP. Utilizing it as a transition region model involved only several lines of code that set the eddy viscosity to zero at the beginning of the domain.